U-NET BASED DEEP LEARNING ARCHITECTURES FOR OBJECT SEGMENTATION IN BIOMEDICAL IMAGES

by

Nahian Siddique

A Thesis

Submitted to the Faculty of Purdue University

In Partial Fulfillment of the Requirements for the degree of

Master of Science

Department of Electrical and Computer Engineering

Hammond, Indiana

August 2021

THE PURDUE UNIVERSITY GRADUATE SCHOOL
STATEMENT OF COMMITTEE APPROVAL

Dr. Vijay Devabhaktuni
School of Engineering

Dr. Quamar Niyaz
School of Engineering

Dr. Colin Elkin
School of Engineering

Dr. Xiaoli Yang
School of Engineering

Approved by:
Dr. Xiaoli Yang

To past me, you did it!

To future me, you can do whatever else comes next!

ACKNOWLEDGMENTS

I would like to express my gratitude to my advisors, Dr. Vijay Devabhaktuni and Dr. Sidike Paheding, for their patience, help, and support. Their guidance and mentorship made it possible for me to complete my research. I would also like to extend my gratitude towards my committee members, Dr. Quamar Niyaz, Dr. Colin Elkin, and Dr. Xiaoli Yang. I would like to acknowledge Dr. Md. Zahangir Alom for his contribution to my research work. Finally, I would like to recognize all of my course instructors and fellow graduate research students who have helped me in my journey.

TABLE OF CONTENTS

LIST OF TABLES

LIST OF FIGURES

GLOSSARY

CNN: Convolutional neural network. A type of neural network layer most commonly applied in computer vision applications.

Max pooling: A downsampling method where the max value from a chosen rectangular region is outputted.

ReLU: Rectified Linear Unit. A common activation function applied to the output of neural network layers, particularly in CNNs. Defined by the function $f(x) = \max(x, 0)$.

Leaky ReLU: A ReLU that allows a small positive gradient when the unit is not active. Defined by the function $f(x) = \max(x, ax)$, where a is the leakage rate.

Batch normalization: A method used to make neural networks faster and more stable through normalization of the layers' inputs by re-centering and re-scaling the gradients.

Dropout: A regularization technique for reducing overfitting in neural networks by preventing complex co-adaptations on training data. The process involves randomly omitting units during training steps.

Learning rate: A tuning parameter in an optimization algorithm that determines the step size at each iteration while moving toward a minimum of a loss function.

ABSTRACT

U-net is an image segmentation technique developed primarily for medical image analysis that can precisely segment images using a scarce amount of training data. These traits provide U-net with a high utility within the medical imaging community and have resulted in extensive adoption of U-net as the primary tool for segmentation tasks in medical imaging. The success of U-net is evident in its widespread use in nearly all major image modalities from CT scans and MRI to X-rays and microscopy. Furthermore, while U-net is largely a segmentation tool, there have been instances of the use of U-net in other applications. Given that U-net's potential is still increasing, this review examines the numerous developments and breakthroughs in the U-net architecture and provides observations on recent trends. We also discuss the many innovations that have advanced in deep learning and discuss how these tools facilitate U-net. In addition, we review the different image modalities and application areas that have been enhanced by U-net.

In recent years, deep learning for health care is rapidly infiltrating and transforming medical fields thanks to the advances in computing power, data availability, and algorithm development. In particular, U-Net, a deep learning technique, has achieved remarkable success in medical image segmentation and has become one of the premier tools in this area. While the accomplishments of U-Net and other deep learning algorithms are evident, there still exist many challenges in medical image processing to achieve human-like performance. In this thesis, we propose a U-net architecture that integrates a residual skip connections and recurrent feedback with EfficientNet as a pretrained encoder. Residual connections help feature propagation in deep neural networks and significantly improve performance against networks with a similar number of parameters while recurrent connections ameliorate gradient learning. We also propose a second model that utilizes densely connected layers aiding deeper neural networks. And the proposed third model that incorporates fractal expansions to bypass diminishing gradients. EfficientNet is a family of powerful pretrained encoders that streamline neural network design. The use of EfficientNet as an encoder provides the network with robust feature extraction that can be used by the U-Net decoder to create highly accurate segmentation maps. The proposed networks are evaluated against state-of-the-art deep learning based segmentation techniques to demonstrate their superior performance.

1. INTRODUCTION

A version of this chapter was previously published by IEEE Access [1] [https://doi.org/10.1109/ACCESS.2021.3086020].

Thanks to recent advances in deep learning in computer vision within the past decade, deep learning has been increasingly utilized in the analysis of medical images. While the use of deep learning in computer vision has seen rapid growth in many different fields, it still faces some challenges in the medical imaging field. There have been many breakthrough techniques over the years to overcome these various challenges, and new research is continuously leading to the development of more novel and innovative methods. One such technique that will be discussed in this literature review will be the U-net, a deep learning technique widely adopted within the medical imaging community.

U-net is a neural network architecture designed primarily for image segmentation [2]. The basic structure of a U-net architecture consists of two paths. The first path is the contracting path, also known as the encoder or the analysis path, which is similar to a regular convolution network and provides classification information. The second is an expansion path, also known as the decoder or the synthesis path, consisting of up-convolutions and concatenations with features from the contracting path. This expansion allows the network to learn localized classification information. Additionally, the expansion path also increases the resolution of the output, which can then pass to a final convolutional layer to create a fully segmented image. The resulting network is almost symmetrical, giving it a u-like shape. The main canonical task performed by most convolutional networks is to classify the whole image into a single label. However, classification networks fail to provide pixel-level contextual information, which is of vital importance in medical image analysis. While there have been previous attempts at segmentation tasks, it was not until U-net by Ronneberger et al. [2] that a significant improvement in medical image segmentation performance occurred. The U-net network was developed based on the works of Long, J et al. [3] using fully convolutional networks. Their implementation achieved better performance than the previous best on the ISBI 2012 challenge and won the ISBI cell tracking challenge in 2015, beating the state of the art at the time by a considerable margin.

What makes U-net particularly useful is its creation of highly detailed segmentation maps using highly limited training samples. The latter trait is of great importance in the medical imaging community, as properly labeled images are often limited. This is achieved by utilizing random elastic deformation on the training data, which enables the network to learn these variations without requiring new labeled data [2]. Another challenge is to separate touching objects of the same class, which is resolved by applying a weighted loss function that penalizes the model if it fails to separate the two objects. Finally, U-net is also much faster to train than most other segmentation models due to its context-based learning.

Since its inception in 2015, U-net has seen an explosion in usage in medical imaging. And naturally, there have been many advancements in U-net architecture by researchers implementing new methods or incorporating other imaging methods into U-net. In this thesis, we examine papers that utilize U-net in the application of medical image analysis. To avoid redundancy, we only reviewed papers from 2017 onward. Given that there are numerous sources of scientific publicization, in order to find the most relevant quality of research papers, we limited ourselves to three major publishers: IEEE, Springer, and Elsevier. From there, we searched their databases with related keywords to find the top papers in each database and collected the appropriate publications. Since new papers are being published regularly, we selected a designated endpoint of 12/31/2020. Figure 1 showcases some statistics from our survey.

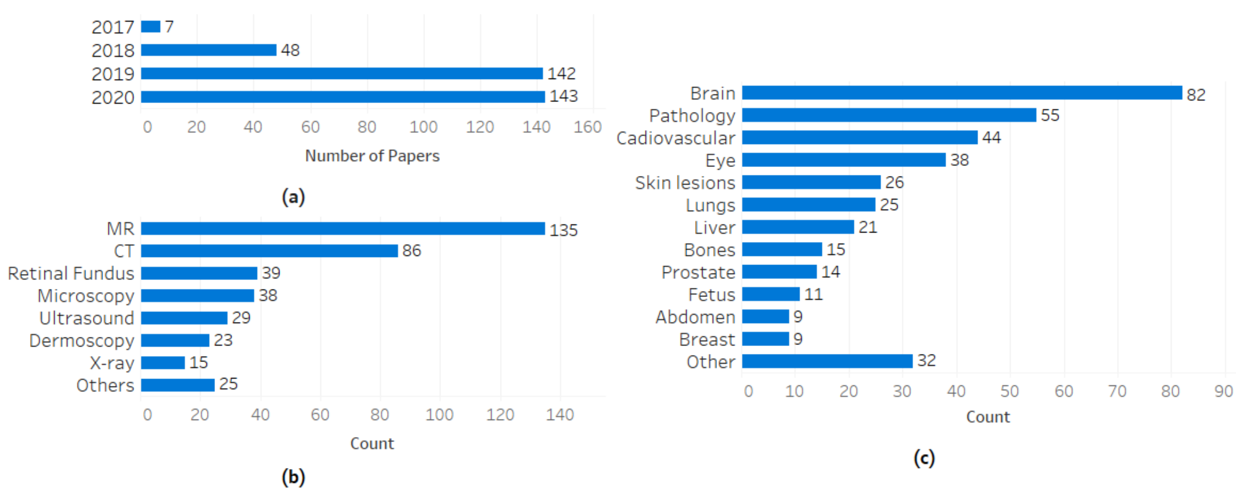

Figure 1. Distribution of (a) U-net related papers in our survey by year of publication starting with 2017, (b) image modality in U-net related papers, and (c) application area in U-net related papers. It should be noted that some papers had multiple image modalities and application areas, and each instance was counted separately.

The novel coronavirus (COVID-19) pandemic has created a staggering global medical crisis. As of June 7th 2021, a total of 172,956,039 confirmed cases and 3,726,466 confirmed deaths have been recorded globally [4]. To combat this challenge, the medical imaging community has involved itself in the research of multiple deep learning techniques, including U-net, for the diagnosis of COVID-19. The primary diagnostic images taken for COVID-19 are chest CT scans, which are ideal given that U-net has seen extensive exploration in that modality. The versatility of the U-net network has allowed rapid development and deployment of early screening diagnostic algorithms for field use as early as March 2020 [5]. Further improvements on early screening tests have been made by augmenting attention and residual methods with U-net [6], [7]. Wu et al. [8] have implemented a hybrid network with U-net for segmentation and a classifier for classification, while Yan et al. [9] developed a network with feature variation that allowed for an easier distinction of COVID-19 infection. U-net research has also been ongoing in X-ray-based screening of COVID-19 [10], [11], and Alom et al. [12] established a multi-stage model to detect COVID-19 from X-ray and CT images. A survey on deep learning techniques for COVID-19 diagnosis reveals that U-net is one of the primary models of choice for segmentation-related tasks [13]. This is no surprise, as we have already explored the various utilities of U-net based models. We expect research on U-net-based algorithms for the diagnosis of COVID-19 to continue and to be a major asset to the medical imaging community during this global crisis.

2. LITERATURE REVIEW

A version of this chapter was previously published by IEEE Access [1] [https://doi.org/10.1109/ACCESS.2021.3086020].

2.1 U-net Architectures

In this section, we explore the different variations and augmentations that have been applied to the U-net model. While there are numerous implementations of U-net, we selected the most commonly implemented architectures for this review.

2.1.1 Base U-net

As mentioned earlier, the U-net network can be divided into two parts: The first is the contracting path that uses a typical CNN architecture. Each block in the contracting path consists of two successive 3x3 convolutions followed by a ReLU activation unit and a max-pooling layer. This arrangement is repeated several times. The novelty of U-net comes in the second part, called the expansive path, in which each stage upsamples the feature map using 2x2 up-convolution. Then, the feature map from the corresponding layer in the contracting path is cropped and concatenated onto the upsampled feature map. This is followed by two successive 3x3 convolutions and ReLU activation. At the final stage, an additional 1x1 convolution is applied to reduce the feature map to the required number of channels and produce the segmented image. The cropping is necessary since pixel features in the edges have the least amount of contextual information and therefore need to be discarded. This results in a network resembling a u-shape and, more importantly, propagates contextual information along the network, which allows it to segment objects in an area using context from a larger overlapping area. Figure 2 illustrates the overall U-net architecture.

The energy function for the network is given by:

$$E = \sum w(x) \log\left(p_{k(x)}(x)\right) \tag{1}$$

where p_k is the pixel-wise SoftMax function applied over the final feature map, defined as:

$$p_k = \exp\left(a_k(x)\right) / \sum_{k'=1}^{K} \exp\left(a_k(x)'\right) \tag{2}$$

and a_k denotes the activation in channel k.

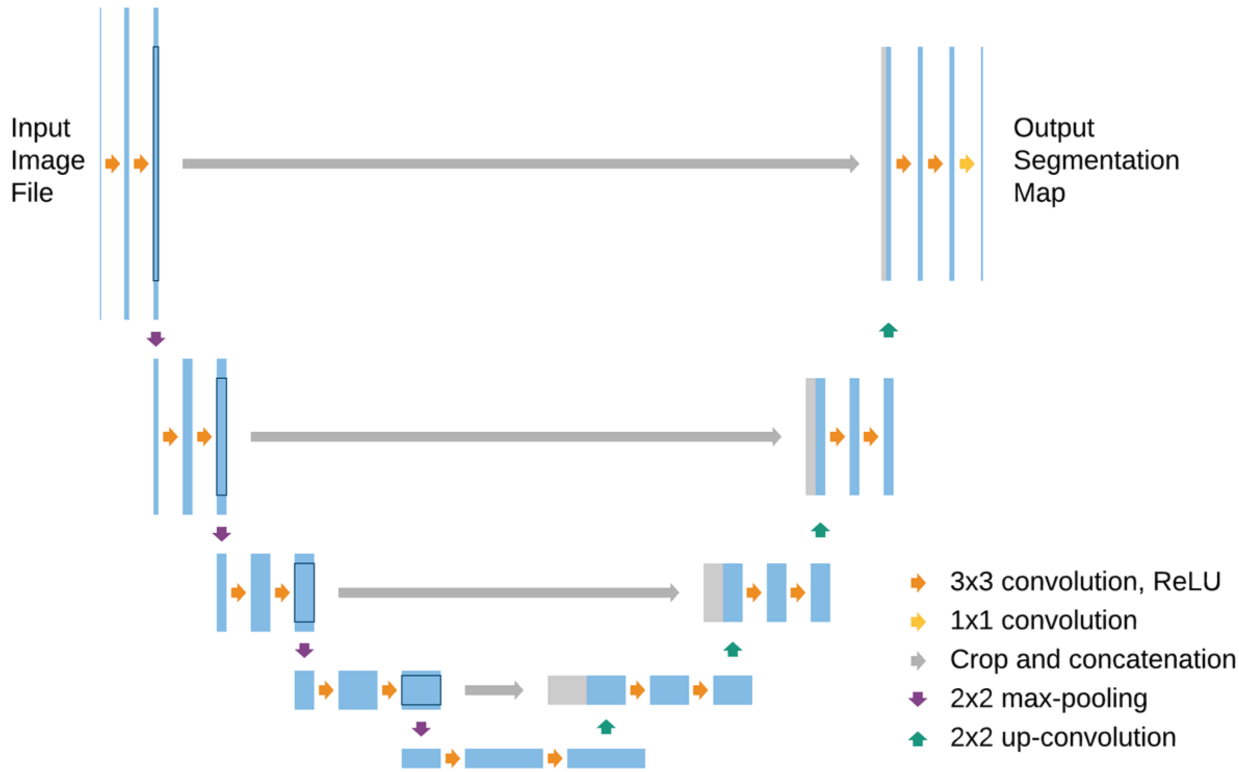

Figure 2. Basic U-net architecture. The arrows represent the different operations, the blue boxes represent the feature map at each layer, and the gray boxes represent the cropped feature maps from the contracting path.

2.1.2 **3D U-net**

3D U-net is an augmentation of the basic U-net framework that enables 3D volumetric segmentation [14]. The core structure still contains a contracting and expansive path. However, all of the 2D operations are replaced with corresponding 3D operations, namely 3D convolutions, 3D max pooling, and 3D up-convolutions, thereby resulting in a three-dimensional segmented image. This network is able to segment images using minimal annotated examples. This is due to 3D images having many repeating structures and shapes, thereby enabling a faster training process even with scarcely labeled data. 3D U-net has seen extensive use in volumetric CT and MR image segmentation applications, including diagnosis of the cardiac structures [15]–[22], bone structures [23]–[26], vertebral column [27], [28], brain tumors [29]–[31], liver tumors [32]–[34], lung nodules [35], nasopharyngeal cancer [36], multi-organ segmentation [37]–[39], head and neck organ at risk assessment [40], and white matter tracts segmentation [41]. 3D U-net has been used to great effect in many biomedical applications. Zeng et al. [23] created a network that produced multi-level segmented images that allow abstraction when making a diagnosis.

2.1.3 **Attention U-net**

An often-desirable trait in an image processing network is the ability to focus on specific objects that are of importance while ignoring unnecessary areas. The attention U-net achieves this by making use of the attention gate [42], [43]. An attention gate is a unit that trims features that are not relevant to the ongoing task. Each layer in the expansive path has an attention gate through which the corresponding features from the contracting path must pass through before the features are concatenated with the upsampled features in the expansive path. Repeated uses of the attention gate after each layer significantly improves segmentation performance without adding excessive computational complexity to the model.

The attention unit is useful in encoder-decoder models such as the U-net since it can provide localized classification information as opposed to global classification. In U-net, this allows different parts of the network to focus on segmenting different objects. Furthermore, with properly labeled training data, the network can attune to particular objects in an image. The attention gate applies a function in which the feature map is weighted according to each class, and the network can be tuned to focus on a particular class [44] and hence pay attention to particular objects in an image. While there are different types of attention gates, additive attention is more popular in image processing due to it resulting in higher accuracy [32]. Figure 3 illustrates a basic additive attention gate. The additive attention gate is described by:

$$q_{att}^{l} = \psi^{T}\left(\sigma_1\left(W_x^T x_i^l + W_g^T g_i + b_g\right)\right) + b_\psi \tag{3}$$

$$\alpha_i^l = \sigma_2(q_{att}^l(x_i^l, g_i; \Theta_{att})) \tag{4}$$

where x^l is the features from the contracting path and g is the gating signal. The term $\sigma_2\left(x_{i,c}\right)$ represents the sigmoid function:

$$\sigma_2\left(x_{i,c}\right) = \frac{1}{1 + \exp\left(-x_{i,c}\right)} \tag{5}$$

Attention U-net has been successfully applied to problems such as ocular disease diagnosis [45]–[49], melanoma [50], lung cancer [45], cervical cancer [51], abdominal structure segmentation [43], fetus development [43], and brain tissue quantification [52].

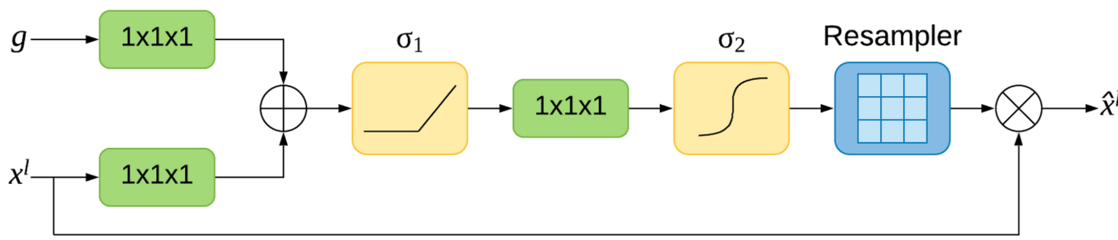

Figure 3. Additive attention gate schematic. The input signal xl and the gating signal g both pass through separate 1x1x1 convolutions. The signals are then added and undergo a series of linear transformation which are ReLU activation (σ1), a 1x1x1 convolution, sigmoid activation (σ2), and an optional grid resampler. Finally, the original input is concatenated to the output from the sigmoid unit or the resampler.

2.1.4 **Inception U-net**

Most image processing algorithms tend to use fixed-size filters for convolutions. However, tuning the model to find the correct filter size can often be cumbersome. Moreover, fixed-size filters are appropriate only for images with similar-sized salient parts. In many applications, the analysis looks through images with large variations in shapes and sizes in the salient region. One solution to this problem would be to use deeper networks that can read high-level details across a spectrum of sizes and shapes. However, such deep networks are quite computationally expensive. An alternative solution, called the inception network, uses filters of multiple sizes on the same layer in the network. [53]. The outputs from the different filters are concatenated and transferred onto the next layer. The inception network is able to analyze images with different salient regions quite effectively due to the different filter sizes. To reduce computational complexity, the inception network adds a 1x1 convolution before every 3x3 or larger filter for dimensionality reduction. Additionally, pooling layers may also be added in parallel in each inception module.

The original inception network, called GoogLeNet, attained the state of the art outcomes in the ILSVRC14 competition [53]. This was soon followed by more improvements to the network, including the application of factorization methods and the replacement of 5x5 convolution with two successive 3x3 convolutions. In the latter case, a single 5x5 convolution is 2.78 times more computationally expensive than two equivalent 3x3 convolutions [54]. Further factorization can be applied by splitting *n*x*n* filters into a 1x*n* and *n*x1 filter, respectively. Factorizing a 3x3 filter by this method makes the network 33% less expensive. Figure 4 displays two configurations of the inception module.

Inception modules of different configurations have been applied on a multitude of U-net applications, including brain tumor detection [30], [55], [56], brain tissue mapping [57], cardiac segmentation [18], [58], lung nodule detection [59], human embryo segmentation [60], and ultrasound nerve segmentation [61].

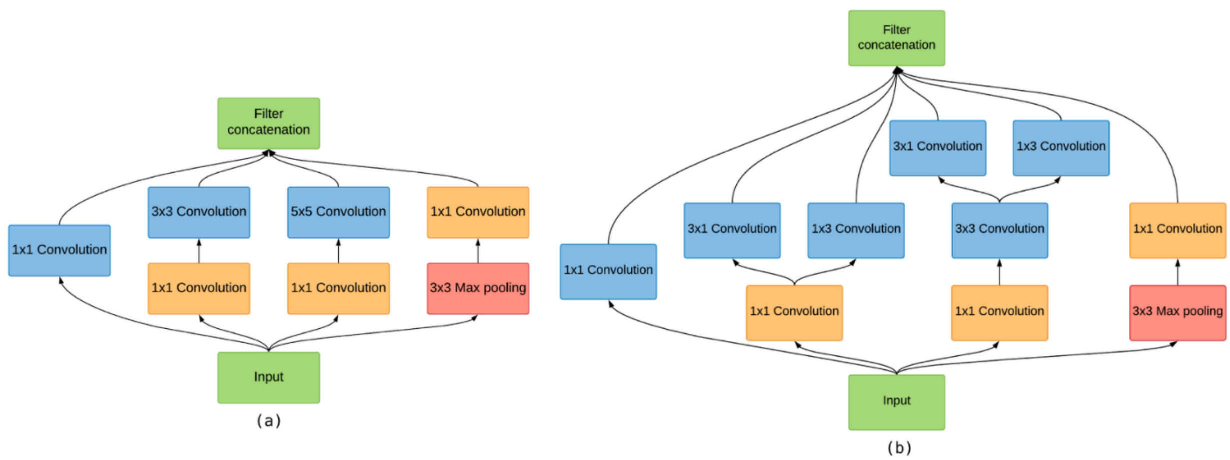

Figure 4. (a) The original inception block used in GoogLeNet. (b) Improved inception block with factorized filters. At the end of the inception block, the feature maps from each filter are concatenated together and passed onto the next layer. It should be noted that both networks in figures (a) and (b) are equivalent, though the factorized network requires less computational power.

2.1.5 **Residual U-net**

This variant of U-net is based on the ResNet [62] architecture. The motivation behind ResNet was to overcome the difficulty in training highly deep neural networks. It is known that neural networks are able to converge faster to a solution when more layers are present. However, experimental results have shown that increasing the number of layers results in saturation, and further increases can cause degradation of performance [62]. This degradation arises due to the loss of feature identities in deeper neural networks caused by diminishing gradients in the weight vector. ResNet lessens this problem by utilizing skip connections, which take the feature map from one layer and add it to another layer deeper in the network. This behavior allows the network to better preserve feature maps in deeper neural networks and provide improved performance for such deeper networks. The unit design of ResNet blocks is pictured in Fig 5.

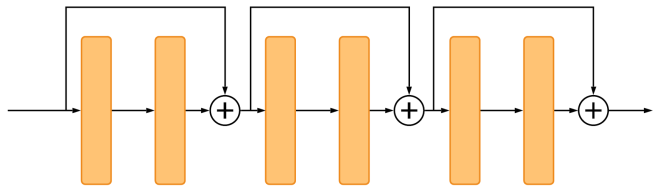

Figure 5. Three successive ResNet blocks with skip connections. The skipped signal is joined with the channel output via element-wise addition. The most common ResNet implementations are double-layer skips (as shown in this figure) or triple-layer skips.

In the residual U-net, at each block in the network, the input to the first convolutional layer is added to the output from the second convolutional layer using a skip connection. This skip connection is applied before the downsampling or upsampling in the corresponding paths in the U-net. The usage of residual skip connections helps to alleviate the vanishing gradient problem [62], thereby allowing for U-net models with deeper neural networks to be designed. Each residual unit can be denoted by:

$$y_l = h(x_l) + \mathcal{F}(x_l, \mathcal{W}_l) \tag{6}$$

$$x_{l+1} = f(y_l) \tag{7}$$

where x_l and x_{l+1} correspond to the input and output of the residual unit, $\mathcal{F}(\cdot)$ corresponds to the residual function, $f(\cdot)$ is the activation function, and $h(\cdot)$ is the identity mapping function.

We have found papers in which deep residual U-nets have been used to great effect in many biomedical imaging applications such as nuclei segmentation [63], [64], brain tissue quantification [52], brain structure mapping [65], retinal vessel segmentation [66], breast cancer [67], liver cancer [34], [68], prostate cancer [69], endoscopy [70], melanoma [70], osteosarcoma [71], bone structure analysis [72], and cardiac structure analysis [69], [73]. Deep residual U-nets are ideal for complex image analysis.

2.1.6 **Recurrent U-net**

Recurrent neural networks are a type of neural network initially designed to analyze sequential data such as text or audio data. The network is designed in such a way that a node's output changes based on the previous output from the same nodes, i.e., a feedback loop as opposed to a traditional feedforward network, as illustrated in Figure 6. This feedback loop also called a recurrent connection, creates an internal state or memory that provides the node with temporal properties that change the output at discrete time steps. When extended to the entire layer, this allows the network to process contextual information from the preceding data.

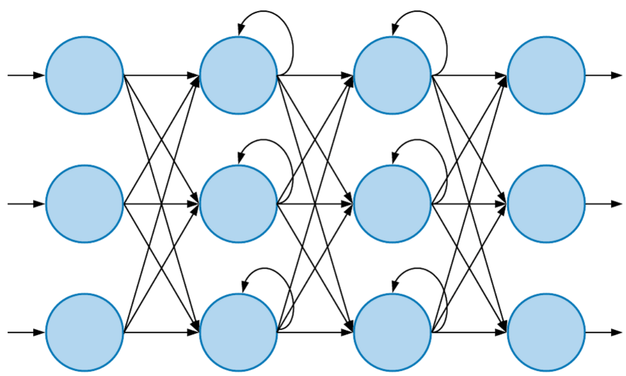

Figure 6. Recurrent neural network. In this simple network, the second and third layers are recurrent layers. Each neuron in a recurrent layer receives feedback from its output as well as new information from the previous layer at discrete time periods and correspondingly produces a new output. This component allows the network to process sequential information.

The recurrent U-net makes use of recurrent convolutional neural networks (RCNN) [74], by incorporating the recurrent feedback loops into a convolutional layer. The feedback is applied after both convolution and an activation function and feeds the feature map produced by a filter back into the associated layer. The feedback property allows the units to update their feature maps based on context from adjoining units, providing better accuracy and performance. The output y of the recurrent convolutional neural network can be expressed as:

$$y_{ijk}^{l}(t) = \left(w_k^f\right)^T x_l^{f(i,j)}(t) + (w_k^r)^T x_l^{r(i,j)}(t-1) + b_k \tag{8}$$

where $x_l^f(t)$ is the feedforward input and $x_l^r(t-1)$ is the recurrent input for the l^{th} layer, w_k^f is the feedforward weight, w_k^r is the recurrent weight, and b_k is the bias of the k^{th} feature map. Recurrent U-nets have been used in [75], [76]. Alom et al. [63], [77] devised a U-net model containing both recurrent connections and residual connections. The resulting network outperformed solely residual and recurrent U-net models as well as prior state of the art methods using a similar number of parameters.

2.1.7 **Dense U-net**

Dense U-nets employ DenseNet [78] blocks in place of regular layers. While the ResNet model allows for deeper neural networks, it does not eliminate the problem of vanishing gradients. The ResNet architecture also eventually degrades in performance with increasing layers. To remedy this, DenseNet is a deep learning architecture built on top of ResNet with two key changes. Firstly, every layer in a block receives the feature or identity map from all of its preceding layers [78]. The second major change is that the identity maps are combined via channel-wise concatenation into tensors [78], as opposed to ResNet in which the identity maps are summed via element-wise addition. Therefore, the identity mapping of each layer is dependent not only on the previous layer but on all of the layers before it in the block. This configuration is visualized in Figure 7. This allows DenseNet to preserve all identity maps from prior layers and significantly promote gradient propagation. The implication is that each layer can have fewer channels, as information is more easily preserved between layers, thereby resulting in higher accuracy with fewer computations, which in turn allows deep learning models with a greater number of layers. The output for each layer in a dense block is described as:

$$x_l = H_l([x_0, x_1, x_2, \dots, x_{l-1}]) \tag{9}$$

where $H_l(\cdot)$ represents the dense mapping function, which typically includes batch normalization, ReLU activation, and a convolutional layer while $[\cdot]$ denotes channel-wise concatenation.

When implementing a U-net, each traditional U-net block is replaced with a dense block of two or more convolutional layers. The adoption of dense blocks allows for deeper U-net models, which can segment objects in an image with greater distinction. This attribute of dense U-nets is highly desired in medical image analysis due to objects in such images being highly close together, often to the point of overlapping. Applications of dense U-net have been found in analysis of brain tumors [31], [56], retinal blood vessel segmentation [56], cerebral blood vessel segmentation [79], [80], melanoma [81], lung cancer [81], liver cancer [82], and multi-organ segmentation [83].

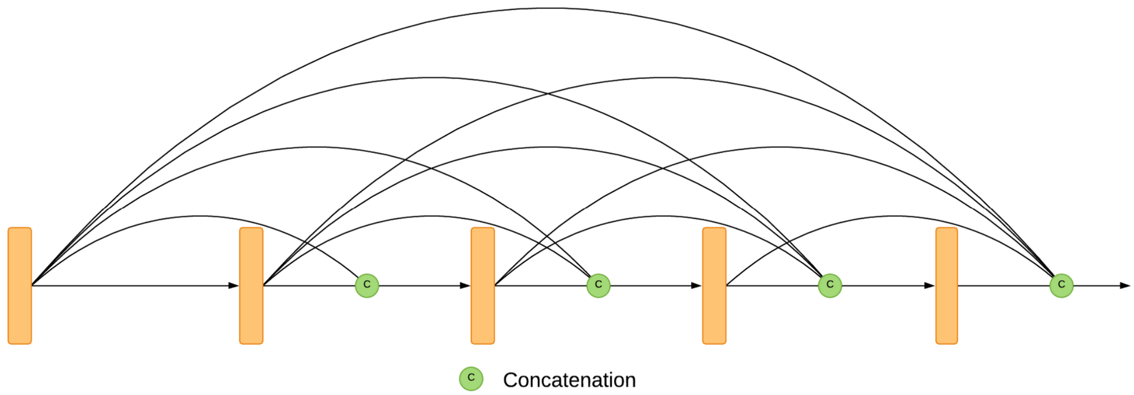

Figure 7. A five-layer dense block. The concatenation unit receives the feature map from all previous layers and passes it onto the next layer. This ensures that any given layer has contextual information from any of the previous layers in the block.

2.1.8 **U-net++**

U-net++ is another powerful form of the U-net architecture inspired from DenseNet [78]. It uses a dense network of skip connections as an intermediary grid between the contracting and expansive paths [84]. This aids the network by propagating more semantic information between the two paths, thereby enabling it to segment images more accurately.

In traditional U-net, the feature maps of the contracting path are directly concatenated onto the corresponding layers in the expansive path. U-net++, however, has a number of skip connection nodes between each corresponding layer, as represented in Figure 8. Each skip connection unit receives all of the feature maps from all previous units at the same level, as well as an upsampled feature map from its immediate lower unit. Therefore, each level is equivalent to a dense block. This arrangement minimizes the loss of semantic information between the two paths. The operation of the skip connection unit in which x represents the feature map and i and j correspond to the index down the contracting path and across the skip connections, respectively, is defined as:

$$x^{i,j} = \begin{cases} \mathcal{H}\left(x^{i-1,j}\right), & j = 0 \\ \mathcal{H}\left(\left[\left[x^{i,k}\right]_{k=0}^{j-1}, \mathcal{U}\left(x^{i+1,j-1}\right)\right]\right), & j > 0 \end{cases} \tag{10}$$

Here, $\mathcal{H}(\cdot)$ denotes a convolution and the activation operation, $\mathcal{U}(\cdot)$, represents the upsampling operation, and [] signifies a concatenation. The number of intermediary skip connection units depends on the layer number and decreases linearly when traversing the contracting path. Applications in U-net++ include segmentation of cell nuclei [84], cancer tissue [84], cardiac structures and vessels [85], [86], and pelvic organs [87].

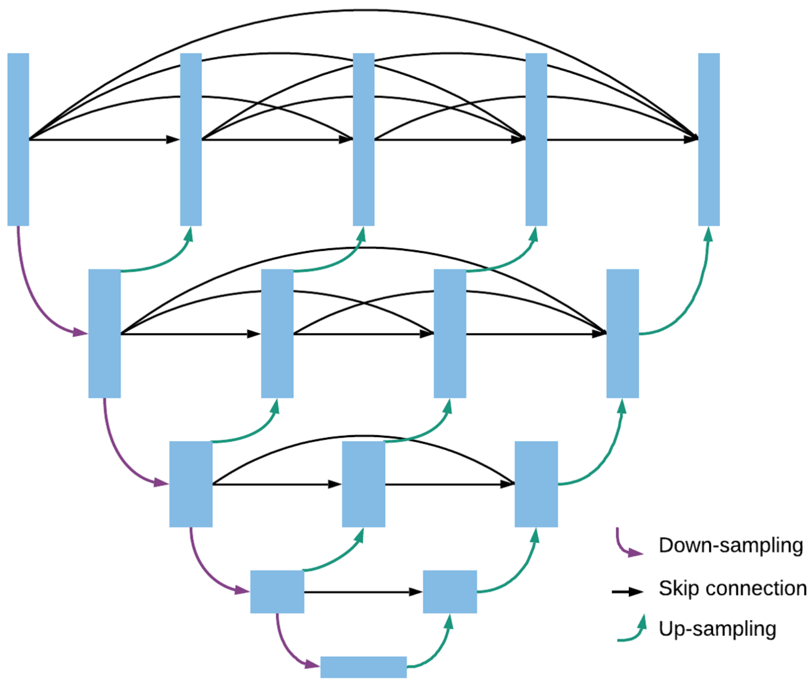

Figure 8. U-net++ schematic representation. Each square denotes a convolutional block. Unlike the base U-net, which has a single direct concatenation from the contracting path to the expansive path, U-net++ has a series of intermediary convolutional blocks between the two paths. Each intermediary and expansive block receives the concatenated feature maps from all of the previous blocks at the same level as well as the upsampled feature map from the block immediately below it.

2.1.9 **Adversarial U-net**

An adversarial model is a setup in which two networks compete against each other in order to improve their performance. Generative adversarial networks (GAN) are a novel type of adversarial process used to generate new data [88]. The framework consists of two networks: a discriminator and a generator. The discriminator network, *D*, is a classifier that is trained to identify whether a given input image is from the data set or is produced by the generator *G*. *D* undergoes standard CNN supervised training, and for each image input, it outputs the probability of the image being produced by *G* with the goal of minimizing its error rate of classifying 'fakes' as real data set images. The generator *G* produces images that are periodically fed to the discriminator. To help the generator produce convincing images, the generator's gradient function is a function of the discriminator's gradient function during the step in which the discriminator is fed a fake image. This allows the generator to adjust its weight in response to the output of the discriminator. Furthermore, to create variations in the images produced by the generator, random noise is passed to it. The goal of the generator is to deceive the discriminator, i.e., maximize the error rate of the discriminator. This minimax relationship results in an adversarial network in which the two networks compete with each other, defined as:

$$\min_G \max_D V(D,G) = \mathbb{E}_{x\sim p_{data}(x)} \log D(x) + \mathbb{E}_{z\sim p_z(z)} \log\left(1 - D\big(G(z)\big)\right) \tag{11}$$

where given enough time, the adversarial network should reach an optimal state in which the discriminator always outputs a probability of ½ regardless of whether the image is from the data set or the generator [88], meaning that it can no longer distinguish the real images from the synthetic images produced by the generator. The resulting generator can then be used to artificially create images of a particular subject. Figure 9 presents the basic relational diagram of a GAN.

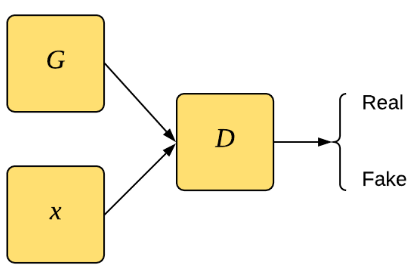

Figure 9. GAN block diagram. The goal of network *D* is to classify all inputs from *x* and network *G* as real and fake respectively. The goal of *G* is to have its output evaluated as real.

This framework can be further extended to restrict the GAN into producing a limited band of synthetic images by controlling its labels and input images. This alteration is known as a conditional GAN [89]. Adversarial U-nets are a type of conditional GANs. The generator network is constructed based on the U-net architecture while the discriminator remains the same. The U-net design allows the generator to take an image as an input instead of random noise. The key difference in adversarial U-nets is that the goal of the generator is not to produce new images but rather transformed images. This output of *G* is evaluated against *D*, which is trained on manually transformed images. Figure 10 provides an example of this design. Ideally, after proper training, the generator will be able to achieve the same transformation ability as the manual human transformation. The resulting generator can then be used to apply its transformation function on new images, which would be considerably faster than a physician manually converting the image. Adversarial U-nets have seen a wide spectrum of applications, including quantitative susceptibility mapping of the brain [90], detection of brain tumors [91], [92] and breast cancer [93], segmentation of retinal vessels [49], segmentation of cardiac structures [94], and image registration of brain structures [95].

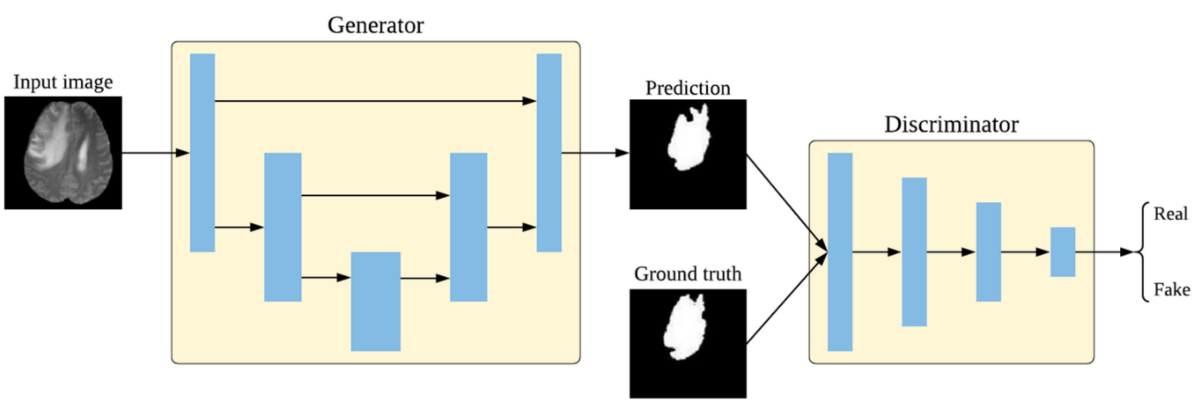

Figure 10. Simplified schematic of U-net based GAN. The generator synthesizes predictions for the tumor area from the input images. The predictions are fed into the discriminator, which in turn judges the accuracy of the prediction by evaluating its similarity to the ground truth. If the prediction is similar to the ground truth, then the discriminator will be unable to distinguish between them and classify the prediction as real. Given enough training, the GAN will be able to segment images to the same accuracy and precision as manual annotations [81].

2.1.10 **Ensemble U-net**

In addition to the aforementioned architectures, many other network configurations have also been tested that make use of an ensemble of U-nets together. One such method is cascading two or more U-nets. In this arrangement, the first U-net performs a high-level segmentation, with each successive U-net performing segmentation on smaller objects. Feng et al. [96] designed a two-stage U-net model in which the first U-net segments the liver from other organs and the second U-net segments tumors within the liver. Liu et al. [68] designed a two-stage U-net for liver segmentation with an intermediate processing module between the two U-nets. Xu et al. [19] and Li et al. [55] have both designed two-stage cascaded U-nets in which the first network is a 2D U-net and the second network is a 3D U-net. Other two-stage U-net models are implemented in [16], [17], [40], [64], [82], [97]–[100]. While two-stage networks are the most common type of cascaded U-nets, we have found two instances of cascaded U-nets with variable numbers of stages [101], [102]. In all of these papers, the cascaded U-net performed better than a single U-net.

Yet another arrangement of the overall architecture can be found in the form of a parallel arrangement of part or the entirety of a U-net network. Abd-Ellah et al. [103] arranged two parallel U-nets and aggregated the results for improved segmentation accuracy. Soltanpour et al. [104] implemented four parallel U-nets with each segmenting a different CT map and then merging the results. A halfway point can be achieved by parallel encoders, which allow for better extraction of features [105]–[107]. Murugesan et al. [108] implemented a network with parallel decoders that provide different levels of segmentation.

2.5D U-net is a special architecture where three 2D U-net networks are run parallelly on different 2D projections of a 3D image to produce a 3D segmentation map. The 2D U-nets perform slice-by-slice segmentation on the 3D volume along three different axes, and the final 3D segmentation is computed by fusing the results [109]–[112]. The advantage of the 2.5D parallel arrangement is reduced computational load for segmentation when juxtaposed with an equivalent 3D network.

2.1.11 **Comparison with Other Architectures**

While there have been numerous deep learning models developed for segmentation, in this section, we briefly describe some of the popular alternatives to U-net, namely FCN, Segnet, FPN, and DeepLab. The first deep learning models for semantic segmentation were fully convolutional networks (FCN) [3]. FCNs use regular downsampling paths to extract contextual information and a single upsampling layer to produce a fully segmented image. FCNs also employ optional skip connections; however, due to the design of FCNs, the skipped gradients are often of different dimensions and require additional processing to be upscaled. One of the significant disadvantages of FCNs is their inability to learn global context information [113]. FCNs ultimately fall behind other state-of-the-art segmentation models in terms of performance [113]. Following U-net came Segnet, another encoder-decoder model [114]. However, Segnet does not use skip connections to send low-level contextual information to deeper layers. The main advantage Segnet enjoys over other segmentation models is its lower number of training parameters.

Feature pyramid networks (FPN) also have an encoder-decoder structure that was initially designed for object detection [115]. Similar to U-net, here, gradient information is concatenated to the decoder via skip connections from the encoder. However, unlike U-net, the decoder also transmits gradient information from each layer to another series of convolution layers. FPNs are designed to detect objects from each layer in the decoder and are particularly useful in producing multi-class segmentation maps [116]. DeepLab is yet another popular segmentation model that utilizes atrous spatial pyramid pooling [117]. Spatial pyramid pooling enables DeepLab models to take input of different sizes. Atrous or dilated convolution allows the layer to extract contextual information from a larger area without increasing the filter size. Combining these two techniques enables DeepLab models to be highly robust without a significant increase in computational complexity.

2.2 Image Modalities

Segmentation is the primary task for U-net models. The goal of segmentation tasks is to outline and separate different objects in an image, i.e., to classify different objects rather than classifying the whole image. This is of particular importance in the medical imaging community, as the diagnosis of medical conditions requires careful analysis of local regions in an image. For instance, the diagnosis of brain tumors would require separating the tumors from the rest of the brain structures. We have found extensive use of the U-net architecture for a wide assortment of medical imaging analysis. Figure 11 illustrates some applications of U-net in various areas. In the next section, we discuss the major image modalities on which U-net has been applied.

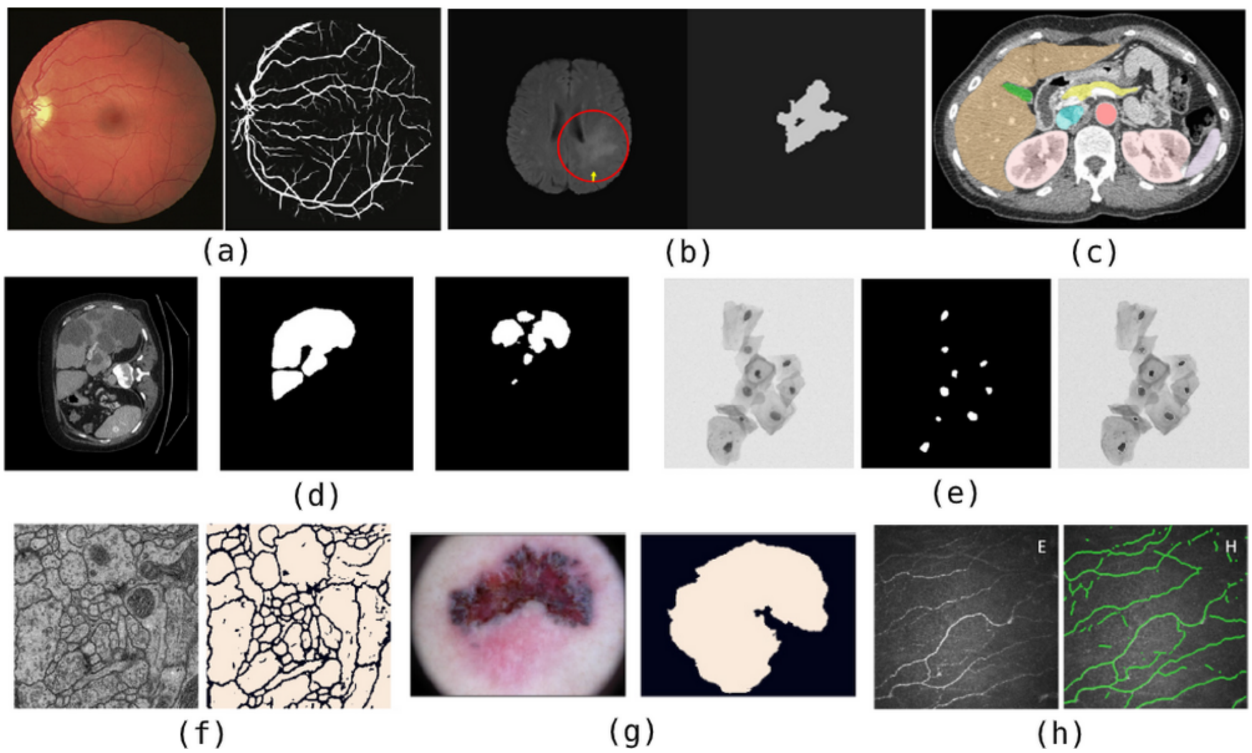

Figure 11. Examples of U-net applications. Images have been collected from papers in this survey, including: (a) Retinal vessel segmentation [118]; (b) Brain tumor detection and segmentation [119]; (c) Multi-organ abdominal segmentation (liver; spleen; left and right kidneys; pancreas; gallbladder; aorta; and inferior vena cava) on CT scans [38]; (d) Liver tumor segmentation, left to right: original CT image, liver segmentation image, and lesion segmentation image [120]; (e) Nuclei prediction, from left to right: original cell images, prediction of nuclei, labeling nuclei in the original images [51]; (f) Cell segmentation [70]; (g) Skin lesion segmentation [70]; and (h) Corneal nerve segmentation [121].

2.2.1 **Magnetic Resonance Imaging (MRI)**

MRI is a very popular radiology imaging technique used to take pictures of soft tissue inside the body. In our review, we have found MRI to be the most popular image modality for segmentation using U-net. MRI is a useful diagnostic tool, particularly for the analysis of the brain. U-net has been used extensively in this regard for the segmentation of brain structures as many different U-net models have been applied on MR images for brain tumor diagnosis [29], [30], [55], [56], [70], [92], [98], [103], [122]–[136]. U-net has also been applied on brain tissue for investigation of neurological conditions [65], [112], [119], [137]–[140], analysis of white matter tissue [141]–[143], [100], fetal brain development [144]–[147], and stroke lesions [80], [148]–[152]. U-net has also been implemented on cardiovascular MR images [15]–[17], [19]–[22], [58], [69], [73], [85], [94], [97], [101], [153]–[162] to segment structures of the heart. Cancer is a leading cause of death worldwide, and MR is one of the strongest methods for the proper prognosis of different types of cancers. In addition to brain cancer, we have found applications on prostate cancer [58], [64], [152]–[156], liver cancer [32], [168], [169], nasopharyngeal cancer [36], [109], [170], and breast cancer [110], [171]. Other implementations include segmentation of the femur [23]–[25], spinal cord [172], [173], blood vessels [111], vertebral column [28], human placenta [174], and the uterus [175]. Table 1 indexes all of the papers that used MRI as an image mode, as well as the application area and the methods used in the corresponding U-net.

2.2.2 **Computed Tomography (CT)**

CT scans are another major non-invasive medical analysis tool for analyzing internal organs and tissue. As with MRI, cancer diagnosis is a major that involves the application of CT imaging; including liver cancer [33], [34], [68], [82], [84], [96], [105], [120], [176]–[178], lung cancer [35], [45], [56], [59], [81], [84], [179]–[183], bone cancer [71], and cervical cancer [184]. CT scans are also used for multiorgan abdominal segmentation [37], [38], [43], [83], [167], [185] as well as the segmentation of hard tissue such as bones [25]–[27], [71], [87], [186]. Along with MR imaging, CT is one of the few imaging techniques that can produce 3D images. The versatility of CT imaging makes it a favored modality in medical diagnosis. Table 2 indexes all of the papers that used CT scans as an image mode in our review, as well as the application area and the methods used.

Table 1. Applications of U-net based models for MR image analysis.

Reference	Model/Methods used
Brain tumor	
[122], [123], [126]–[128], [130]–[134], [187]–[193]	Base U-net
[29], [125], [136]	3D U-net
[92]	Adversarial net; GAN
[197]	Attention gate
[70], [124], [198], [199]	Residual block
[129]	Dense block
[201]	U-net++
[98]	Cascaded U-net
[203]	Dense block; Residual block
[205]	3D U-net; Attention gate
[103]	Residual block; Parallel U-net
[55]	Inception block; Up skip connections
[56]	Dense block; Inception block
[135]	3D U-net; Residual block
[30]	3D U-net; Inception block; Residual block
Brain tissue	
[119], [137]–[140], [208]	Base U-net
[39], [209]–[211]	3D U-net
[212]	2.5D U-net
[65]	Residual block
[112]	Parallel U-net
[52]	Attention gate; Residual block
White matter tracts	
[142], [143]	U-net with modified skip connections
[141]	Base U-net
[100]	Cascaded U-net
Fetal brain	
[144]–[146]	Base U-net
[147]	Base U-net; 3D U-net
Stroke lesion/thrombus	
[149]–[152]	Base U-net
[148]	3D U-net
[80]	Dense block; Inception block
Spinal cord	
[172], [173]	Base U-net
Femur	
[23]–[25]	3D U-net
Placenta	
[174]	Base U-net

Reference	Model/Methods used
Cardiovascular structures	
[154], [156]–[158], [160], [162], [194], [195]	Base U-net
[69], [73], [155], [159], [161], [196]	Residual block
[15], [20], [21], [39]	3D U-net
[97], [101]	Cascaded U-net
[200]	Attention gate
[16], [19]	Cascaded 3D U-net
[22], [202]	Base U-net; 3D U-net
[94], [204]	Adversarial net; GAN
[206]	Attention gate; Dense block
[118]	3D U-net; Attention gate
[153]	Dense block
[85]	U-net++
[58]	Inception block; Residual block
[17]	Cascaded 3D U-net; Residual block
Prostate cancer	
[163], [165]–[167], [207]	Base U-net
[39]	3D U-net
[202]	Base U-net; 3D U-net
[213]	Attention gate
[204]	Adversarial net; GAN
[75]	Recurrent net
[69]	Residual block
Liver cancer	
[168], [169]	Base U-net
[32]	3D U-net
[214]	Attention gate; U-net++
Nasopharyngeal cancer	
[36]	3D U-net; Residual block
[109]	Parallel U-net
[170]	Modified convolution block
Breast cancer	
[171]	Base U-net
[110]	Parallel U-net
Blood vessels	
[111]	Base U-net
Uterus	
[175]	Base U-net
Vertebral column	
[28]	3D U-net

Table 2. Applications of U-net based models for CT image analysis.

Reference	Model/Methods used	Reference	Model/Methods used
Liver cancer		**Lung cancer**	
[120], [176], [177], [215]	Base U-net	[179]–[181], [216]	Base U-net
[33], [39]	3D U-net	[217], [218]	3D U-net
[34]	3D U-net; Residual block	[182], [183], [219]–[221]	Residual block
[84]	U-net++	[45]	Attention gate
[96], [222]	Cascaded U-net	[35], [223]	3D U-net; Residual block
[68]	Cascaded U-net; Residual block	[59]	Dense block; Inception block
		[224]	Dense block; Residual block
[82]	Cascaded U-net; Dense block	[84]	U-net++
[214]	Attention gate; U-net++		
[225]	Dense block; Inception block	**Pulmonary tissue**	
[105]	Modified U-net with dual parallel encoders	[226], [227]	Base U-net
		[228], [229]	Residual block
Cardiovascular structures			
[15]	3D U-net	**Abdominal organs**	
[230]	Attention gate	[167], [185], [232]	Base U-net
[231]	Adversarial net; GAN	[37], [38]	3D U-net
[97]	Cascaded U-net	[43]	Attention gate
[16]	Cascaded 3D U-net	[83]	Dense block
[135]	3D U-net; Residual block		
[18]	3D U-net; Inception block	**Pancreas**	
[86]	U-net++	[172], [232]–[234]	Base U-net
		[39]	3D U-net
Bones			
[186]	Base U-net	**Stroke lesions**	
[25]	3D U-net	[104], [235]	Base U-net
[26]	3D U-net; Residual block	[148]	Base U-net; 3D U-net
[71]	Residual block	[80]	Dense block; Inception block
[87]	U-net++		
		Gallstones	
Head and neck		[237]	U-net++
[236]	3D U-net	[99]	Cascaded U-net
[40]	Cascaded 3D U-net		
		Prostate cancer	
Kidney tumor		[240]	Base U-net
[238], [239]	3D U-net	[241]	Attention gate
Liver and spleen		**Blood vessels**	
[178]	Dense block	[242]	Attention gate
		[243]	Residual block
Brain			
[244]	Base U-net	**Cervical cancer**	
[245]	Attention gate	[184]	Base U-net
[57]	Inception block; Residual block		
[106]	Modified U-net with dual parallel encoders	**Fetus**	
		[43]	Attention gate
Stomach cancer			
[246]	Residual block	**Melanoma**	
		[81]	Dense block
Vertebral column			
[247]	Base U-net	**Muscle tissue**	
[27]	3D U-net	[248]	Base U-net

2.2.3 **Retinal Fundus Imaging**

Color fundus imaging is an ophthalmology technique used for the detection and diagnosis of ocular diseases such as glaucoma, diabetic retinopathy, and age-related macular degeneration (AMD). Proper prognosis depends on the precise segmentation of key structures such as retinal blood vessel segmentation [66], [249]. Accurate screening is of chief importance since such diseases often need to be diagnosed early for treatment. Though ophthalmic imaging has a far narrower scope than MR and CT, the retinal fundus is one of the most analyzed structures in our survey, after the brain and cardiovascular system. Given that it is the primary method of imaging the retina, we expect more research on fundus image analysis to continue as well as research on more complex retinal fundus images. Table 3 collects all of the use cases of U-net models applied in the analysis of the retinal fundus.

Table 3. Applications of U-net based models for fundus image analysis

Reference	Model/Methods used
[249]–[262]	Base U-net
[45]–[47], [242], [263], [264]	Attention gate
[66], [183], [265]–[268]	Residual block
[81]	Dense block
[269]	U-net++
[49]	Adversarial net; GAN; Attention gate
[102]	Cascaded U-net
[270]	Cascaded U-net; Residual block
[271]	Attention gate; Residual block
[56]	Dense block; Inception block
[224], [272]	Dense block; Residual block
[273]	Inception block; Residual block
[274]	Attention gate; Dense block; Residual block
[108]	U-net with parallel decoders
[275]	Recurrent residual block; Up skip connections

2.2.4 **Microscopy**

Microscopy refers to the examination of microscopic objects that cannot be observed with the naked eye. It should be noted that in our survey, we refer to microscopy to mean only optical microscopy. This modality is used extensively in pathology. One of the major challenges in microscopy imaging is identifying overlapping cells as well as identifying the boundary between cells. These are unique challenges to microscopy, as smaller structures such as cells and tissues often do not have well-defined landmarks and similarities, thereby making the image processing much more difficult. However, U-net has overcome such challenges [2] and continues to be a strong implementation for this modality. Applications of U-net based models applied on microscopy imaging are collected and indexed in Table 4.

Table 4. Applications of U-net based models for ultrasound image analysis.

Reference	Model/Methods used	Reference	Model/Methods used
Cell nuclei		**Cell contour**	
[276], [277]	Base U-net	[191], [278]–[281]	Base U-net
[70], [282], [283]	Residual U-net	[51]	Attention gate
[63]	Recurrent net; Residual block	[284]	Cascaded U-net
[64]	Cascaded U-net; Residual block	[285]	Attention gate; Recurrent residual block
[286]	Cascaded U-net; Dense block		
[84]	U-net++	[287]	Dense block; Inception block; Residual block
Human embryo		**Corneal nerve**	
[288]	Base U-net	[121]	Base U-net
[60]	Inception block	[47]	Attention gate
Chromosomes		**Blood vessels**	
[289]–[291]	Base U-net	[292]	Base U-net
Pathogen detection		**Cancer cell detection**	
[293], [294]	Base U-net	[295]–[297]	Base U-net
		[298]	Residual U-net
Sclerosis			
[299]	Base U-net		

2.2.5 **Dermoscopy**

Dermoscopy is a detailed examination of the skin. It is almost exclusively used to examine skin diseases such as skin lesions. The primary medical condition diagnosed using Dermoscopy images in our survey is melanoma or skin cancer, though we have also found a single paper on psoriasis diagnosis [300]. The performance of Dermoscopy image analysis methods is of keen interest in the medical imaging community since it is often used for early detection of melanoma and is less costly than other noninvasive diagnostic tools. Table 5 summarizes the papers and models focusing on Dermoscopy images.

Table 5. Applications of U-net based models for Dermoscopy image analysis.

Reference	Model/Methods used
Melanoma	
[259], [301]–[311]	Base U-net
[50]	Attention gate
[70], [221]	Residual block
[81]	Dense block
[271], [312]	Attention gate; Residual block
[274]	Attention gate; Recurrent residual block
[203]	Dense block; Residual block
[284]	Cascaded U-net
[275]	Up skip connections
Psoriasis	
[300]	Base U-net

2.2.6 Ultrasound

Medical ultrasound is yet another noninvasive imaging technique for the analysis of internal structures. Ultrasound is mostly used for early and real-time diagnosis. Additionally, unlike many other image modalities, ultrasound devices are more maneuverable and can capture images from multiple angles. Ultrasound is also safe since it does not use radiation; hence it is the primary imaging modality for pregnancy-related diagnosis [313]–[315]. Medical ultrasound use cases also include analysis of soft tissue such as nerve bundles [50], [61], [167], [316], [317]. Its real-time image capture abilities make it a vital tool for tracking objects [107]. Applications of U-net in ultrasound imaging are outlined in Table 6.

2.2.7 X-ray

X-ray is a radiograph method used mainly for the imaging of hard tissue. It is the most widely used technique for the analysis of bones. U-net models have been applied to X-rays of bones for diagnosis of rheumatoid arthritis and osteoporosis [72], [318], as well as other bone-related diseases. Chest x-rays are also fairly prevalent and are used for the detection of a myriad of pulmonary diseases such as tuberculosis [271]. Aside from that, we have found applications of U-net in the detection of coronary stenosis [319], breast tumors [93], and surgical catheters [320]. Table 7 encapsulates all of the papers that used X-ray as an image mode for analysis.

Table 6. Applications of U-net based models for ultrasound image analysis.

Reference	Model/Methods used	Reference	Model/Methods used
Nerve segmentation		**Breast lesion**	
[167], [316]	Base U-net	[321]	Base U-net
[61]	Inception block	[50], [322]	Attention gate
[317]	Residual block	[323]	Cascaded U-net
[324]	Modified parallel U-net		
		Cardiovascular structures	
Arterial wall		[325]	Base U-net
[326]–[328]	Base U-net	[192]	Attention gate
[329]	Cascaded U-net	[330]	Residual block
Fetal head		**Gastrointestinal tumor**	
[313], [331]	Base U-net	[332]	Base U-net
[333]	Cascaded U-net		
		Preterm birth prediction	
Knee cartilage		[314]	Base U-net
[107]	U-net with dual parallel encoders		
		Transcranial detection	
Thyroid		[315]	Base U-net
[334]	Residual block		
		Kidney	
Cervical lymph node		[335]	Base U-net
[336]	Dense block; Residual block; Inception block		
		Ovary detection	
		[337]	Base U-net

Table 7. Applications of U-net based models for X-ray image analysis.

Reference	Model/Methods used	Reference	Model/Methods used
Phalange bones		**Pelvic bones**	
[318], [338]	Base U-net	[339]	Base U-net
[72]	Residual block		
		Calcaneus bones	
Chest organs		[340]	Base U-net
[341]–[343]	Base U-net		
[45], [192]	Attention gate	**Blood vessels**	
[271]	Attention gate; Residual block	[319], [344]	Base U-net
Surgical catheter detection		**Breast tumor**	
[320]	Residual block	[93]	Adversarial net; GAN

2.2.8 Other Modalities

In addition to commonly used image modalities, we have also found U-net applications on more inconspicuous modalities. Endoscopy is an invasive imaging procedure in which the imaging device is inserted into an organ or cavity to take pictures. U-net has been applied to endoscopy images for segmentation of polyps in the gastrointestinal tract [108], [284], [312], [345], colon objects [70], detection of laryngeal leukoplakia [76], and detection of surgical instruments [346].

On electron microscopy images, applications include the detection of neuronal structures [172], [347], cell contour [172], [183], [242], and viruses [348]. Optical coherence tomography (OCT) is an imaging method for taking cross-sectional images of the retina. OCT is used for the diagnosis of different ocular diseases, such as age-related macular degeneration (AMD), retinal vein occlusion, and diabetic macular edema [349]. U-net has been used on OCT for segmentation of retinal layers [350]–[352], blood vessels [353], fluid regions [354], [355], and Drusen [356]. Other uncommon applications are segmentation of blood vessels in digital subtraction angiography (DSA) [79], [357], [358], white matter tract segmentation in diffusion tensor imaging (DTI) [41], iris segmentation in iris imaging [48], tumor detection in mammograms [67], and capillary segmentation in nailfold capillaroscopy [359]. Table 8 collects the applications of U-net based models on some uncommon image modalities.

Table 8. Applications of U-net based models for various image modalities.

Reference	Model/Methods used	Image Modality
[119], [345]	Base U-net	Endoscopy
[70]	Residual block	Endoscopy
[284]	Cascaded U-net	Endoscopy
[312]	Attention gate; Residual block	Endoscopy
[76]	Cascaded U-net; Recurrent residual net	Endoscopy
[108]	Modified U-net with parallel decoders	Endoscopy
[172], [347], [348]	Base U-net	Electron microscopy
[242]	Attention gate	Electron microscopy
[183]	Residual block	Electron microscopy
[349], [352]–[354], [356]	Base U-net	OCT
[350], [351]	Residual block	OCT
[355]	Adversarial net	OCT
[357], [358]	Base U-net	DSA
[79]	Dense block	DSA
[41]	3D U-net	DTI
[48]	Attention gate	Iris imaging
[67]	Residual block	Mammogram
[359]	Residual block	Nailfold capillaroscopy

2.3 Other Canonical Tasks By U-Net

Even though U-net is an algorithm developed for segmentation, it has seen a modest amount of augmentation for other types of tasks. Image analysis is often hampered by the presence of noise or loss of detail during imaging. Consequently, we have found three papers that implemented U-net to remove artifacts from images by reconstructing the images [90], [360]–[363], as well as a paper that used U-net for de-aliasing [91]. Image registration is also an area in which U-net models have seen experimentation [95], [364]–[367]. Other reconstruction tasks include the correction of infant cortical surface [368] and EPID dosimetry correction of the cerebrospinal region [369]. Other outlier usages include synthesis of medical images [370], image super-resolution [31], and data augmentation for enabling easier annotation of medical images [371]. Applications of U-net based models applied on canonical tasks other than segmentation tasks are summarized in Table 9.

Table 9. Applications of U-net based models on other canonical tasks.

Reference	Image modality	Canonical task	Model/Methods	Application area
[360]	CT	Denoising	Modified U-net	Cervix
[361]	Ultrasound	Denoising	Base U-net	Brain tissue
[90]	MR	Denoising	3D adversarial net	Brain tumor
[362]	MR	Denoising	Cascaded U-net	Brain tissue
[363]	Photoacoustic tomography	Denoising	Base U-net	Blood vessels
[91]	MR	De-aliasing	Adversarial net	Brain tumor
[364]–[366]	MR	Image registration	Base U-net	Brain tissue
[367]	MR	Image registration	3D U-net	Liver tissue
[95]	MR	Image registration	Adversarial net	Brain tissue
[368]	MR	Image correction	3D U-net	Brain surface
[369]	EPID dosimetry	Image correction	Base U-net	Brain and spinal cord
[370]	CT; MR	Image synthesis	Base U-net	Brain tissue
[371]	MR	Data augmentation	Base U-net	Brain tissue
[31]	MR	Superresolution	3D U-net; Dense block	Brain tumor

2.4 **Limitations**

In this survey, we present the most popular U-net architectures as well as their typical applications. However, it should be highlighted that this survey does not cover all possible U-net variations due to the large body of ongoing research in medical image segmentation. Many other network designs incorporate novel ideas into U-net, such as Bayesian U-net [372] and Capsule U-net [218]. Furthermore, many U-net implementations have hitherto unique modifications, and it is beyond the scope of this survey to cover them all on a case-by-case basis. Nevertheless, we have tried to present the most prevalent and generalized U-net algorithms in this survey.
Additionally, almost all of the U-net architectures surveyed in this study were supervised models.

This is ostensible since the majority of medical image segmentation tasks involve supervised learning due to the low acceptable margin of error. Unsupervised U-net models are quite primitive and rare in biomedical imaging; however, there has been steady ongoing research in this area. For completeness, in this section, we present some unsupervised U-net models not limited to the biomedical imaging domain. Xia et al. [373] developed a network with two cascaded U-nets, where the reconstruction loss of the whole network and the normalized cut loss of the first U-net is minimized iteratively to saliently segment images. Khan et al. [374] designed a dense U-net that segments images via representation oriented clustering. Chen et al. [375] developed an attention gated U-net that had promising results on the ISBI 2017 Challenge.

2.5 **Challenges**

The success of deep learning is vital for improved medical diagnosis. Although there has been tremendous progress in deep learning techniques such as U-net in the past decade, the nature of medical analysis demands algorithms to perform with minimal error. A major limitation of reducing this error in deep learning techniques is computational power. Powerful deep learning algorithms require more time to train and hence are less feasible. U-net algorithms have applied transfer learning as one solution to alleviate this problem [341]. EfficientNet is a framework for optimizing neural network construction that has the potential to streamline U-net design, thereby making it more powerful using a similar number of parameters [376]. Another critical problem is the scarcity of annotated data for training. Ronneberger et al. [2] proposed a solution in their original U-net paper of applying random deformation to create new samples. An alternative solution is the use of adversarial models like GAN to synthesize new image samples. GAN, in particular, has seen tremendous success in synthesizing medical images [377]. Finally, deep learning models have the problem of being ‘black boxes’; the input and output to the network are well understood, but the behavior of the internal hidden layers is not. This creates a problem in which researchers often do not understand how to fix errors in the network or which layers or filters are more important to the task. Additionally, black boxes are difficult to interpret properly, and their properties are difficult to replicate [378]. These are some key reasons why deep learning is yet to be used in any large-scale real-world medical trial [379], despite its tremendous promise. However, day by day, these problems are becoming easier to overcome, and we expect to see even greater adoption of deep learning within the medical imaging community in the future. In this regard, we expect U-net to be a major stepping stone in deep learning within the realm of medical image analysis.

3. METHODOLOGY

A portion of this chapter was previously published by SPIE [380] [https://doi.org/10.1117/12.2591343].

A significant advantage of the U-net design is its high modularity and adaptability. The low-level design of U-net can be easily altered with other modules and architectures while keeping the high-level design the same. This allows U-net to be tuned for specific applications. Furthermore, this means that U-net can be continually improved with novel state-of-the-art methods. Such modifications have allowed U-net variants to outperform base U-net [77]. In our implementation, we have combined the U-net architecture with R2U-net [63], [77], DenseNet [78], FractalNet [381], and EfficientNet [382].

3.1 **Efficient R2U-net**

R2U-net borrows and combines deep residual learning (ResNet) [62] and recurrent convolutional neural network (RCNN) [74] onto U-net. The motivation behind this is twofold. Firstly, residual learning allows for the building of deeper neural networks. Standard CNNs can suffer from degradation of performance if too many hidden layers are introduced. This is due to the loss of feature identities in deeper neural networks caused by diminishing gradients in the weight vector [62]. ResNets overcome this problem by application of residual skip connections that transfer feature maps from a prior layer to a layer deeper in the network. Repeated use of such residual skip connections can significantly improve gradient propagation, allowing for deeper neural networks. By skipping layers, this configuration helps adjacent layers and their activations learn their weights to avoid the problem of diminishing gradients.

The second novel aspect of R2U-net is the integration of RCNN. RCNN incorporates the recurrent feedback loops into a convolutional layer. These recurrent connections provide the output feature map as input to the preceding layer at discrete time steps. The recurrent connections allow RCNNs to be better able to extract contextual information [74]. R2U-net incorporated both ResNet and RCNN modules. The design of these modules is provided in Figure 12.

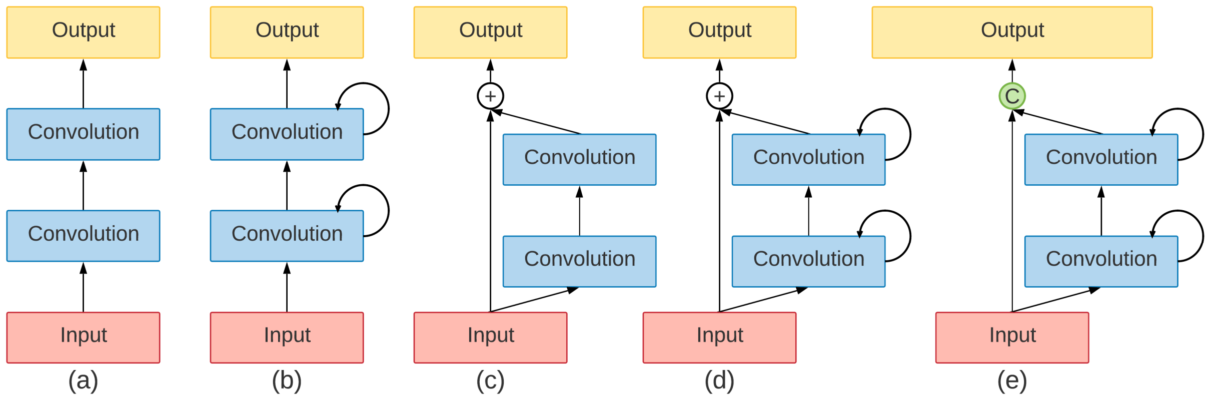

Figure 12. Different variants of residual and recurrent convolutional blocks (a) Forward only block, (b) Recurrent block, (c) Residual block, (d) Recurrent Residual block (R2), (e) Proposed R2 block with channel-wise concatenation.

Considering the input of the lth as x_l and i, j as the pixel locations of kth feature map, the output of the residual RCNN block is expressed as:

$$O_{ijk}^{l}(t) = (w_k^f)^T \times x_l^{f(i,j)}(t) + (w_k^r)^T \times x_l^{r(i,j)}(t-1) + b_k \tag{12}$$

where $f(\cdot)$ and $r(\cdot)$ correspond to the activation of the forward and recurrent output, respectively, while w_k^f and w_k^r denote the weights of the forward layer and recurrent layer of the kth feature map. The term b_k is a bias term. The output of a recurrent convolution layer is passed into a ReLU activation function:

$$\mathcal{F}(x_l, w_l) = \max\left(0, O_{ijk}^{l}(t)\right) \tag{13}$$

The overall output of the residual RCNN block can be simplified as:

$$x_{l+1} = x_l + \mathcal{F}(x_l, w_l) \tag{14}$$

Here x_{l+1} is the output of the residual RCNN block. Finally, we propose a small modification in our implementation of the residual RCNN block. We replace channel-wise addition in favor of channel-wise concatenation. This is because summing the layers can cause the information to be altered between layers [78]. Additionally, the kth feature map across different layers are not necessarily correlated. Performing concatenation preserves the features maps as they were, thereby improving information flow in the network. Our proposal alters Equation 14 into:

$$x_{l+1} = [x_l, \mathcal{F}(x_l, w_l)] \tag{15}$$

where [·] represents channel-wise concatenation. Our proposed model replaces all standard convolutional blocks in the expansive path with the modified residual RCNN blocks. We designate this model as Efficient R2U-net.

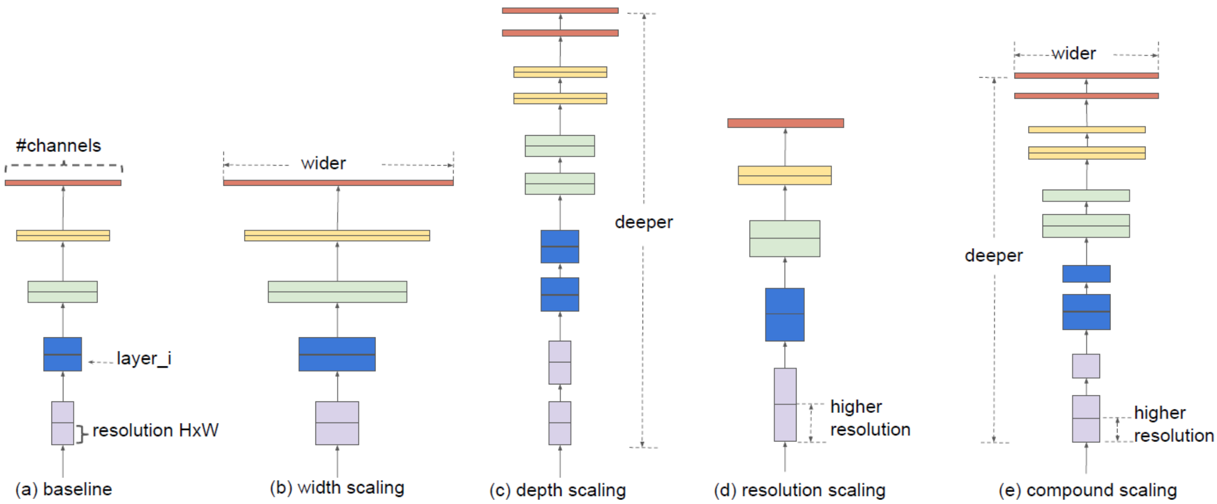

Figure 13. (a) Baseline network. (b)-(d) Conventional scaling methods that only increase one dimension of the network: width, depth, or resolution. (e) Compound scaling method that uniformly scales all three dimensions with a fixed ratio [382].

Yet another challenging aspect of designing deep neural networks is allocating resources efficiently. While scaling up to improve the performance of the network, it is often unclear what is the best approach. The common ways of scaling up a network are usually done by adding more layers or more filters. EfficientNet is a family of pretrained encoders that uses compound scaling to determine the network design [382]. Compound scaling uses fixed ratios to automatically select the appropriate depth, width, and resolutions for the model. Figure 13. illustrates the different network scaling methods. When applied to a suitable baseline network, compound scaling can scale it up more optimally than other methods. EfficientNet encoders require up to 8 times fewer parameters when juxtaposed with similarly performing models [382]. This is ideal when building deep neural networks with limited resources. In our proposed model, we replace the contracting path of the U-net with an EfficientNet encoder. The application of the EfficientNet encoder allows us to have a much deeper contracting path that can perform classification with higher accuracy. Furthermore, since EfficientNet is a fixed budget network, we can divert our focus on optimizing the decoder with residual RCNNs. Another advantage of EfficientNet is that these encoders are pretrained, which allows for significantly faster training allowing us to save up on valuable research time. The proposed model is illustrated in Figure 14.

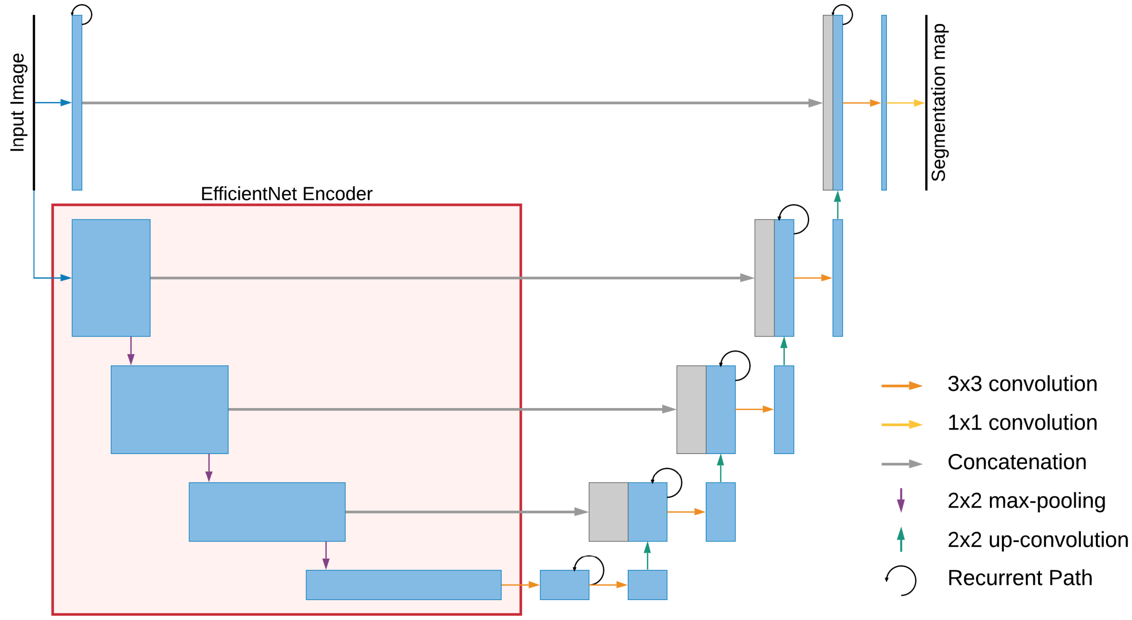

Figure 14. Our proposed model of residual recurrent U-net, using EfficientNet encoder.

3.2 Efficient Dense U-net

We also implemented a second convolution block based on densely connected convolutional networks (DenseNet) [78]. DenseNet is a design inspired by residual connections. While residual learning does indeed improve the problem of vanishing gradients, it does not entirely remove it. As such, ResNet models also degrade in performance after a certain threshold of layers is added. Unlike ResNet, DenseNet utilizes skip connections between every layer in the block. This configuration is presented in Figure 15. The concatenation block receives the feature maps from all previous layers and passes them onto the next layer. This ensures that any given layer has contextual information from all of the previous layers in the block. This significantly improves gradient propagation and allows for the building of deeper neural networks. The output for each layer in a dense block is described as:

$$x_l = H_l([x_1, x_2, x_3, \cdots, x_{l-1}]) \tag{16}$$

where H_l represents the dense mapping function. Our second U-net model replaces all standard convolutional blocks in the expansive path with the DenseNet blocks. We designate this model as Efficient Dense U-net.

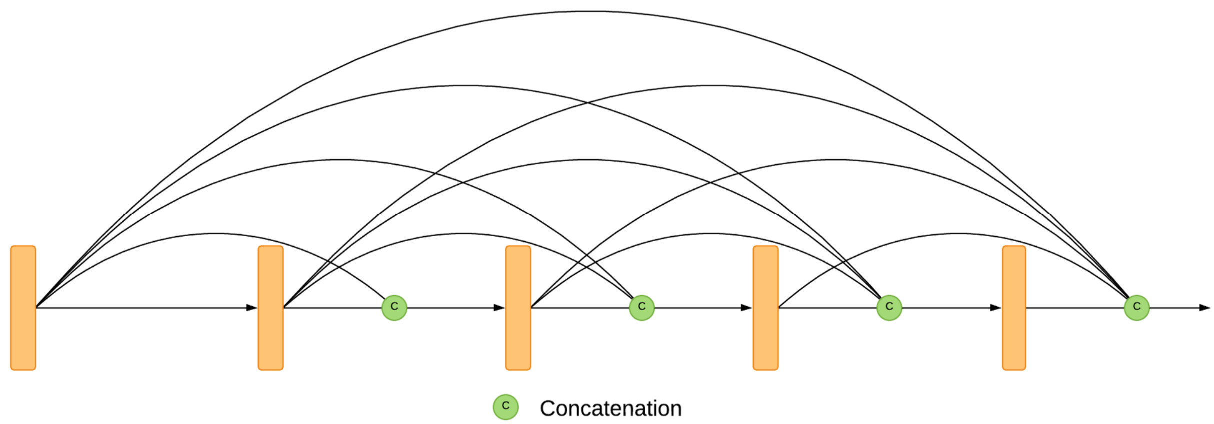

Figure 15. A five-layer DenseNet block.

3.3 **Efficient Fractal U-net**

FractalNet is a neural network architecture design based on the principle of fractal geometry expansion and similarity. This network uses repeated fractal expansions to generate unit blocks with multiple paths where each path has a geometrically increasing number of hidden layers [381]. Widening the network by adding multiple paths is an idea partially inspired by the Inception module [53]. Intermediary join layers merge outputs from different paths at regular geometric intervals. The final result is a network architecture that promotes gradient propagation without the typical residual skip connections. This behavior is achieved due to the different paths outputting different levels of gradient information. The fractal neural network designed by Larsson et al. [381] outperformed the ResNet architecture by a significant margin. Figure 16 showcases the basic representation of the fractal architecture. Let $f_C(x)$ denote the output of the *Cth* fractal truncation. $f_1(x)$ is defined as the unit base case, which can be customized according to the needs of the algorithms.

$$f_1(x) = \text{layer\_operation}(x) \tag{17}$$

With $f_1(x)$ defined, successive fractals can be generated by the following relationship:

$$f_{C+1}(x) = f_c\big(f_c(x)\big) \oplus f_1(x) \tag{18}$$

where $\oplus$ represents the join operation. The join operation aggregates the output of two or more hidden layers. A consequence of this expansion rule is that the number of operations increases exponentially as C increases. It is also possible to generate networks with different expansion rules to produce the desired result, though this requires further experimentation.

The fractal architecture has seen some adoption in U-net applications. Bai et al. [383] implemented a U-net model where the fractal block employs variable filter sizes and a residual skip connection. Kumar et al. [384] designed a U-net model where the fractal expansion resembles the original FractalNet architecture. The unit block consists of a convolution layer, batch normalization, leaky ReLU, and dropout in our implementation. For the join operation, there are several choices of layers. The original execution of FractalNet employed channel-wise addition. However, in our application, we replace channel-wise addition with channel-wise concatenation. This is due to the same reasons outlined in section 3.1.1; summing the layers can cause the information to be altered between layers and feature maps across different layers are not necessarily correlated [78]. Performing concatenation, therefore, preserves the features maps as they were and improves information flow in the network. The expansion rule of our implementation is simplified in Equation 19.

$$f_{C+1}(x) = \big[f_c\big(f_c(x)\big), f_1(x)\big] \tag{19}$$

We perform two tests, with two different fractal U-net models. The first model is an entirely fractal-based network. This is used for a baseline comparison against R2U-net where is narrowly outperforms R2U-net. The second implementation is a combination of EfficientNet with the fractal architectures, dubbed, Efficient Fractal U-net. Both models had $C = 3$.

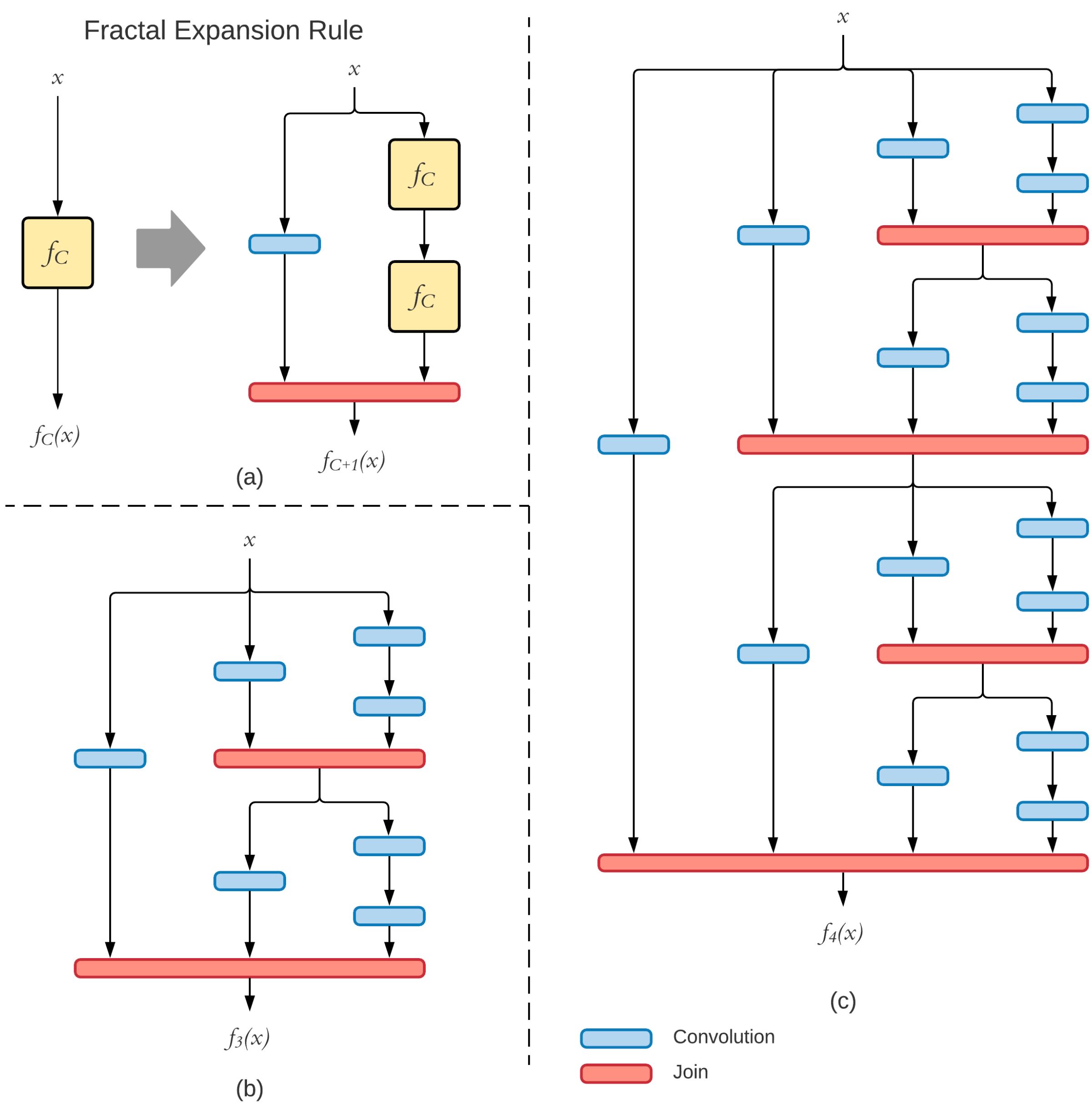

Figure 16. (a) Expansion rule to generate fractal architecture. The base case $f_1(x)$ has a single set of chosen layers. (b) Fractal block with *C*=3. (c) Fractal block with *C*=4.

3.4 **Loss Functions**

Aside from network architecture, one of the essential characteristics of a deep learning model is its loss function. In this section, we briefly describe some key loss functions used in image segmentation. One of the most common loss functions used in medical image segmentation is cross-entropy loss.

$$L_{CE} = -\sum_{i=1}^{n} t_i \log(p_i) \tag{20}$$

Here, t_i denotes to the ground truth, p_i denotes the probability for the ith class, and n denotes the number of classes [385]. One variant of cross-entropy loss is the weighted cross-entropy loss. This loss function gives certain weights to classes based on class imbalance. Another emerging variant of cross-entropy loss is the focal loss, where well-classified training samples are weighted down.

Besides cross-entropy, the other standard loss function in image segmentation is the Dice loss, obtained from the Sørensen–Dice coefficient [386]. Here GT refers to the ground truth, and SR refers to the segmentation result.

$$Dice = \frac{2|GT \cap SR|}{|GT| + |SR|} \tag{21}$$

Intersection over union (IoU) loss, derived from the Jaccard index, measures the ratio of the intersection of the samples to their union [387]. Dice loss and IoU loss are often used to strengthen their respective evaluation metrics.

$$Jaccard/IoU = \frac{|GT \cap SR|}{|GT \cup SR|} \tag{22}$$

Tversky loss is a modification of the Dice loss that gives different weights to false positive and false negative results [388]. This makes it useful in training datasets with unbalanced classes.

$$L = \frac{|GT \cap SR|}{|GT \cap SR| + \alpha|SR \backslash GT| + \beta|GT \backslash SR|} \tag{23}$$

Lastly, boundary loss is a family of loss functions that aim to minimize the distance between the ground truth and the segmentation results on a regional basis [389]. This loss function is useful for training models on highly unbalanced data.

4. RESULTS AND DISCUSSION

A portion of this chapter was previously published by SPIE [380] [https://doi.org/10.1117/12.2591343] and IEEE Access [1] [https://doi.org/10.1109/ACCESS.2021.3086020].

4.1 Datasets

Our proposed network model is tested on two popular medical image datasets, CHASE_DB1 [390] and ISIC 2018 [391], [392]. CHASE_DB1 is a retinal fundus dataset consisting of 28 colored images of dimensions 999×960 pixels, as well as their corresponding blood vessel segmentation maps. 23 of the images are selected for training, and the remaining 5 are left for testing the model, for an approximate 82:18 split. Due to the limited data samples, we opt for a patch-based approach. Each sample in the training and testing sets is randomly sampled to produce 160 patches of size 192×192 pixels. This results in a total of 3680 patches for training and 800 patches for testing. ISIC 2018 is a skin lesion dataset comprising of 2594 Dermoscopy images of different resolutions. Due to resource constraints, and to standardize the data, all images and ground truths have been resized to 256×256 pixels. The resized dataset is randomly split in an 80:20 ratio, resulting in 2075 training samples and 519 testing samples. Examples of both datasets are shown in Figure 17.

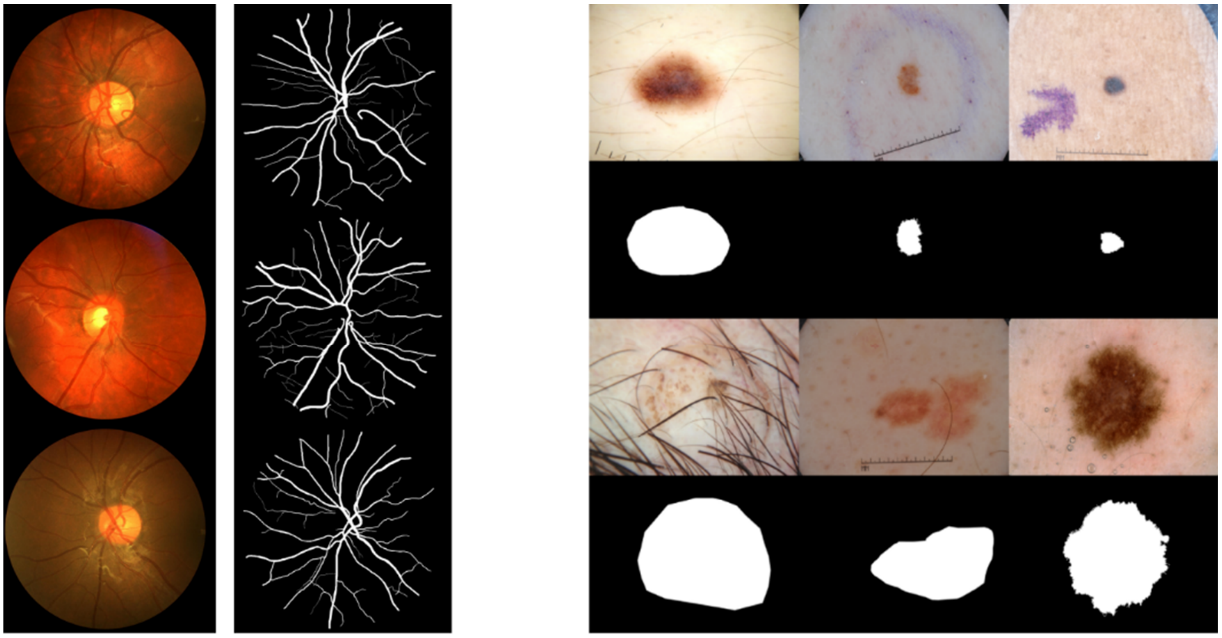

(a) (b)

Figure 17. Samples from (a) CHASE_DB1 and (b) ISIC 2018 datasets, including both images and segmentation maps.

4.2 Evaluation Metrics

As crucial as designing image processing models are, it is equally important to evaluate their performance correctly. In this section, presented are some of the most popular and widely used image segmentation evaluation metrics. Many of these metrics have been derived from the resulting confusion matrix and the associated true positive (TP), true negative (TN), false positive (FP), and false negative (FN) values.

The accuracy metric measures the number of correctly predicted samples against the total number of samples. In image processing, these samples are usually pixels or voxels. Accuracy, however, is not helpful in unbalanced data distributions that may arise in image processing and is rarely considered by itself [393].

$$Accuracy = \frac{TP + TN}{TP + TN + FP + FN} \tag{24}$$

Precision measures the number of correctly predicted positive samples against all positive predictions. Analogous to precision, specificity measures the number of correctly predicted negative samples among all negative samples. Both precision and specificity are useful to evaluate the number of false positive pixels in an image [393].

$$Precision = \frac{TP}{TP + FP} \tag{25}$$

$$Specificity = \frac{TN}{TN + FP} \tag{26}$$

Recall or sensitivity measures the proportion of positive samples that have been identified correctly as positive. Recall/sensitivity is useful to gauge the number of false negative pixels in an image [393]. It is common practice to pair precision with recall or specificity with sensitivity to get a much broader evaluation of a model or algorithm.

$$Recall/Sensitivity = \frac{TP}{TP + FN} \tag{27}$$

F-score, F1-score, or F-measure, is the harmonic mean of precision and recall. The F-score is often used to measure the overall performance of a model by combining precision and recall [393].

$$F\ score = \frac{2 \cdot Precision \cdot Recall}{Precision + Recall} \tag{28}$$

The Sørensen–Dice coefficient, commonly known as Dice score, compares the similarity between two samples [386]. Equation 21 describes the Dice score. In binary data evaluation, the Dice score is equivalent to F-score.

The Jaccard index, also known as intersection over union (IoU), is a measure of the overlap between two samples [387]. The Jaccard index is expressed in Equation 22.

The area under curve score (AUC) is another popular metric in image processing, particularly in biomedical image processing. It uses receiver operating characteristics (ROC) to evaluate different thresholds to convert continuous data to discrete data for classification [394]. It is a measure of how easily a model can distinguish between different classes [394].

4.3 **Parameter Settings**

In our implementation of EfficientNet based U-net architectures, we use EfficientNet-B7 [382] as the encoder, which is the deepest pretrained encoder in the EfficientNet family. The encoder layers are not modified. All other convolutional blocks are replaced with either DenseNet blocks, modified residual RCNN blocks, or fractal blocks.

We apply batch normalization after each convolution, where the output from each layer is normalized to have zero mean and a variance of one. This helps deal with training problems that arise due to poor initialization and helps gradient flow in deeper models [395]. The activation function used in our models is leaky ReLU. Leaky ReLU allows a small, positive gradient when a unit is not active, improving the overall performance of the network [396]. Finally, dropout is also applied to prevent overfitting issues [397]. The models are trained using adaptive learning rate for up to 500 epochs with early stopping criteria. The batch size for training the CHASE_DB1 dataset is 16, while for ISIC 2018, it is 8.

The EfficientNet models had 20,127,897 (Dense), 17,638,169 (R2), and 18,879,328 (Fractal) parameters. The experimental environment was TensorFlow 2.1. implementation of Keras written in Python 3. The experiment was run on Google Colab Pro. Google Colab Pro provides access to T4 or P100 GPU based on availability and a RAM size of 25.6 GB. The average training time for each model on each dataset was about 10 hours. It should be noted that training was done in multiple sessions by taking model checkpoints in between. The testing time was less than 2 minutes.

4.4 **Results**

We first evaluate the performance of our models on the CHASE_DB1 dataset. The segmentation results for CHASE_DB1 are presented in Figure 18, alongside the fundus images and the ground truths. From observation, it is evident that most of the structures are properly identified and segmented. The quantitative results of our models are compared against state-of-the-art models and presented in Table 10. Our proposed models achieve better accuracy and F1-scores against other segmentation models.

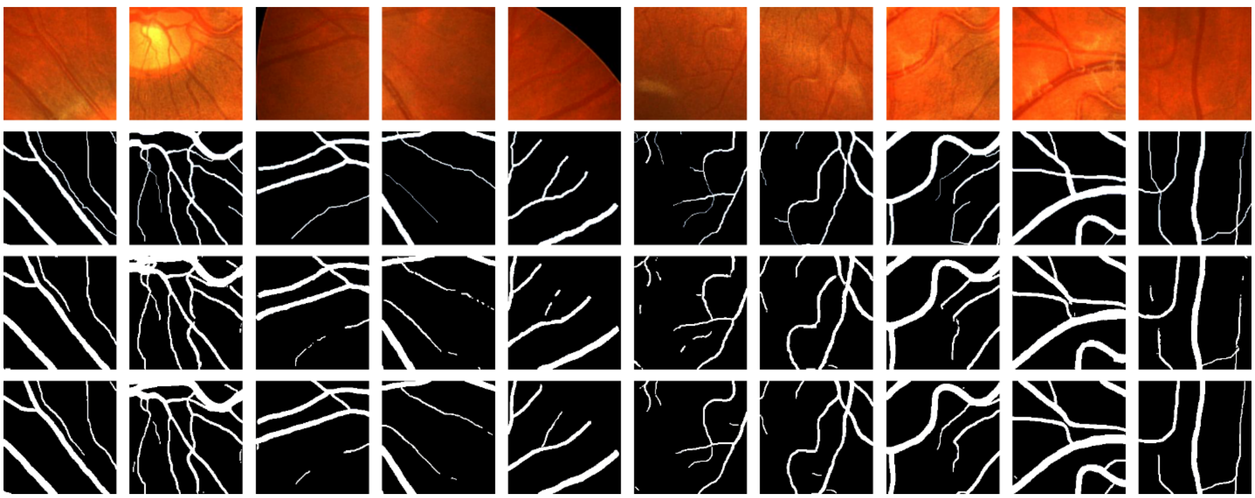

Figure 18. Sample segmentation results on the CHASE_DB1 dataset. Top to bottom: input patches; ground truths; Efficient Dense U-net segmentation result; Efficient R2U-net segmentation result.

Table 10. Evaluation metrics between other state-of-the-art and the proposed models on the CHASE_DB1 dataset.

Model	Year	Acc	F1	AUC
U-net [2]	2015	0.9578	0.7783	0.9772
Residual U-Net [398]	2017	0.9553	0.7800	0.9779
R2U-Net [77]	2018	0.9634	0.7928	0.9815
VGN [399]	2018	–	0.8034	0.9830
LadderNet [400]	2019	0.9656	0.8031	0.9839
IterNet [401]	2019	0.9655	0.8073	**0.9851**
Fractal U-net	2021	0.9665	0.8035	0.9816
Efficient Dense U-net	2021	0.9667	0.8092	0.9777
Efficient R2U-net	2021	**0.9668**	**0.8103**	0.9808

Our second evaluation is on the ISIC 2018 dataset. The segmentation results are previewed in Figure 19. The quantitative metrics for the dataset are presented in Table 11 against other comparable models.

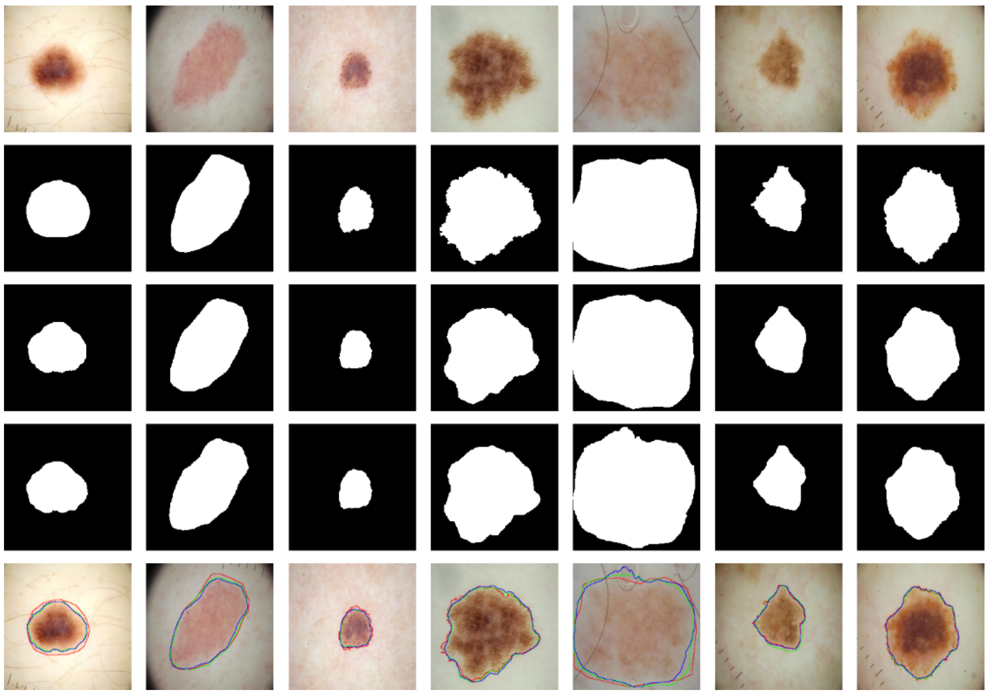

Figure 19. Sample segmentation results on the ISIC 2018 dataset. Top to bottom: input images; ground truths; Efficient Dense U-net segmentation result; Efficient R2U-net segmentation result; images with contours for ground truth (red), Efficient Dense U-net result (green), and Efficient R2U-net result (blue).

Table 11. Evaluation metrics between other state-of-the-art and the proposed models on the ISIC 2018 dataset.

Model	Year	Dice	JAC
U-Net 46 [301]	2019	–	0.9336
U-Net + FTL [50]	2018	0.8290	–
BCDU-Net [81]	2019	0.8510	0.9370
Attn U-Net + Multi-Input + FTL [50]	2018	0.8560	–
U-Net + DCNN-SVM [302]	2020	0.8700	0.8000
Fractal U-net	2021	0.8599	0.9476
Efficient Fractal U-net	2021	0.8702	0.9480
Efficient R2U-net	2021	0.8794	0.9519
Efficient Dense U-net	2021	**0.8862**	**0.9534**

4.5 Ablation Study

We perform ablation studies on our results to compare the metrics of the different network architectures and note which structure resulted in improved performance.

4.5.1 Comparison between EfficientNet and non-EfficientNet models

The first comparison is between models with and without the EfficientNet encoder. For the ISIC 2018 dataset, all of the EfficientNet models outperformed the non-EfficientNet models. In the case of the CHASE_DB1 dataset, the EfficientNet models outperformed the other models in accuracy and F1-score. However, they lagged behind in the area under curve (AUC) score. The improved performance scores can be attributed to the increased number of layers in the Efficient encoder and the compound scaling which distributes them for optimal performance. The lag in the AUC score between IterNet [401] and the EfficientNet models can be attributed to a narrow classification threshold in the latter models.

A possible reason this could arise is due to shortcomings in the decoder segment of the EfficientNet models. Since EfficientNet compound scaling is not available as a decoder, we had to implement different architectures for the decoder. In particular, the decoder has significantly fewer parameters than the encoder. As such, some of the performance gains in the encoder could be lost in the decoder. This loss has two consequences; firstly, it is plausible that the decoder bottlenecks all U-net models that use the EfficientNet encoder. Secondly, this implies that there is further room for improvement in such models by adjusting the decoder. Overall, the expansion of networks with the EfficientNet encoder increases networks' segmentation capabilities. It should be noted that we did not take the number of parameters or training time into consideration when making these comparisons. However, it can be confidently assumed that the Efficient U-net models have a higher number of parameters and greater training time than the non-Efficient U-net models, although this tradeoff does result in better performance metrics.

4.5.2 Comparison between Fractal U-net and non-EfficientNet models

Our second comparison is between vanilla Fractal U-net and other models. We ignore the EfficientNet models to evaluate the practicality of the fractal block on its own. Fractal U-net performs comparably with other models in its metrics. In particular, we would like to point out its performance against other simplified models; Fractal U-net outperformed vanilla U-net, Residual U-net, and R2U-net. These results show the potential of fractal designs over residual connections and recurrent connections. This result is significant since the design goal of all of the mentioned modules is to promote gradient propagation. In this regard, we can confidently say that the fractal mode is more effective in promoting gradient propagation in deep neural networks than both the recurrent and residual blocks.

The other important observation is against the attention models. It has a similar performance to models utilizing attention gate models. In the ISIC 2018 dataset Fractal U-net outperformed the attention gate models (Attn U-Net + Multi-Input + FTL [50]). In the CHASE_DB1 dataset, Fractal U-net had mixed results against LadderNet [400] and IterNet [401], both of which use some variant of the attention module. Fractal U-net had higher accuracy but lowered F1-score and AUC. The inconsistent result shows that the attention gate model to be on par or superior to the fractal block. This result is more intriguing since the fractal block, and the attention gates have different purposes. The key insight here is that the fractal block provides improved gradient propagation, resulting in higher pixel accuracy. However, the attention gate designed to target objects in an image produces more relevant improvements. Furthermore, since neither design competes with each other in terms of functionality, combining them could result in much more desirable results. The final observation is that the VGN [399] and DCNN-SVM [302] models outperform the vanilla Fractal U-net.

4.5.3 **Comparison within EfficientNet models**

The final evaluation comparison is within the Efficient U-net models themselves. For the CHASE_DB1 dataset, we compare Efficient R2U-net and Efficient Dense U-net. In this dataset, the Efficient R2U-net was better in all metrics versus the Efficient Dense U-net. This phenomenon is somewhat unexpected since the dense block has greater skip connections than the R2 block. As such, it should result in better gradient propagation and perform better in a one-to-one comparison. Furthermore, the number of convolution layers has been consistent across both. This surprising behavior might be explained due to the Dense block having more frequent concatenations, which results in a higher number of parameters. A higher number of parameters can lead to slight overfitting problems [113], and this might be why the Efficient R2U-net outperforms the Efficient

Dense U-net. Overfitting issues can be solved by specialized techniques such as compound scaling in EfficientNet [382] or supplementing other modules.

For the ISIC 2018 dataset, we compare Efficient R2U-net, Efficient Dense U-net, and Efficient Fractal U-net. In this dataset, the Dense block does indeed outperform the R2 block, as we hypothesized prior. We expect the Dense block to produce better segmentation maps than the R2 block, all other things being equal. And it is plausible that training on this dataset does not cause overfitting for the dense block. We also have the Efficient Fractal U-net for comparison, which is the worst of the three. This result is also unforeseen since the base Fractal U-net has better metrics than the base R2U-net; one would assume the same trend for their EfficientNet variants. This disparity could be explained due to the addition of the EfficientNet encoder itself. The fractal block has a higher number of parameters than the R2 block. The addition of the EfficientNet encoder could result in the fractal U-net architecture crossing the ideal parameter threshold and becoming overfitted. Overfitting does not happen in the vanilla variants since the number of parameters is sufficiently low, but the Efficient encoder adds a significantly higher number of layers and operations. Lastly, Efficient Dense U-net has higher performance metrics than Efficient Fractal U-net. There is no direct comparison between vanilla Dense U-net and Fractal U-net; however, we can still theorize a possible reason for the Dense block performing better. The Dense block has greater interconnectivity between its convolution layers than the fractal block since every layer is connected to all preceding layers in a Dense block. The fractal block ends up with a similar number of parameters as the Dense block since the fractal block in our models had seven convolution layers across all its paths versus the four layers in the Dense block. As such, it can be concluded that the higher interconnectivity makes up for the reduced number of layers in the Dense block, which makes it superior to the fractal block.

5. CONCLUSION

U-net is a powerful deep learning architecture that has been successfully applied to many biomedical image segmentation problems. In this thesis, we explored the many variants of U-net and its diverse applications on a multitude of image modalities. We also examined the major deep learning methods and their application areas for all of the papers in this thesis. Indeed U-net based architecture is quite ground-breaking and valuable in medical image analysis. The growth of U-net papers since 2017 lends credence to its status as a premier deep learning technique in medical image diagnosis. Thus, despite the many challenges remaining in deep learning-based image analysis, we expect U-net to be one of the major paths forward.

Precise segmentation of medical images is of vital importance for proper diagnosis by physicians. In this regard, U-net is a powerful deep learning architecture that achieves very strong performance on biomedical image segmentation. Additionally, U-net itself is quite adaptable and can be integrated with more deep learning techniques. The implementation of residual skip connections and recurrent feedback connections allows for the design of a much deeper U-net with a higher number of convolutions. Similar performance is achieved using densely connected convolutional networks. And finally, the addition of EfficientNet allows us to leverage the performance of a powerful pretrained classifier for our U-net encoder. Our proposed models achieve anticipated results on two popular benchmarking datasets.

Future work for this topic should be focused on implementing compound scaling for the expansive path to have symmetry on both U-net paths and produce further performance enhancement on segmentation tasks.

APPENDIX A. FRAMEWORKS AND SDKS

FRAMEWORKS

There are many open-source deep learning frameworks, among which some of the more popular and widely used frameworks are listed below:

- TensorFlow (Python, C, Java, Go, JavaScript, Swift): https://www.tensorflow.org/
- Keras (Python): https://keras.io/
- PyTorch (Python, C++): https://pytorch.org/
- Caffe (Python, MATLAB): http://caffe.berkeleyvision.org/
- Chainer (Python): https://chainer.org/
- Deeplearning4j (Java, Scala, Python, Clojure, Kotlin): https://deeplearning4j.org/
- Microsoft Cognitive Toolkit (CNTK) (Python, C#, C++): https://docs.microsoft.com/en-us/cognitive-toolkit/
- Theano (Python): http://www.deeplearning.net/software/theano/
- MXNet (Python, Scala, Julia, R, Clojure, Java, C++, Perl): https://mxnet.apache.org/
- ONNX (Python): https://microsoft.github.io/onnxruntime/
- Sonnet (Python): https://github.com/deepmind/sonnet
- PaddlePaddle (Python): https://github.com/PaddlePaddle/Paddle
- DeepGraphLibrary (Python): https://www.dgl.ai/

SDK

- NVIDIA CUDA-X AI platforms: https://developer.nvidia.com/deep-learning-software
- Qualcomm mobile platforms: https://developer.qualcomm.com/solutions/artificial-intelligence

APPENDIX B. DATASETS

The following includes some popular benchmarking datasets and databases for medical image segmentation tasks:

- ISBI 2012 cell segmentation challenge: Electron microscopy cell slices. http://brainiac2.mit.edu/isbi_challenge/
- ISBI cell tracking challenge: Database collecting 2D and 3D time-lapse videos of moving cells from past and ongoing ISBI challenges. http://celltrackingchallenge.net/
- LiTS: Liver CT scans for tumor detection. https://competitions.codalab.org/competitions/17094
- LIDC-IDRI: Lung CT scans for cancer detection. https://wiki.cancerimagingarchive.net/display/Public/LIDC-IDRI
- DRIVE: A popular retinal fundus image dataset. https://drive.grand-challenge.org/
- CT Colonography: CT scan dataset for colon cancer detection. https://wiki.cancerimagingarchive.net/display/Public/CT+COLONOGRAPHY
- Kaggle Data Science Bowl 2018: Nuclei segmentation challenge in microscopy images. https://www.kaggle.com/c/data-science-bowl-2018
- ISIC archive: Database of Dermoscopy images from past and ongoing ISIC challenges. https://www.isic-archive.com/
- SICAS Medical Image Repository: Archive for MICCAI Brain Tumor Segmentation Challenge (BRATS), MICCAI Ischemic Stroke Lesion Segmentation Challenge (ISLES), and ISBI Statistical Shape Model Challenge (SHAPE). https://www.smir.ch/Home/Browse
- Medical Segmentation Decathlon: Collection of MR and CT databases for various target areas. http://medicaldecathlon.com/
- OASIS: Brain MRI and PET images. https://www.oasis-brains.org/
- ABIDE: Brain MRI datasets. http://fcon_1000.projects.nitrc.org/indi/abide/
- ICCVB: Prostate MRI and retinal fundus datasets. http://i2cvb.github.io/
- STARE: Retinal fundus dataset. http://cecas.clemson.edu/~ahoover/stare/
- CHASE_DB1: Retinal fundus dataset. https://blogs.kingston.ac.uk/retinal/chasedb1/
- SCR: Chest X-ray dataset. http://www.isi.uu.nl/Research/Databases/SCR/

- DDSM: Mammogram dataset. http://www.eng.usf.edu/cvprg/Mammography/Database.html
- BCDR: Mammogram database. https://bcdr.eu/
- mini-MIAS: Mammogram dataset. http://peipa.essex.ac.uk/info/mias.html
- PanNuke: Histology dataset for nuclei instance segmentation. https://jgamper.github.io/PanNukeDataset/
- University of Cyprus: Multiple sclerosis MRI, tele-orthopedics X-ray, and carotid ultrasound datasets. http://www.ehealthlab.cs.ucy.ac.cy/index.php/facilities/32-software/218-datasets
- The cancer imaging archive: A large public repository of cancer image datasets. https://www.cancerimagingarchive.net/
- Cardiac atlas project: Repository of cardiovascular image datasets. http://www.cardiacatlas.org/

COVID-19 DATASETS

The following are some publicly available COVID-19 image datasets.

- COVID-CT: https://github.com/UCSD-AI4H/COVID-CT
- COVID-19 CT: http://medicalsegmentation.com/covid19/
- University of Montreal COVID-19 Image Data Collection: https://github.com/ieee8023/covid-chestxray-dataset
- RadiologyAi Consortium: https://www.radiologyaiconsortium.org/view

REFERENCES

[1] N. Siddique, P. Sidike, C. Elkin, and V. Devabhaktuni, “U-net and its variants for medical image segmentation: A review of theory and applications,” *IEEE Access*, Jun. 2021, doi: https://doi.org/10.1109/ACCESS.2021.3086020.

[2] O. Ronneberger, P. Fischer, and T. Brox, “U-net: Convolutional networks for biomedical image segmentation,” in *International Conference on Medical image computing and computer-assisted intervention*, 2015, pp. 234–241.

[3] J. Long, E. Shelhamer, and T. Darrell, “Fully convolutional networks for semantic segmentation,” in *Proceedings of the IEEE conference on computer vision and pattern recognition*, 2015, pp. 3431–3440.

[4] World Health Organization, “Weekly operational update on COVID-19 - 7 June 2021.” https://www.who.int/publications/m/item/weekly-operational-update-on-covid-19---7-june-2021 (accessed Jun. 08, 2021).

[5] S. Jin *et al.*, “AI-assisted CT imaging analysis for COVID-19 screening: Building and deploying a medical AI system in four weeks,” *medRxiv*, 2020.

[6] X. Chen, L. Yao, and Y. Zhang, “Residual Attention U-Net for Automated Multi-Class Segmentation of COVID-19 Chest CT Images,” *ArXiv Prepr. ArXiv200405645*, 2020.

[7] T. Zhou, S. Canu, and S. Ruan, “An automatic COVID-19 CT segmentation based on U-Net with attention mechanism,” *ArXiv Prepr. ArXiv200406673*, 2020.

[8] Y.-H. Wu *et al.*, “JCS: An explainable COVID-19 diagnosis system by joint classification and segmentation,” *ArXiv Prepr. ArXiv200407054*, 2020.

[9] Q. Yan *et al.*, “COVID-19 Chest CT Image Segmentation--A Deep Convolutional Neural Network Solution,” *ArXiv Prepr. ArXiv200410987*, 2020.

[10] G. Gaál, B. Maga, and A. Lukács, “Attention u-net based adversarial architectures for chest x-ray lung segmentation,” *ArXiv Prepr. ArXiv200310304*, 2020.

[11] T. Ozturk, M. Talo, E. A. Yildirim, U. B. Baloglu, O. Yildirim, and U. R. Acharya, “Automated detection of COVID-19 cases using deep neural networks with X-ray images,” *Comput. Biol. Med.*, p. 103792, 2020.

[12] M. Z. Alom, M. Rahman, M. S. Nasrin, T. M. Taha, and V. K. Asari, “COVID_MTNet: COVID-19 Detection with Multi-Task Deep Learning Approaches,” *ArXiv Prepr. ArXiv200403747*, 2020.

[13] F. Shi *et al.*, “Review of artificial intelligence techniques in imaging data acquisition, segmentation and diagnosis for covid-19,” *IEEE Rev. Biomed. Eng.*, 2020.

[14] Ö. Çiçek, A. Abdulkadir, S. S. Lienkamp, T. Brox, and O. Ronneberger, “3D U-Net: learning dense volumetric segmentation from sparse annotation,” in *International conference on medical image computing and computer-assisted intervention*, 2016, pp. 424–432.

[15] Q. Tong, M. Ning, W. Si, X. Liao, and J. Qin, “3D deeply-supervised U-net based whole heart segmentation,” in *International Workshop on Statistical Atlases and Computational Models of the Heart*, 2017, pp. 224–232.

[16] C. Wang, T. MacGillivray, G. Macnaught, G. Yang, and D. Newby, “A Two-Stage U-Net Model for 3D Multi-class Segmentation on Full-Resolution Cardiac Data,” in *International Workshop on Statistical Atlases and Computational Models of the Heart*, 2018, pp. 191–199.

[17] S. Jia *et al.*, “Automatically segmenting the left atrium from cardiac images using successive 3D U-nets and a contour loss,” in *International Workshop on Statistical Atlases and Computational Models of the Heart*, 2018, pp. 221–229.

[18] S. R. Ravichandran *et al.*, “3D Inception U-Net for Aorta Segmentation using Computed Tomography Cardiac Angiography,” in *2019 IEEE EMBS International Conference on Biomedical & Health Informatics (BHI)*, 2019, pp. 1–4.

[19] H. Xu, Z. Xu, W. Gu, and Q. Zhang, “A Two-Stage Fully Automatic Segmentation Scheme Using Both 2D and 3D U-Net for Multi-sequence Cardiac MR,” in *International Workshop on Statistical Atlases and Computational Models of the Heart*, 2019, pp. 309–316.

[20] T. Wang *et al.*, “MSU-Net: Multiscale Statistical U-Net for Real-time 3D Cardiac MRI Video Segmentation,” in *International Conference on Medical Image Computing and Computer-Assisted Intervention*, 2019, pp. 614–622.

[21] J. Wu, Y. Zhang, and X. Tang, “Simultaneous Tissue Classification and Lateral Ventricle Segmentation via a 2D U-net Driven by a 3D Fully Convolutional Neural Network,” in *2019 41st Annual International Conference of the IEEE Engineering in Medicine and Biology Society (EMBC)*, 2019, pp. 5928–5931.

[22] D. Yang, Q. Huang, L. Axel, and D. Metaxas, “Multi-component deformable models coupled with 2D-3D U-Net for automated probabilistic segmentation of cardiac walls and blood,” in *2018 IEEE 15th International Symposium on Biomedical Imaging (ISBI 2018)*, 2018, pp. 479–483.

[23] G. Zeng, X. Yang, J. Li, L. Yu, P.-A. Heng, and G. Zheng, “3D U-net with multi-level deep supervision: fully automatic segmentation of proximal femur in 3D MR images,” in *International workshop on machine learning in medical imaging*, 2017, pp. 274–282.

[24] G. Zeng *et al.*, “Latent3DU-net: Multi-level latent shape space constrained 3D U-net for automatic segmentation of the proximal femur from radial MRI of the hip,” in *International Workshop on Machine Learning in Medical Imaging*, 2018, pp. 188–196.

[25] G. Zeng and G. Zheng, “3D Tiled Convolution for Effective Segmentation of Volumetric Medical Images,” in *International Conference on Medical Image Computing and Computer-Assisted Intervention*, 2019, pp. 146–154.

[26] J. C. G. Sánchez, M. Magnusson, M. Sandborg, Å. C. Tedgren, and A. Malusek, “Segmentation of bones in medical dual-energy computed tomography volumes using the 3D U-Net,” *Phys. Med.*, vol. 69, pp. 241–247, 2020.

[27] H.-J. Bae *et al.*, “Fully automated 3D segmentation and separation of multiple cervical vertebrae in CT images using a 2D convolutional neural network,” *Comput. Methods Programs Biomed.*, vol. 184, p. 105119, 2020.

[28] C. Wang, Y. Guo, W. Chen, and Z. Yu, “Fully Automatic Intervertebral Disc Segmentation Using Multimodal 3D U-Net,” in *2019 IEEE 43rd Annual Computer Software and Applications Conference (COMPSAC)*, 2019, vol. 1, pp. 730–739.

[29] R. Mehta and T. Arbel, “3D U-Net for brain tumour segmentation,” in *International MICCAI Brainlesion Workshop*, 2018, pp. 254–266.

[30] W. Chen, B. Liu, S. Peng, J. Sun, and X. Qiao, “S3D-UNet: separable 3D U-Net for brain tumor segmentation,” in *International MICCAI Brainlesion Workshop*, 2018, pp. 358–368.

[31] M. Kolarik, R. Burget, V. Uher, and L. Povoda, “Superresolution of MRI brain images using unbalanced 3D Dense-U-Net network,” in *2019 42nd International Conference on Telecommunications and Signal Processing (TSP)*, 2019, pp. 643–646.

[32] J. Owler, B. Irving, G. Ridgeway, M. Wojciechowska, J. McGonigle, and M. Brady, "Comparison of Multi-atlas Segmentation and U-Net Approaches for Automated 3D Liver Delineation in MRI," in *Annual Conference on Medical Image Understanding and Analysis*, 2019, pp. 478–488.
[33] Q. Huang, J. Sun, H. Ding, X. Wang, and G. Wang, "Robust liver vessel extraction using 3D U-Net with variant dice loss function," *Comput. Biol. Med.*, vol. 101, pp. 153–162, 2018.
[34] W. Yu, B. Fang, Y. Liu, M. Gao, S. Zheng, and Y. Wang, "Liver Vessels Segmentation Based on 3d Residual U-NET," in *2019 IEEE International Conference on Image Processing (ICIP)*, 2019, pp. 250–254.
[35] C. Zhao, J. Han, Y. Jia, and F. Gou, "Lung nodule detection via 3D U-Net and contextual convolutional neural network," in *2018 International Conference on Networking and Network Applications (NaNA)*, 2018, pp. 356–361.
[36] Y. He, X. Yu, C. Liu, J. Zhang, K. Hu, and H. C. Zhu, "A 3D Dual Path U-Net of Cancer Segmentation Based on MRI," in *2018 IEEE 3rd International Conference on Image, Vision and Computing (ICIVC)*, 2018, pp. 268–272.
[37] M. P. Heinrich, O. Oktay, and N. Bouteldja, "OBELISK-Net: Fewer layers to solve 3D multi-organ segmentation with sparse deformable convolutions," *Med. Image Anal.*, vol. 54, pp. 1–9, 2019.
[38] H. Kakeya, T. Okada, and Y. Oshiro, "3D U-JAPA-Net: mixture of convolutional networks for abdominal multi-organ CT segmentation," in *International Conference on Medical Image Computing and Computer-Assisted Intervention*, 2018, pp. 426–433.
[39] C. Huang, H. Han, Q. Yao, S. Zhu, and S. K. Zhou, "3D U^2-Net: A 3D Universal U-Net for Multi-domain Medical Image Segmentation," in *International Conference on Medical Image Computing and Computer-Assisted Intervention*, 2019, pp. 291–299.
[40] Y. Wang, L. Zhao, M. Wang, and Z. Song, "Organ at Risk Segmentation in Head and Neck CT Images Using a Two-Stage Segmentation Framework Based on 3D U-Net," *IEEE Access*, vol. 7, pp. 144591–144602, 2019.
[41] B. Li, M. de Groot, M. W. Vernooij, M. A. Ikram, W. J. Niessen, and E. E. Bron, "Reproducible white matter tract segmentation using 3D U-Net on a large-scale DTI dataset," in *International Workshop on Machine Learning in Medical Imaging*, 2018, pp. 205–213.
[42] O. Oktay *et al.*, "Attention u-net: Learning where to look for the pancreas," *ArXiv Prepr. ArXiv180403999*, 2018.
[43] J. Schlemper *et al.*, "Attention gated networks: Learning to leverage salient regions in medical images," *Med. Image Anal.*, vol. 53, pp. 197–207, 2019.
[44] A. Vaswani *et al.*, "Attention is all you need," in *Advances in neural information processing systems*, 2017, pp. 5998–6008.
[45] Z. Zhang, H. Fu, H. Dai, J. Shen, Y. Pang, and L. Shao, "ET-Net: A Generic Edge-aTtention Guidance Network for Medical Image Segmentation," in *International Conference on Medical Image Computing and Computer-Assisted Intervention*, 2019, pp. 442–450.
[46] Z. Si, D. Fu, and J. Li, "U-Net with Attention Mechanism for Retinal Vessel Segmentation," in *Image and Graphics*, Cham, 2019, pp. 668–677.
[47] L. Mou *et al.*, "CS-Net: Channel and Spatial Attention Network for Curvilinear Structure Segmentation," in *Medical Image Computing and Computer Assisted Intervention – MICCAI 2019*, Cham, 2019, pp. 721–730.
[48] S. Lian, Z. Luo, Z. Zhong, X. Lin, S. Su, and S. Li, "Attention guided U-Net for accurate iris segmentation," *J. Vis. Commun. Image Represent.*, vol. 56, pp. 296–304, 2018.

[49] C. Wu, Y. Zou, and Z. Yang, "U-GAN: Generative Adversarial Networks with U-Net for Retinal Vessel Segmentation," in *2019 14th International Conference on Computer Science & Education (ICCSE)*, Aug. 2019, pp. 642–646. doi: 10.1109/ICCSE.2019.8845397.
[50] N. Abraham and N. M. Khan, "A novel focal tversky loss function with improved attention u-net for lesion segmentation," in *2019 IEEE 16th International Symposium on Biomedical Imaging (ISBI 2019)*, 2019, pp. 683–687.
[51] H. Zhang, H. Zhu, and X. Ling, "Polar coordinate sampling-based segmentation of overlapping cervical cells using attention U-Net and random walk," *Neurocomputing*, vol. 383, pp. 212–223, 2020.
[52] Z. Fang, Y. Chen, D. Nie, W. Lin, and D. Shen, "RCA-U-Net: Residual Channel Attention U-Net for Fast Tissue Quantification in Magnetic Resonance Fingerprinting," in *International Conference on Medical Image Computing and Computer-Assisted Intervention*, 2019, pp. 101–109.
[53] C. Szegedy *et al.*, "Going deeper with convolutions," in *Proceedings of the IEEE conference on computer vision and pattern recognition*, 2015, pp. 1–9.
[54] C. Szegedy, V. Vanhoucke, S. Ioffe, J. Shlens, and Z. Wojna, "Rethinking the inception architecture for computer vision," in *Proceedings of the IEEE conference on computer vision and pattern recognition*, 2016, pp. 2818–2826.
[55] H. Li, A. Li, and M. Wang, "A novel end-to-end brain tumor segmentation method using improved fully convolutional networks," *Comput. Biol. Med.*, vol. 108, pp. 150–160, 2019.
[56] Z. Zhang, C. Wu, S. Coleman, and D. Kerr, "DENSE-INception U-net for medical image segmentation," *Comput. Methods Programs Biomed.*, vol. 192, p. 105395, 2020.
[57] L. Chen, P. Bentley, K. Mori, K. Misawa, M. Fujiwara, and D. Rueckert, "DRINet for medical image segmentation," *IEEE Trans. Med. Imaging*, vol. 37, no. 11, pp. 2453–2462, 2018.
[58] A. H. Curiale, F. D. Colavecchia, and G. Mato, "Automatic quantification of the LV function and mass: a deep learning approach for cardiovascular MRI," *Comput. Methods Programs Biomed.*, vol. 169, pp. 37–50, 2019.
[59] H. Cheng, Y. Zhu, and H. Pan, "Modified U-Net block network for lung nodule detection," in *2019 IEEE 8th Joint International Information Technology and Artificial Intelligence Conference (ITAIC)*, 2019, pp. 599–605.
[60] R. M. Rad, P. Saeedi, J. Au, and J. Havelock, "Trophectoderm segmentation in human embryo images via inceptioned U-Net," *Med. Image Anal.*, vol. 62, p. 101612, 2020.
[61] H. Zhao and N. Sun, "Improved U-Net Model for Nerve Segmentation," in *Image and Graphics*, Cham, 2017, pp. 496–504.
[62] K. He, X. Zhang, S. Ren, and J. Sun, "Deep residual learning for image recognition," in *Proceedings of the IEEE conference on computer vision and pattern recognition*, 2016, pp. 770–778.
[63] M. Z. Alom, C. Yakopcic, T. M. Taha, and V. K. Asari, "Nuclei segmentation with recurrent residual convolutional neural networks based U-Net (R2U-Net)," in *NAECON 2018-IEEE National Aerospace and Electronics Conference*, 2018, pp. 228–233.
[64] S. Das, A. Deka, Y. Iwahori, M. Bhuyan, T. Iwamoto, and J. Ueda, "Contour-Aware Residual W-Net for Nuclei Segmentation," *Procedia Comput. Sci.*, vol. 159, pp. 1479–1488, 2019.
[65] H. Li, A. Zhygallo, and B. Menze, "Automatic brain structures segmentation using deep residual dilated U-net," in *International MICCAI Brainlesion Workshop*, 2018, pp. 385–393.

[66] T. Mostafiz, I. Jarin, S. A. Fattah, and C. Shahnaz, “Retinal Blood Vessel Segmentation Using Residual Block Incorporated U-Net Architecture and Fuzzy Inference System,” in *2018 IEEE International WIE Conference on Electrical and Computer Engineering (WIECON-ECE)*, Dec. 2018, pp. 106–109. doi: 10.1109/WIECON-ECE.2018.8783182.
[67] H. Li, D. Chen, W. H. Nailon, M. E. Davies, and D. Laurenson, “Improved breast mass segmentation in mammograms with conditional residual u-net,” in *Image Analysis for Moving Organ, Breast, and Thoracic Images*, Springer, 2018, pp. 81–89.
[68] Y. Liu, N. Qi, Q. Zhu, and W. Li, “CR-U-Net: Cascaded U-Net with Residual Mapping for Liver Segmentation in CT Images,” in *2019 IEEE Visual Communications and Image Processing (VCIP)*, 2019, pp. 1–4.
[69] M. Baldeon-Calisto and S. K. Lai-Yuen, “AdaResU-Net: Multiobjective adaptive convolutional neural network for medical image segmentation,” *Neurocomputing*, 2019.
[70] N. Ibtehaz and M. S. Rahman, “MultiResUNet: Rethinking the U-Net architecture for multimodal biomedical image segmentation,” *Neural Netw.*, vol. 121, pp. 74–87, 2020.
[71] R. Zhang, L. Huang, W. Xia, B. Zhang, B. Qiu, and X. Gao, “Multiple supervised residual network for osteosarcoma segmentation in CT images,” *Comput. Med. Imaging Graph.*, vol. 63, pp. 1–8, 2018.
[72] K. Kawagoe, K. Hatano, S. Murakami, H. Lu, H. Kim, and T. Aoki, “Automatic Segmentation Method of Phalange Regions Based on Residual U-Net and MSGVF Snakes,” in *2019 19th International Conference on Control, Automation and Systems (ICCAS)*, Oct. 2019, pp. 1046–1049. doi: 10.23919/ICCAS47443.2019.8971740.
[73] E. Kerfoot, J. Clough, I. Oksuz, J. Lee, A. P. King, and J. A. Schnabel, “Left-ventricle quantification using residual u-net,” in *International Workshop on Statistical Atlases and Computational Models of the Heart*, 2018, pp. 371–380.
[74] M. Liang and X. Hu, “Recurrent convolutional neural network for object recognition,” in *Proceedings of the IEEE conference on computer vision and pattern recognition*, 2015, pp. 3367–3375.
[75] P. Q. Lee *et al.*, “Model-free prostate cancer segmentation from dynamic contrast-enhanced MRI with recurrent convolutional networks: A feasibility study,” *Comput. Med. Imaging Graph.*, vol. 75, pp. 14–23, 2019.
[76] B. Ji *et al.*, “A multi-scale recurrent fully convolution neural network for laryngeal leukoplakia segmentation,” *Biomed. Signal Process. Control*, vol. 59, p. 101913, 2020.
[77] M. Z. Alom, M. Hasan, C. Yakopcic, T. M. Taha, and V. K. Asari, “Recurrent residual convolutional neural network based on u-net (r2u-net) for medical image segmentation,” *ArXiv Prepr. ArXiv180206955*, 2018.
[78] G. Huang, Z. Liu, L. Van Der Maaten, and K. Q. Weinberger, “Densely connected convolutional networks,” in *Proceedings of the IEEE conference on computer vision and pattern recognition*, 2017, pp. 4700–4708.
[79] C. Meng, K. Sun, S. Guan, Q. Wang, R. Zong, and L. Liu, “Multiscale dense convolutional neural network for DSA cerebrovascular segmentation,” *Neurocomputing*, vol. 373, pp. 123–134, 2020.
[80] J. Dolz, I. B. Ayed, and C. Desrosiers, “Dense multi-path U-Net for ischemic stroke lesion segmentation in multiple image modalities,” in *International MICCAI Brainlesion Workshop*, 2018, pp. 271–282.

[81] R. Azad, M. Asadi-Aghbolaghi, M. Fathy, and S. Escalera, "Bi-Directional ConvLSTM U-Net with Densley Connected Convolutions," in *Proceedings of the IEEE International Conference on Computer Vision Workshops*, 2019, pp. 0–0.
[82] X. Li, H. Chen, X. Qi, Q. Dou, C.-W. Fu, and P.-A. Heng, "H-DenseUNet: hybrid densely connected UNet for liver and tumor segmentation from CT volumes," *IEEE Trans. Med. Imaging*, vol. 37, no. 12, pp. 2663–2674, 2018.
[83] Z.-H. Wang, Z. Liu, Y.-Q. Song, and Y. Zhu, "Densely connected deep U-Net for abdominal multi-organ segmentation," in *2019 IEEE International Conference on Image Processing (ICIP)*, 2019, pp. 1415–1419.
[84] Z. Zhou, M. M. R. Siddiquee, N. Tajbakhsh, and J. Liang, "Unet++: A nested u-net architecture for medical image segmentation," in *Deep Learning in Medical Image Analysis and Multimodal Learning for Clinical Decision Support*, Springer, 2018, pp. 3–11.
[85] J. Ren, H. Sun, Y. Huang, and H. Gao, "Knowledge-Based Multi-sequence MR Segmentation via Deep Learning with a Hybrid U-Net++ Model," in *International Workshop on Statistical Atlases and Computational Models of the Heart*, 2019, pp. 280–289.
[86] H. Cui, X. Liu, and N. Huang, "Pulmonary vessel segmentation based on orthogonal fused u-net++ of chest ct images," in *International Conference on Medical Image Computing and Computer-Assisted Intervention*, 2019, pp. 293–300.
[87] S. Wu, Z. Wang, C. Liu, C. Zhu, S. Wu, and K. Xiao, "Automatical segmentation of pelvic organs after hysterectomy by using dilated convolution u-net++," in *2019 IEEE 19th International Conference on Software Quality, Reliability and Security Companion (QRS-C)*, 2019, pp. 362–367.
[88] I. Goodfellow *et al.*, "Generative adversarial nets," 2014, pp. 2672–2680.
[89] M. Mirza and S. Osindero, "Conditional generative adversarial nets," *ArXiv Prepr. ArXiv14111784*, 2014.
[90] Y. Chen, A. Jakary, S. Avadiappan, C. P. Hess, and J. M. Lupo, "Qsmgan: Improved quantitative susceptibility mapping using 3d generative adversarial networks with increased receptive field," *NeuroImage*, vol. 207, p. 116389, 2020.
[91] G. Yang *et al.*, "DAGAN: Deep de-aliasing generative adversarial networks for fast compressed sensing MRI reconstruction," *IEEE Trans. Med. Imaging*, vol. 37, no. 6, pp. 1310–1321, 2017.
[92] Y. Xue, T. Xu, H. Zhang, L. R. Long, and X. Huang, "Segan: Adversarial network with multi-scale l 1 loss for medical image segmentation," *Neuroinformatics*, vol. 16, no. 3–4, pp. 383–392, 2018.
[93] T. Shen, C. Gou, F.-Y. Wang, Z. He, and W. Chen, "Learning from adversarial medical images for X-ray breast mass segmentation," *Comput. Methods Programs Biomed.*, vol. 180, p. 105012, Oct. 2019, doi: 10.1016/j.cmpb.2019.105012.
[94] R. R. Upendra, S. Dangi, and C. A. Linte, "An Adversarial Network Architecture Using 2D U-Net Models for Segmentation of Left Ventricle from Cine Cardiac MRI," in *International Conference on Functional Imaging and Modeling of the Heart*, 2019, pp. 415–424.
[95] G. Li, L. Zhang, S. Hu, D. Fu, and M. Liu, "Adversarial Network with Dual U-net Model and Multiresolution Loss Computation for Medical Images Registration," in *2019 12th International Congress on Image and Signal Processing, BioMedical Engineering and Informatics (CISP-BMEI)*, 2019, pp. 1–5.

[96] X. Feng, C. Wang, S. Cheng, and L. Guo, “Automatic Liver and Tumor Segmentation of CT Based on Cascaded U-Net,” in *Proceedings of 2018 Chinese Intelligent Systems Conference*, 2019, pp. 155–164.
[97] T. Liu, Y. Tian, S. Zhao, X. Huang, and Q. Wang, “Automatic Whole Heart Segmentation Using a Two-Stage U-Net Framework and an Adaptive Threshold Window,” *IEEE Access*, vol. 7, pp. 83628–83636, 2019.
[98] H. Liu, X. Shen, F. Shang, F. Ge, and F. Wang, “CU-Net: Cascaded U-Net with Loss Weighted Sampling for Brain Tumor Segmentation,” in *Multimodal Brain Image Analysis and Mathematical Foundations of Computational Anatomy*, Springer, 2019, pp. 102–111.
[99] X. Fu *et al.*, “M-Net: A Novel U-Net With Multi-Stream Feature Fusion and Multi-Scale Dilated Convolutions for Bile Ducts and Hepatolith Segmentation,” *IEEE Access*, vol. 7, pp. 148645–148657, 2019.
[100] J. Hong, B. Park, M. J. Lee, C.-S. Chung, J. Cha, and H. Park, “Two-step deep neural network for segmentation of deep white matter hyperintensities in migraineurs,” *Comput. Methods Programs Biomed.*, vol. 183, p. 105065, 2020.
[101] D. M. Vigneault, W. Xie, C. Y. Ho, D. A. Bluemke, and J. A. Noble, “Ω-net (omega-net): fully automatic, multi-view cardiac MR detection, orientation, and segmentation with deep neural networks,” *Med. Image Anal.*, vol. 48, pp. 95–106, 2018.
[102] J. Hu *et al.*, “S-UNet: A Bridge-Style U-Net Framework With a Saliency Mechanism for Retinal Vessel Segmentation,” *IEEE Access*, vol. 7, pp. 174167–174177, 2019, doi: 10.1109/ACCESS.2019.2940476.
[103] M. K. Abd-Ellah, A. A. Khalaf, A. I. Awad, and H. F. Hamed, “TPUAR-Net: Two Parallel U-Net with Asymmetric Residual-Based Deep Convolutional Neural Network for Brain Tumor Segmentation,” in *International Conference on Image Analysis and Recognition*, 2019, pp. 106–116.
[104] M. Soltanpour, R. Greiner, P. Boulanger, and B. Buck, “Ischemic Stroke Lesion Prediction in CT Perfusion Scans Using Multiple Parallel U-Nets Following by a Pixel-Level Classifier,” in *2019 IEEE 19th International Conference on Bioinformatics and Bioengineering (BIBE)*, 2019, pp. 957–963.
[105] L. Zhang and L. Xu, “An Automatic Liver Segmentation Algorithm for CT Images U-Net with Separated Paths of Feature Extraction,” in *2018 IEEE 3rd International Conference on Image, Vision and Computing (ICIVC)*, 2018, pp. 294–298.
[106] D. Kwon *et al.*, “Siamese U-Net with Healthy Template for Accurate Segmentation of Intracranial Hemorrhage,” in *International Conference on Medical Image Computing and Computer-Assisted Intervention*, 2019, pp. 848–855.
[107] M. Dunnhofer *et al.*, “Siam-U-Net: encoder-decoder siamese network for knee cartilage tracking in ultrasound images,” *Med. Image Anal.*, vol. 60, p. 101631, Feb. 2020, doi: 10.1016/j.media.2019.101631.
[108] B. Murugesan, K. Sarveswaran, S. M. Shankaranarayana, K. Ram, J. Joseph, and M. Sivaprakasam, “Psi-Net: Shape and boundary aware joint multi-task deep network for medical image segmentation,” in *2019 41st Annual International Conference of the IEEE Engineering in Medicine and Biology Society (EMBC)*, 2019, pp. 7223–7226.
[109] K. Hu, C. Liu, X. Yu, J. Zhang, Y. He, and H. Zhu, “A 2.5 D Cancer Segmentation for MRI Images Based on U-Net,” in *2018 5th International Conference on Information Science and Control Engineering (ICISCE)*, 2018, pp. 6–10.

[110] G. Piantadosi, M. Sansone, R. Fusco, and C. Sansone, “Multi-planar 3D breast segmentation in MRI via deep convolutional neural networks,” *Artif. Intell. Med.*, vol. 103, p. 101781, 2020.

[111] C. Angermann and M. Haltmeier, “Random 2.5 D U-net for Fully 3D Segmentation,” in *Machine Learning and Medical Engineering for Cardiovascular Health and Intravascular Imaging and Computer Assisted Stenting*, Springer, 2019, pp. 158–166.

[112] J. Wei, Y. Xia, and Y. Zhang, “M3Net: A multi-model, multi-size, and multi-view deep neural network for brain magnetic resonance image segmentation,” *Pattern Recognit.*, vol. 91, pp. 366–378, 2019.

[113] S. Minaee, Y. Boykov, F. Porikli, A. Plaza, N. Kehtarnavaz, and D. Terzopoulos, “Image Segmentation Using Deep Learning: A Survey,” *ArXiv200105566 Cs*, Apr. 2020, Accessed: Jun. 08, 2020. [Online]. Available: http://arxiv.org/abs/2001.05566

[114] V. Badrinarayanan, A. Kendall, and R. Cipolla, “Segnet: A deep convolutional encoder-decoder architecture for image segmentation,” *IEEE Trans. Pattern Anal. Mach. Intell.*, vol. 39, no. 12, pp. 2481–2495, 2017.

[115] T.-Y. Lin, P. Dollár, R. Girshick, K. He, B. Hariharan, and S. Belongie, “Feature pyramid networks for object detection,” 2017, pp. 2117–2125.

[116] S. Seferbekov, V. Iglovikov, A. Buslaev, and A. Shvets, “Feature pyramid network for multi-class land segmentation,” 2018, pp. 272–275.

[117] L.-C. Chen, G. Papandreou, I. Kokkinos, K. Murphy, and A. L. Yuille, “Deeplab: Semantic image segmentation with deep convolutional nets, atrous convolution, and fully connected crfs,” *IEEE Trans. Pattern Anal. Mach. Intell.*, vol. 40, no. 4, pp. 834–848, 2017.

[118] S. Dong *et al.*, “DeU-Net: Deformable U-Net for 3D Cardiac MRI Video Segmentation,” Oct. 2020, pp. 98–107. doi: 10.1007/978-3-030-59719-1_10.

[119] S. K. Hasan and C. A. Linte, “A Modified U-Net Convolutional Network Featuring a Nearest-neighbor Re-sampling-based Elastic-Transformation for Brain Tissue Characterization and Segmentation,” in *2018 IEEE Western New York Image and Signal Processing Workshop (WNYISPW)*, 2018, pp. 1–5.

[120] L. Song, K. Geoffrey, and H. Kaijian, “Bottleneck feature supervised U-Net for pixel-wise liver and tumor segmentation,” *Expert Syst. Appl.*, vol. 145, p. 113131, 2020.

[121] A. Colonna, F. Scarpa, and A. Ruggeri, “Segmentation of corneal nerves using a U-Net-based convolutional neural network,” in *Computational Pathology and Ophthalmic Medical Image Analysis*, Springer, 2018, pp. 185–192.

[122] H. Dong, G. Yang, F. Liu, Y. Mo, and Y. Guo, “Automatic brain tumor detection and segmentation using u-net based fully convolutional networks,” in *annual conference on medical image understanding and analysis*, 2017, pp. 506–517.

[123] H. T. Le and H. T.-T. Pham, “Brain Tumor Segmentation Using U-Net Based Deep Neural Networks,” in *International Conference on the Development of Biomedical Engineering in Vietnam*, 2018, pp. 39–42.

[124] A. Kermi, I. Mahmoudi, and M. T. Khadir, “Deep convolutional neural networks using U-Net for automatic brain tumor segmentation in multimodal MRI volumes,” in *International MICCAI Brainlesion Workshop*, 2018, pp. 37–48.

[125] S. Chen, C. Ding, and M. Liu, “Dual-force convolutional neural networks for accurate brain tumor segmentation,” *Pattern Recognit.*, vol. 88, pp. 90–100, 2019.

[126] X. Kong, G. Sun, Q. Wu, J. Liu, and F. Lin, “Hybrid pyramid U-Net model for brain tumor segmentation,” in *International Conference on Intelligent Information Processing*, 2018, pp. 346–355.

[127] A. Bousselham, O. Bouattane, M. Youssfi, and A. Raihani, “Improved Brain Tumor Segmentation in MRI Images Based on Thermal Analysis Model Using U-Net and GPUs,” in *International Conference on Advanced Intelligent Systems for Sustainable Development*, 2019, pp. 80–87.

[128] Y. Chen, Z. Cao, C. Cao, J. Yang, and J. Zhang, “A modified U-net for brain MR image segmentation,” in *International Conference on Cloud Computing and Security*, 2018, pp. 233–242.

[129] Z. Wu, F. Chen, and D. Wu, “A Novel Framework Called HDU for Segmentation of Brain Tumor,” in *2018 15th International Computer Conference on Wavelet Active Media Technology and Information Processing (ICCWAMTIP)*, 2018, pp. 81–84.

[130] T. Yang and J. Song, “An Automatic Brain Tumor Image Segmentation Method Based on the U-net,” in *2018 IEEE 4th International Conference on Computer and Communications (ICCC)*, 2018, pp. 1600–1604.

[131] J. Dutta, D. Chakraborty, and D. Mondal, “Multimodal Segmentation of Brain Tumours in Volumetric MRI Scans of the Brain Using Time-Distributed U-Net,” in *Computational Intelligence in Pattern Recognition*, Springer, 2020, pp. 715–725.

[132] R. Mehta, T. Christinck, T. Nair, P. Lemaitre, D. Arnold, and T. Arbel, “Propagating Uncertainty Across Cascaded Medical Imaging Tasks for Improved Deep Learning Inference,” in *Uncertainty for Safe Utilization of Machine Learning in Medical Imaging and Clinical Image-Based Procedures*, Springer, 2019, pp. 23–32.

[133] A. K. Dhara *et al.*, “Segmentation of post-operative glioblastoma in mri by u-net with patient-specific interactive refinement,” in *International MICCAI Brainlesion Workshop*, 2018, pp. 115–122.

[134] A. Rafi *et al.*, “U-Net Based Glioblastoma Segmentation with Patient’s Overall Survival Prediction,” in *International Symposium on Intelligent Computing Systems*, 2020, pp. 22–32.

[135] P. X. Nguyen, Z. Lu, W. Huang, S. Huang, A. Katsuki, and Z. Lin, “Medical Image Segmentation with Stochastic Aggregated Loss in a Unified U-Net,” in *2019 IEEE EMBS International Conference on Biomedical & Health Informatics (BHI)*, 2019, pp. 1–4.

[136] Y. Xu, M. Gong, H. Fu, D. Tao, K. Zhang, and K. Batmanghelich, “Multi-scale masked 3-D U-net for brain tumor segmentation,” in *International MICCAI Brainlesion Workshop*, 2018, pp. 222–233.

[137] K. B. Dev, P. S. Jogi, S. Niyas, S. Vinayagamani, C. Kesavadas, and J. Rajan, “Automatic detection and localization of Focal Cortical Dysplasia lesions in MRI using fully convolutional neural network,” *Biomed. Signal Process. Control*, vol. 52, pp. 218–225, 2019.

[138] A. Zaman, L. Zhang, J. Yan, and D. Zhu, “Multi-modal Image Prediction via Spatial Hybrid U-Net,” in *International Workshop on Multiscale Multimodal Medical Imaging*, 2019, pp. 1–9.

[139] M. Jafari *et al.*, “FU-Net: Multi-class Image Segmentation Using Feedback Weighted U-Net,” in *International Conference on Image and Graphics*, 2019, pp. 529–537.

[140] W. Yao, S. Wang, and H. Fu, “Hippocampus Segmentation in MRI Using Side U-Net Model,” in *International Conference on Neural Information Processing*, 2019, pp. 143–150.

[141] Y. Zhang, W. Chen, Y. Chen, and X. Tang, “A post-processing method to improve the white matter hyperintensity segmentation accuracy for randomly-initialized U-net,” in *2018 IEEE 23rd International Conference on Digital Signal Processing (DSP)*, 2018, pp. 1–5.
[142] J. Wu, Y. Zhang, K. Wang, and X. Tang, “Skip Connection U-Net for White Matter Hyperintensities Segmentation From MRI,” *IEEE Access*, vol. 7, pp. 155194–155202, 2019.
[143] Y. Zhang *et al.*, “Fully Automatic White Matter Hyperintensity Segmentation using U-net and Skip Connection,” in *2019 41st Annual International Conference of the IEEE Engineering in Medicine and Biology Society (EMBC)*, 2019, pp. 974–977.
[144] S. S. M. Salehi, D. Erdogmus, and A. Gholipour, “Auto-context convolutional neural network (auto-net) for brain extraction in magnetic resonance imaging,” *IEEE Trans. Med. Imaging*, vol. 36, no. 11, pp. 2319–2330, 2017.
[145] A. Rampun, D. Jarvis, P. Griffiths, and P. Armitage, “Automated 2D Fetal Brain Segmentation of MR Images Using a Deep U-Net,” in *Asian Conference on Pattern Recognition*, 2019, pp. 373–386.
[146] J. Lou *et al.*, “Automatic Fetal Brain Extraction Using Multi-stage U-Net with Deep Supervision,” in *International Workshop on Machine Learning in Medical Imaging*, 2019, pp. 592–600.
[147] G. Wang *et al.*, “Interactive medical image segmentation using deep learning with image-specific fine tuning,” *IEEE Trans. Med. Imaging*, vol. 37, no. 7, pp. 1562–1573, 2018.
[148] G. R. Pinheiro, R. Voltoline, M. Bento, and L. Rittner, “V-Net and U-Net for Ischemic Stroke Lesion Segmentation in a Small Dataset of Perfusion Data,” in *International MICCAI Brainlesion Workshop*, 2018, pp. 301–309.
[149] R. Karthik, U. Gupta, A. Jha, R. Rajalakshmi, and R. Menaka, “A deep supervised approach for ischemic lesion segmentation from multimodal MRI using Fully Convolutional Network,” *Appl. Soft Comput.*, vol. 84, p. 105685, 2019.
[150] A. Bousselham, O. Bouattane, M. Youssfi, and A. Raihani, “Ischemic Stroke Lesion Segmentation Based on Thermal Analysis Model Using U-Net Fully Convolutional Neural Networks on GPUs,” in *International Conference on Advanced Intelligent Systems for Sustainable Development*, 2019, pp. 99–106.
[151] L. K. S. Cornelio, M. A. V. del Castillo, and P. C. Naval Jr, “U-ISLES: Ischemic Stroke Lesion Segmentation Using U-Net,” in *Proceedings of SAI Intelligent Systems Conference*, 2018, pp. 326–336.
[152] J. Kobold *et al.*, “Stroke Thrombus Segmentation on SWAN with Multi-Directional U-Nets,” in *2019 Ninth International Conference on Image Processing Theory, Tools and Applications (IPTA)*, 2019, pp. 1–6.
[153] H. Yang, Z. Liu, and X. Yang, “Right Ventricle Segmentation in Short-Axis MRI Using a Shape Constrained Dense Connected U-Net,” in *International Conference on Medical Image Computing and Computer-Assisted Intervention*, 2019, pp. 532–540.
[154] Y.-C. Kim, K. R. Kim, and Y. H. Choe, “Automatic myocardial segmentation in dynamic contrast enhanced perfusion MRI using Monte Carlo dropout in an encoder-decoder convolutional neural network,” *Comput. Methods Programs Biomed.*, vol. 185, p. 105150, 2020.
[155] W. Yan, Y. Wang, Z. Li, R. J. Van Der Geest, and Q. Tao, “Left ventricle segmentation via optical-flow-net from short-axis cine MRI: preserving the temporal coherence of cardiac motion,” in *International Conference on Medical Image Computing and Computer-Assisted Intervention*, 2018, pp. 613–621.

[156] J. Zhang, J. Du, H. Liu, X. Hou, Y. Zhao, and M. Ding, “LU-NET: An improved U-Net for ventricular segmentation,” *IEEE Access*, vol. 7, pp. 92539–92546, 2019.

[157] S. Charmchi, K. Punithakumar, and P. Boulanger, “Optimizing U-net to segment left ventricle from magnetic resonance imaging,” in *2018 IEEE International Conference on Bioinformatics and Biomedicine (BIBM)*, 2018, pp. 327–332.

[158] G. Borodin and O. Senyukova, “Right ventricle segmentation in cardiac MR images using u-net with partly dilated convolution,” in *International Conference on Artificial Neural Networks*, 2018, pp. 179–185.

[159] X. Wang *et al.*, “SK-Unet: an improved u-net model with selective kernel for the segmentation of multi-sequence cardiac MR,” in *International Workshop on Statistical Atlases and Computational Models of the Heart*, 2019, pp. 246–253.

[160] X.-Y. Zhou, P. Li, Z.-Y. Wang, and G.-Z. Yang, “U-net training with instance-layer normalization,” in *International Workshop on Multiscale Multimodal Medical Imaging*, 2019, pp. 101–108.

[161] W. Yan, Y. Wang, R. J. van der Geest, and Q. Tao, “Cine MRI analysis by deep learning of optical flow: Adding the temporal dimension,” *Comput. Biol. Med.*, vol. 111, p. 103356, 2019.

[162] F. Guo, M. Ng, and G. Wright, “Cardiac MRI Left Ventricle Segmentation and Quantification: A Framework Combining U-Net and Continuous Max-Flow,” in *International Workshop on Statistical Atlases and Computational Models of the Heart*, 2018, pp. 450–458.

[163] R. J. Nowling *et al.*, “Classification before Segmentation: Improved U-Net Prostate Segmentation,” in *2019 IEEE EMBS International Conference on Biomedical & Health Informatics (BHI)*, 2019, pp. 1–4.

[164] Y. Zhang, J. Wu, W. Chen, Y. Chen, and X. Tang, “Prostate segmentation using Z-net,” in *2019 IEEE 16th International Symposium on Biomedical Imaging (ISBI 2019)*, 2019, pp. 11–14.

[165] L. Rundo *et al.*, “USE-Net: Incorporating Squeeze-and-Excitation blocks into U-Net for prostate zonal segmentation of multi-institutional MRI datasets,” *Neurocomputing*, vol. 365, pp. 31–43, 2019.

[166] S. Elguindi *et al.*, “Deep learning-based auto-segmentation of targets and organs-at-risk for magnetic resonance imaging only planning of prostate radiotherapy,” *Phys. Imaging Radiat. Oncol.*, vol. 12, pp. 80–86, 2019.

[167] Y. Weng, T. Zhou, Y. Li, and X. Qiu, “NAS-Unet: Neural architecture search for medical image segmentation,” *IEEE Access*, vol. 7, pp. 44247–44257, 2019.

[168] A. Fabijańska *et al.*, “U-CatcHCC: An Accurate HCC Detector in Hepatic DCE-MRI Sequences Based on an U-Net Framework,” in *International Conference on Computer Vision and Graphics*, 2018, pp. 319–328.

[169] Y. Wang *et al.*, “A Two-Step Automated Quality Assessment for Liver MR Images Based on Convolutional Neural Network,” *Eur. J. Radiol.*, p. 108822, 2020.

[170] B. Zhao, J. Soraghan, G. Di Caterina, and D. Grose, “Segmentation of head and neck tumours using modified U-net,” in *2019 27th European Signal Processing Conference (EUSIPCO)*, 2019, pp. 1–4.

[171] G. Piantadosi, S. Marrone, A. Galli, M. Sansone, and C. Sansone, “DCE-MRI Breast Lesions Segmentation with a 3TP U-Net Deep Convolutional Neural Network,” in *2019 IEEE 32nd International Symposium on Computer-Based Medical Systems (CBMS)*, 2019, pp. 628–633.

[172] M. AskariHemmat *et al.*, “U-Net Fixed-Point Quantization for Medical Image Segmentation,” in *Large-Scale Annotation of Biomedical Data and Expert Label Synthesis and Hardware Aware Learning for Medical Imaging and Computer Assisted Intervention*, Springer, 2019, pp. 115–124.

[173] F. Paugam *et al.*, “Open-source pipeline for multi-class segmentation of the spinal cord with deep learning,” *Magn. Reson. Imaging*, vol. 64, pp. 21–27, 2019.

[174] M. Han *et al.*, “Automatic Segmentation of Human Placenta Images With U-Net,” *IEEE Access*, vol. 7, pp. 180083–180092, 2019.

[175] Y. Kurata *et al.*, “Automatic segmentation of the uterus on MRI using a convolutional neural network,” *Comput. Biol. Med.*, vol. 114, p. 103438, 2019.

[176] Z. Liu *et al.*, “Liver CT sequence segmentation based with improved U-Net and graph cut,” *Expert Syst. Appl.*, vol. 126, pp. 54–63, 2019.

[177] B. Sakboonyara and P. Taeprasartsit, “U-Net and Mean-Shift Histogram for Efficient Liver Segmentation from CT Images,” in *2019 11th International Conference on Knowledge and Smart Technology (KST)*, 2019, pp. 51–56.

[178] T.-Y. Su and Y.-H. Fang, “Automatic Liver and Spleen Segmentation with CT Images Using Multi-channel U-net Deep Learning Approach,” in *International Conference on Biomedical and Health Informatics*, 2019, pp. 33–41.

[179] B. A. Skourt, A. El Hassani, and A. Majda, “Lung CT image segmentation using deep neural networks,” *Procedia Comput. Sci.*, vol. 127, pp. 109–113, 2018.

[180] W. Tan, Y. Liu, H. Liu, J. Yang, X. Yin, and Y. Zhang, “A Segmentation Method of Lung Parenchyma From Chest CT Images Based on Dual U-Net,” in *2019 IEEE International Conference on Bioinformatics and Biomedicine (BIBM)*, 2019, pp. 1649–1656.

[181] H. Shaziya, K. Shyamala, and R. Zaheer, “Automatic Lung Segmentation on Thoracic CT Scans Using U-Net Convolutional Network,” in *2018 International Conference on Communication and Signal Processing (ICCSP)*, 2018, pp. 0643–0647.

[182] G. Tong, Y. Li, H. Chen, Q. Zhang, and H. Jiang, “Improved U-NET network for pulmonary nodules segmentation,” *Optik*, vol. 174, pp. 460–469, 2018.

[183] Z. Gu *et al.*, “CE-Net: context encoder network for 2D medical image segmentation,” *IEEE Trans. Med. Imaging*, vol. 38, no. 10, pp. 2281–2292, 2019.

[184] Z. Liu *et al.*, “Segmentation of organs-at-risk in cervical cancer CT images with a convolutional neural network,” *Phys. Med.*, vol. 69, pp. 184–191, 2020.

[185] N. Yagi, M. Nii, and S. Kobashi, “Abdominal Organ Area Segmentation using U-Net for Cancer Radiotherapy Support,” in *2019 IEEE International Conference on Systems, Man and Cybernetics (SMC)*, 2019, pp. 1210–1214.

[186] C. Wang, B. Connolly, P. F. de Oliveira Lopes, A. F. Frangi, and Ö. Smedby, “Pelvis segmentation using multi-pass U-Net and iterative shape estimation,” in *International Workshop on Computational Methods and Clinical Applications in Musculoskeletal Imaging*, 2018, pp. 49–57.

[187] V. Garg, M. Bansal, A. Sanjana, and M. Dave, “Analysis and Detection of Brain Tumor Using U-Net-Based Deep Learning.,” Jul. 2020, pp. 161–173. doi: 10.1007/978-3-030-52243-8_13.

[188] H. M. Rai and K. Chatterjee, "Detection of brain abnormality by a novel Lu-Net deep neural CNN model from MR images," *Mach. Learn. Appl.*, vol. 2, p. 100004, Dec. 2020, doi: 10.1016/j.mlwa.2020.100004.

[189] S. E. I. El kaitouni and H. Tairi, "Segmentation of medical images for the extraction of brain tumors: A comparative study between the Hidden Markov and Deep Learning approaches," in *2020 International Conference on Intelligent Systems and Computer Vision (ISCV)*, Jun. 2020, pp. 1–5. doi: 10.1109/ISCV49265.2020.9204319.

[190] Z. Wang and L. Zhang, "Semantic Segmentation of Brain MRI Based on U-net Network and Edge Loss," in *2020 19th International Symposium on Distributed Computing and Applications for Business Engineering and Science (DCABES)*, Oct. 2020, pp. 154–157. doi: 10.1109/DCABES50732.2020.00048.

[191] M. A. Ahamed, M. Ali Hossain, and M. Al Mamun, "Semantic Segmentation of Self-Supervised Dataset and Medical Images Using Combination of U-Net and Neural Ordinary Differential Equations," in *2020 IEEE Region 10 Symposium (TENSYMP)*, Jun. 2020, pp. 238–241. doi: 10.1109/TENSYMP50017.2020.9230884.

[192] S. Subramaniam, K. B. Jayanthi, C. Rajasekaran, and R. Kuchelar, "Deep Learning Architectures for Medical Image Segmentation," in *2020 IEEE 33rd International Symposium on Computer-Based Medical Systems (CBMS)*, Jul. 2020, pp. 579–584. doi: 10.1109/CBMS49503.2020.00115.

[193] A. Mehrtash, W. M. Wells, C. M. Tempany, P. Abolmaesumi, and T. Kapur, "Confidence Calibration and Predictive Uncertainty Estimation for Deep Medical Image Segmentation," *IEEE Trans. Med. Imaging*, vol. 39, no. 12, pp. 3868–3878, Dec. 2020, doi: 10.1109/TMI.2020.3006437.

[194] M. Zhao, Y. Wei, Y. Lu, and K. K. L. Wong, "A novel U-Net approach to segment the cardiac chamber in magnetic resonance images with ghost artifacts," *Comput. Methods Programs Biomed.*, vol. 196, p. 105623, Nov. 2020, doi: 10.1016/j.cmpb.2020.105623.

[195] B. Wu, Y. Fang, and X. Lai, "Left ventricle automatic segmentation in cardiac MRI using a combined CNN and U-net approach," *Comput. Med. Imaging Graph.*, vol. 82, p. 101719, Jun. 2020, doi: 10.1016/j.compmedimag.2020.101719.

[196] E. Altunok and I. Öksüz, "Accurate Myocardial Pathology Segmentation with Residual U-Net.," Jan. 2020.

[197] Z. Ji, X. Han, T. Lin, and W. Wang, "A Dense-Gated U-Net for Brain Lesion Segmentation," in *2020 IEEE International Conference on Visual Communications and Image Processing (VCIP)*, Dec. 2020, pp. 104–107. doi: 10.1109/VCIP49819.2020.9301852.

[198] W. Shi, E. Pang, Q. Wu, and F. Lin, "Brain Tumor Segmentation Using Dense Channels 2D U-net and Multiple Feature Extraction Network," Oct. 2019. doi: 10.1007/978-3-030-46640-4_26.

[199] R. Yogesh, N. Malarvizhi, and G. Sasi, "Narcotic Image Segmentation Utilizing MR U-Net Design," in *2020 International Conference on System, Computation, Automation and Networking (ICSCAN)*, Jul. 2020, pp. 1–6. doi: 10.1109/ICSCAN49426.2020.9262362.

[200] H. Yu, S. Zha, Y. Huangfu, C. Chen, M. Ding, and J. Li, "Dual Attention U-Net for Multi-sequence Cardiac MR Images Segmentation.," Jan. 2020.

[201] N. Micallef, D. Seychell, and C. J. Bajada, "A Nested U-Net Approach for Brain Tumour Segmentation," in *2020 IEEE 20th Mediterranean Electrotechnical Conference (MELECON)*, Jun. 2020, pp. 376–381. doi: 10.1109/MELECON48756.2020.9140550.

[202] M. Baldeon Calisto and S. K. Lai-Yuen, “AdaEn-Net: An ensemble of adaptive 2D–3D Fully Convolutional Networks for medical image segmentation,” *Neural Netw.*, vol. 126, pp. 76–94, Jun. 2020, doi: 10.1016/j.neunet.2020.03.007.

[203] M. Jafari, D. Auer, S. Francis, J. Garibaldi, and X. Chen, “DRU-Net: An Efficient Deep Convolutional Neural Network for Medical Image Segmentation,” in *2020 IEEE 17th International Symposium on Biomedical Imaging (ISBI)*, Apr. 2020, pp. 1144–1148. doi: 10.1109/ISBI45749.2020.9098391.

[204] B. Murugesan, K. Sarveswaran, V. Raghavan S., S. M. Shankaranarayana, K. Ram, and M. Sivaprakasam, “A Context Based Deep Learning Approach for Unbalanced Medical Image Segmentation,” in *2020 IEEE 17th International Symposium on Biomedical Imaging (ISBI)*, Apr. 2020, pp. 1949–1953. doi: 10.1109/ISBI45749.2020.9098597.

[205] S. Chen, G. Hu, and J. Sun, “Medical Image Segmentation Based on 3D U-net,” in *2020 19th International Symposium on Distributed Computing and Applications for Business Engineering and Science (DCABES)*, Oct. 2020, pp. 130–133. doi: 10.1109/DCABES50732.2020.00042.

[206] J. Sun, F. Darbehani, M. Zaidi, and B. Wang, “SAUNet: Shape Attentive U-Net for Interpretable Medical Image Segmentation,” Oct. 2020, pp. 797–806. doi: 10.1007/978-3-030-59719-1_77.

[207] P. Hambarde, S. Talbar, A. Mahajan, S. Chavan, M. Thakur, and N. Sable, “Prostate lesion segmentation in MR images using radiomics based deeply supervised U-Net,” *Biocybern. Biomed. Eng.*, vol. 40, no. 4, pp. 1421–1435, Oct. 2020, doi: 10.1016/j.bbe.2020.07.011.

[208] T. Jesus, R. Magalhães, and V. Alves, “Spatial Normalization of MRI Brain Studies Using a U-Net Based Neural Network.,” Apr. 2020, pp. 493–502. doi: 10.1007/978-3-030-45697-9_48.

[209] K. Ryu, N.-Y. Shin, D.-H. Kim, and Y. Nam, “Synthesizing T1 weighted MPRAGE image from multi echo GRE images via deep neural network,” *Magn. Reson. Imaging*, vol. 64, pp. 13–20, 2019.

[210] L. Zhao, X. Feng, C. H. Meyer, and D. C. Alsop, “Choroid Plexus Segmentation Using Optimized 3D U-Net,” in *2020 IEEE 17th International Symposium on Biomedical Imaging (ISBI)*, Apr. 2020, pp. 381–384. doi: 10.1109/ISBI45749.2020.9098443.

[211] D. Ai *et al.*, “Spatial probabilistic distribution map-based two-channel 3D U-net for visual pathway segmentation,” *Pattern Recognit. Lett.*, vol. 138, pp. 601–607, Oct. 2020, doi: 10.1016/j.patrec.2020.09.003.

[212] B. E. Dewey *et al.*, “DeepHarmony: A deep learning approach to contrast harmonization across scanner changes,” *Magn. Reson. Imaging*, vol. 64, pp. 160–170, 2019.

[213] A. Machireddy, N. Meermeier, F. Coakley, and X. Song, “Malignancy Detection in Prostate Multi-Parametric MR Images Using U-net with Attention,” in *2020 42nd Annual International Conference of the IEEE Engineering in Medicine & Biology Society (EMBC)*, Jul. 2020, pp. 1520–1523. doi: 10.1109/EMBC44109.2020.9176050.

[214] C. Li *et al.*, “ANU-Net: Attention-based nested U-Net to exploit full resolution features for medical image segmentation,” *Comput. Graph.*, vol. 90, pp. 11–20, Aug. 2020, doi: 10.1016/j.cag.2020.05.003.

[215] H. Seo, C. Huang, M. Bassenne, R. Xiao, and L. Xing, “Modified U-Net (mU-Net) With Incorporation of Object-Dependent High Level Features for Improved Liver and Liver-Tumor Segmentation in CT Images,” *IEEE Trans. Med. Imaging*, vol. 39, no. 5, pp. 1316–1325, May 2020, doi: 10.1109/TMI.2019.2948320.

[216] J. Rocha, A. Cunha, and A. M. Mendonça, "Conventional Filtering Versus U-Net Based Models for Pulmonary Nodule Segmentation in CT Images.," *J. Med. Syst.*, vol. 44, no. 4, pp. 81–81, Mar. 2020, doi: 10.1007/S10916-020-1541-9.

[217] K. Suzuki, Y. Otsuka, Y. Nomura, K. K. Kumamaru, R. Kuwatsuru, and S. Aoki, "Development and Validation of a Modified Three-Dimensional U-Net Deep-Learning Model for Automated Detection of Lung Nodules on Chest CT Images From the Lung Image Database Consortium and Japanese Datasets," *Acad. Radiol.*, Aug. 2020, doi: 10.1016/j.acra.2020.07.030.

[218] K. Yang *et al.*, "Identification of benign and malignant pulmonary nodules on chest CT using improved 3D U-Net deep learning framework," *Eur. J. Radiol.*, vol. 129, p. 109013, Aug. 2020, doi: 10.1016/j.ejrad.2020.109013.

[219] A. Khanna, N. D. Londhe, S. Gupta, and A. Semwal, "A deep Residual U-Net convolutional neural network for automated lung segmentation in computed tomography images," *Biocybern. Biomed. Eng.*, vol. 40, no. 3, pp. 1314–1327, Jul. 2020, doi: 10.1016/j.bbe.2020.07.007.

[220] Y. Zhou, M. Chen, M. Zhang, T. Wang, F. Yan, and C. Xie, "Automatic Segmentation of Lung Noudles using improved U-Net NetWork," in *2020 Chinese Automation Congress (CAC)*, Nov. 2020, pp. 1609–1613. doi: 10.1109/CAC51589.2020.9326834.

[221] C. Wang *et al.*, "MufiNet: Multiscale Fusion Residual Networks for Medical Image Segmentation," in *2020 International Joint Conference on Neural Networks (IJCNN)*, Jul. 2020, pp. 1–7. doi: 10.1109/IJCNN48605.2020.9207314.

[222] Y.-C. Liu, M. Shahid, W. Sarapugdi, Y.-X. Lin, J.-C. Chen, and K.-L. Hua, "Cascaded atrous dual attention U-Net for tumor segmentation," *Multimed. Tools Appl.*, Oct. 2020, doi: 10.1007/S11042-020-10078-2.

[223] A. G. Rassadin, "Deep Residual 3D U-Net for Joint Segmentation and Texture Classification of Nodules in Lung.," Jun. 2020, pp. 419–427. doi: 10.1007/978-3-030-50516-5_37.

[224] W. Ying, J. Li, Y. Wu, K. Zheng, Y. Deng, and J. Li, "U-Net with Dense Encoder, Residual Decoder and Depth-wise Skip Connections," in *2020 International Joint Conference on Neural Networks (IJCNN)*, Jul. 2020, pp. 1–6. doi: 10.1109/IJCNN48605.2020.9207371.

[225] S. LI, G. K. F. TSO, and K. HE, "Bottleneck feature supervised U-Net for pixel-wise liver and tumor segmentation," *Expert Syst. Appl.*, vol. 145, p. 113131, May 2020, doi: 10.1016/j.eswa.2019.113131.

[226] A. Kumar *et al.*, "Segmentation of Lung Field in HRCT Images Using U-Net Based Fully Convolutional Networks," in *Annual Conference on Medical Image Understanding and Analysis*, 2018, pp. 84–93.

[227] S. Hernández-Juárez *et al.*, "Semantic Segmentation of Lung Tissues in HRCT Images by Means of a U-Net Convolutional Network," in *Latin American Conference on Biomedical Engineering*, 2019, pp. 426–434.

[228] A. Yang, X. Jin, and L. Li, "CT Images Recognition of Pulmonary Tuberculosis Based on Improved Faster RCNN and U-Net," in *2019 10th International Conference on Information Technology in Medicine and Education (ITME)*, 2019, pp. 93–97.

[229] M. O. Ramkumar, D. Jayakumar, and R. Yogesh, "Multi Res U-Net Based Image Segmentation of Pulmonary Tuberculosis Using CT Images," in *2020 7th International Conference on Smart Structures and Systems (ICSSS)*, Jul. 2020, pp. 1–4. doi: 10.1109/ICSSS49621.2020.9202371.

[230] X. Ding, Y. Peng, C. Shen, and T. Zeng, "CAB U-Net: An end-to-end category attention boosting algorithm for segmentation," *Comput. Med. Imaging Graph.*, vol. 84, p. 101764, Sep. 2020, doi: 10.1016/j.compmedimag.2020.101764.

[231] Z. Lou, W. Huo, K. Le, and X. Tian, "Whole Heart Auto Segmentation of Cardiac CT Images Using U-Net Based GAN," in *2020 13th International Congress on Image and Signal Processing, BioMedical Engineering and Informatics (CISP-BMEI)*, Oct. 2020, pp. 192–196. doi: 10.1109/CISP-BMEI51763.2020.9263532.

[232] E. Kurnaz and R. Ceylan, "Pancreas Segmentation in Abdominal CT Images with U-Net Model," in *2020 28th Signal Processing and Communications Applications Conference (SIU)*, Oct. 2020, pp. 1–4. doi: 10.1109/SIU49456.2020.9302180.

[233] Y. Man, Y. Huang, J. Feng, X. Li, and F. Wu, "Deep Q learning driven ct pancreas segmentation with geometry-aware u-net," *IEEE Trans. Med. Imaging*, vol. 38, no. 8, pp. 1971–1980, 2019.

[234] L. Wang, B. Wang, and Z. Xu, "Tumor Segmentation Based on Deeply Supervised Multi-Scale U-Net," in *2019 IEEE International Conference on Bioinformatics and Biomedicine (BIBM)*, 2019, pp. 746–749.

[235] A. Manvel, K. Vladimir, T. Alexander, and U. Dmitry, "Radiologist-Level Stroke Classification on Non-contrast CT Scans with Deep U-Net," in *International Conference on Medical Image Computing and Computer-Assisted Intervention*, 2019, pp. 820–828.

[236] D. Zhang, J. Wang, J. H. Noble, and B. M. Dawant, "HeadLocNet: Deep convolutional neural networks for accurate classification and multi-landmark localization of head CTs," *Med. Image Anal.*, vol. 61, p. 101659, 2020.

[237] T. Song, F. Meng, A. Rodríguez-Patón, P. Li, P. Zheng, and X. Wang, "U-Next: A Novel Convolution Neural Network With an Aggregation U-Net Architecture for Gallstone Segmentation in CT Images," *IEEE Access*, vol. 7, pp. 166823–166832, 2019.

[238] W. Zhao, D. Jiang, J. Peña Queralta, and T. Westerlund, "MSS U-Net: 3D segmentation of kidneys and tumors from CT images with a multi-scale supervised U-Net," *Inform. Med. Unlocked*, vol. 19, p. 100357, Jan. 2020, doi: 10.1016/j.imu.2020.100357.

[239] Z. Li, J. Pan, H. Wu, Z. Wen, and J. Qin, "Memory-Efficient Automatic Kidney and Tumor Segmentation Based on Non-local Context Guided 3D U-Net," Oct. 2020, pp. 197–206. doi: 10.1007/978-3-030-59719-1_20.

[240] J. Chen, A. Cao, Y. Zhang, and T. Xu, "Tumor-assisted Diagnosis based on U-Net Network," in *2020 13th International Congress on Image and Signal Processing, BioMedical Engineering and Informatics (CISP-BMEI)*, Oct. 2020, pp. 739–742. doi: 10.1109/CISP-BMEI51763.2020.9263550.

[241] X. Xu *et al.*, "Asymmetrical Multi-task Attention U-Net for the Segmentation of Prostate Bed in CT Image," Oct. 2020, pp. 470–479. doi: 10.1007/978-3-030-59719-1_46.

[242] J. Ni, J. Wu, J. Tong, Z. Chen, and J. Zhao, "GC-Net: Global context network for medical image segmentation," *Comput. Methods Programs Biomed.*, vol. 190, p. 105121, Jul. 2020, doi: 10.1016/j.cmpb.2019.105121.

[243] L. Bargsten, M. Wendebourg, and A. Schlaefer, "Data Representations for Segmentation of Vascular Structures Using Convolutional Neural Networks with U-Net Architecture," in *2019 41st Annual International Conference of the IEEE Engineering in Medicine and Biology Society (EMBC)*, 2019, pp. 989–992.

[244] G. Cao, Y. Wang, X. Zhu, M. Li, X. Wang, and Y. Chen, "Segmentation of intracerebral hemorrhage based on improved U-Net," in *2020 IEEE Conference on Telecommunications, Optics and Computer Science (TOCS)*, Dec. 2020, pp. 183–185. doi: 10.1109/TOCS50858.2020.9339707.

[245] Z. Kuang, X. Deng, L. Yu, H. Wang, T. Li, and S. Wang, "Ψ-Net: Focusing on the border areas of intracerebral hemorrhage on CT images," *Comput. Methods Programs Biomed.*, vol. 194, p. 105546, Oct. 2020, doi: 10.1016/j.cmpb.2020.105546.

[246] Y. Zhang *et al.*, "HBNet: Hybrid Blocks Network for Segmentation of Gastric Tumor from Ordinary CT Images," in *2020 IEEE 17th International Symposium on Biomedical Imaging (ISBI)*, Apr. 2020, pp. 1–4. doi: 10.1109/ISBI45749.2020.9098425.

[247] G. Sha, J. Wu, and B. Yu, "Spinal fracture lesions segmentation based on U-net," in *2020 IEEE International Conference on Artificial Intelligence and Computer Applications (ICAICA)*, Jun. 2020, pp. 142–144. doi: 10.1109/ICAICA50127.2020.9182574.

[248] Y. Hiasa, Y. Otake, M. Takao, T. Ogawa, N. Sugano, and Y. Sato, "Automated Muscle Segmentation from Clinical CT Using Bayesian U-Net for Personalized Musculoskeletal Modeling," *IEEE Trans. Med. Imaging*, vol. 39, no. 4, pp. 1030–1040, Apr. 2020, doi: 10.1109/TMI.2019.2940555.

[249] L. Luo, D. Chen, and D. Xue, "Retinal blood vessels semantic segmentation method based on modified U-Net," in *2018 Chinese Control And Decision Conference (CCDC)*, Jun. 2018, pp. 1892–1895. doi: 10.1109/CCDC.2018.8407435.

[250] Q. Jin, Z. Meng, T. D. Pham, Q. Chen, L. Wei, and R. Su, "DUNet: A deformable network for retinal vessel segmentation," *Knowl.-Based Syst.*, vol. 178, pp. 149–162, Aug. 2019, doi: 10.1016/j.knosys.2019.04.025.

[251] J. Devda and R. Eswari, "Pathological Myopia Image Analysis Using Deep Learning," *2nd Int. Conf. Recent Trends Adv. Comput. ICRTAC -DISRUP - TIV Innov. 2019 Novemb. 11-12 2019*, vol. 165, pp. 239–244, Jan. 2019, doi: 10.1016/j.procs.2020.01.084.

[252] X. Xu, T. Tan, and F. Xu, "An Improved U-Net Architecture for Simultaneous Arteriole and Venule Segmentation in Fundus Image," in *Medical Image Understanding and Analysis*, Cham, 2018, pp. 333–340.

[253] W. Yijie, L. Shixuan, C. Guogang, C. Cong, L. Mengxue, and Z. Xinyu, "Improved U-net fundus image segmentation method," in *2019 International Conference on Intelligent Informatics and Biomedical Sciences (ICIIBMS)*, Nov. 2019, pp. 110–113. doi: 10.1109/ICIIBMS46890.2019.8991481.

[254] Z. Yan, X. Han, C. Wang, Y. Qiu, Z. Xiong, and S. Cui, "Learning Mutually Local-Global U-Nets For High-Resolution Retinal Lesion Segmentation In Fundus Images," in *2019 IEEE 16th International Symposium on Biomedical Imaging (ISBI 2019)*, Apr. 2019, pp. 597–600. doi: 10.1109/ISBI.2019.8759579.

[255] S. Kumawat and S. Raman, "Local Phase U-net for Fundus Image Segmentation," in *ICASSP 2019 - 2019 IEEE International Conference on Acoustics, Speech and Signal Processing (ICASSP)*, May 2019, pp. 1209–1213. doi: 10.1109/ICASSP.2019.8683390.

[256] C. Guo, M. Szemenyei, Y. Pei, Y. Yi, and W. Zhou, "SD-Unet: A Structured Dropout U-Net for Retinal Vessel Segmentation," in *2019 IEEE 19th International Conference on Bioinformatics and Bioengineering (BIBE)*, Oct. 2019, pp. 439–444. doi: 10.1109/BIBE.2019.00085.

[257] S. Zhang *et al.*, "Simultaneous Arteriole and Venule Segmentation of Dual-Modal Fundus Images Using a Multi-Task Cascade Network," *IEEE Access*, vol. 7, pp. 57561–57573, 2019, doi: 10.1109/ACCESS.2019.2914319.
[258] J. Civit-Masot, F. Luna-Perejón, S. Vicente-Díaz, J. M. Rodríguez Corral, and A. Civit, "TPU Cloud-Based Generalized U-Net for Eye Fundus Image Segmentation," *IEEE Access*, vol. 7, pp. 142379–142387, 2019, doi: 10.1109/ACCESS.2019.2944692.
[259] A. Farahani and H. Mohseni, "Medical image segmentation using customized U-Net with adaptive activation functions," *Neural Comput. Appl.*, pp. 1–17, Oct. 2020, doi: 10.1007/S00521-020-05396-3.
[260] X. -M. Li, G. -S. Chen, and S. -Y. Wang, "Dense-Atrous U-Net with salient computing for Accurate Retina Vessel Segmentation," in *2020 IEEE 15th International Conference on Solid-State & Integrated Circuit Technology (ICSICT)*, Nov. 2020, pp. 1–3. doi: 10.1109/ICSICT49897.2020.9278165.
[261] E. S. Kumar and C. S. Bindu, "An Efficient Approach to Accomplish Automatic Segmentation of Optic Cup Using Modified U-Net," in *2020 11th International Conference on Computing, Communication and Networking Technologies (ICCCNT)*, Jul. 2020, pp. 1–5. doi: 10.1109/ICCCNT49239.2020.9225537.
[262] A. Desai, R. Chauhan, and J. Sivaswamy, "Image Segmentation Using Hybrid Representations," in *2020 IEEE 17th International Symposium on Biomedical Imaging (ISBI)*, Apr. 2020, pp. 1–4. doi: 10.1109/ISBI45749.2020.9098463.
[263] B. Wang, S. Qiu, and H. He, "Dual Encoding U-Net for Retinal Vessel Segmentation," in *Medical Image Computing and Computer Assisted Intervention – MICCAI 2019*, Cham, 2019, pp. 84–92.
[264] Y. Li, Y. Wang, T. Leng, and W. Zhijie, "Wavelet U-Net for Medical Image Segmentation.," Sep. 2020, pp. 800–810. doi: 10.1007/978-3-030-61609-0_63.
[265] P. Xiuqin, Q. Zhang, H. Zhang, and S. Li, "A Fundus Retinal Vessels Segmentation Scheme Based on the Improved Deep Learning U-Net Model," *IEEE Access*, vol. 7, pp. 122634–122643, 2019, doi: 10.1109/ACCESS.2019.2935138.
[266] S. Yu, D. Xiao, S. Frost, and Y. Kanagasingam, "Robust optic disc and cup segmentation with deep learning for glaucoma detection," *Comput. Med. Imaging Graph.*, vol. 74, pp. 61–71, Jun. 2019, doi: 10.1016/j.compmedimag.2019.02.005.
[267] N. Liu, L. Liu, and J. Wang, "Local Adaptive U-net for Medical Image Segmentation," in *2020 IEEE International Conference on Bioinformatics and Biomedicine (BIBM)*, Dec. 2020, pp. 670–674. doi: 10.1109/BIBM49941.2020.9313515.
[268] W. Liu, H. Lei, H. Xie, B. Zhao, G. Yue, and B. Lei, "Multi-level Light U-Net and Atrous Spatial Pyramid Pooling for Optic Disc Segmentation on Fundus Image.," Jan. 2020.
[269] R. Kamble, P. Samanta, and N. Singhal, "Optic Disc, Cup and Fovea Detection from Retinal Images Using U-Net++ with EfficientNet Encoder.," Jan. 2020.
[270] G. Alfonso Francia, C. Pedraza, M. Aceves, and S. Tovar-Arriaga, "Chaining a U-Net With a Residual U-Net for Retinal Blood Vessels Segmentation," *IEEE Access*, vol. 8, pp. 38493–38500, 2020, doi: 10.1109/ACCESS.2020.2975745.
[271] R. Zhao, W. Chen, and G. Cao, "Edge-Boosted U-Net for 2D Medical Image Segmentation," *IEEE Access*, vol. 7, pp. 171214–171222, 2019.

[272] R. Adarsh, G. Amarnageswarao, R. Pandeeswari, and S. Deivalakshmi, "Dense Residual Convolutional Auto Encoder For Retinal Blood Vessels Segmentation," in *2020 6th International Conference on Advanced Computing and Communication Systems (ICACCS)*, Mar. 2020, pp. 280–284. doi: 10.1109/ICACCS48705.2020.9074172.

[273] Y. Wu *et al.*, "Vessel-Net: Retinal Vessel Segmentation Under Multi-path Supervision," in *Medical Image Computing and Computer Assisted Intervention – MICCAI 2019*, Cham, 2019, pp. 264–272.

[274] H. H. Yu, X. Feng, Z. Wang, and H. Sun, "MixModule: Mixed CNN Kernel Module for Medical Image Segmentation," in *2020 IEEE 17th International Symposium on Biomedical Imaging (ISBI)*, Apr. 2020, pp. 1508–1512. doi: 10.1109/ISBI45749.2020.9098498.

[275] K. Chen, G. Xu, J. Qian, and C.-X. Ren, "A Bypass-Based U-Net for Medical Image Segmentation," in *International Conference on Intelligent Science and Big Data Engineering*, 2019, pp. 155–164.

[276] E. B. Kablan, H. Dogan, M. E. Ercin, S. Ersoz, and M. Ekinci, "An ensemble of fine-tuned fully convolutional neural networks for pleural effusion cell nuclei segmentation," *Comput. Electr. Eng.*, vol. 81, p. 106533, 2020.

[277] T. Wan, L. Zhao, H. Feng, D. Li, C. Tong, and Z. Qin, "Robust nuclei segmentation in histopathology using ASPPU-Net and boundary refinement," *Neurocomputing*, vol. 408, pp. 144–156, Sep. 2020, doi: 10.1016/j.neucom.2019.08.103.

[278] Y. Huang, H. Zhu, P. Wang, and D. Dong, "Segmentation of Overlapping Cervical Smear Cells Based on U-Net and Improved Level Set," in *2019 IEEE International Conference on Systems, Man and Cybernetics (SMC)*, 2019, pp. 3031–3035.

[279] M. Zhang, X. Li, M. Xu, and Q. Li, "RBC semantic segmentation for sickle cell disease based on deformable U-Net," in *International Conference on Medical Image Computing and Computer-Assisted Intervention*, 2018, pp. 695–702.

[280] C. E. Akbaş and M. Kozubek, "Condensed U-Net (Cu-Net): An Improved U-Net Architecture for Cell Segmentation Powered by 4x4 Max-Pooling Layers," in *2020 IEEE 17th International Symposium on Biomedical Imaging (ISBI)*, Apr. 2020, pp. 446–450. doi: 10.1109/ISBI45749.2020.9098351.

[281] T. Overton and A. Tucker, "DO-U-Net for Segmentation and Counting," 2020, pp. 391–403.

[282] A. O. Vuola, S. U. Akram, and J. Kannala, "Mask-RCNN and U-net ensembled for nuclei segmentation," in *2019 IEEE 16th International Symposium on Biomedical Imaging (ISBI 2019)*, 2019, pp. 208–212.

[283] J. Zhao *et al.*, "PGU-net+: Progressive Growing of U-net+ for Automated Cervical Nuclei Segmentation," in *International Workshop on Multiscale Multimodal Medical Imaging*, 2019, pp. 51–58.

[284] D. Jha, M. A. Riegler, D. Johansen, P. Halvorsen, and H. D. Johansen, "DoubleU-Net: A Deep Convolutional Neural Network for Medical Image Segmentation," in *2020 IEEE 33rd International Symposium on Computer-Based Medical Systems (CBMS)*, Jul. 2020, pp. 558–564. doi: 10.1109/CBMS49503.2020.00111.

[285] Y. Wang *et al.*, "Segment Medical Image Using U-Net Combining Recurrent Residuals and Attention," in *Medical Imaging and Computer-Aided Diagnosis*, 2020, pp. 77–86. doi: 10.1007/978-981-15-5199-4_8.

[286] B. Zhao *et al.*, “Triple U-net: Hematoxylin-aware nuclei segmentation with progressive dense feature aggregation,” *Med. Image Anal.*, vol. 65, p. 101786, Oct. 2020, doi: 10.1016/j.media.2020.101786.

[287] X. Li, Y. Huang, C. Yan, and L. Liu, “IT-Block: Inverted Triangle Block embedded U-Net for Medical Image Segmentation,” in *2020 International Joint Conference on Neural Networks (IJCNN)*, Jul. 2020, pp. 1–8. doi: 10.1109/IJCNN48605.2020.9207047.

[288] R. M. Rad, P. Saeedi, J. Au, and J. Havelock, “Multi-resolutional ensemble of stacked dilated u-net for inner cell mass segmentation in human embryonic images,” in *2018 25th IEEE International Conference on Image Processing (ICIP)*, 2018, pp. 3518–3522.

[289] H. M. Saleh, N. H. Saad, and N. A. M. Isa, “Overlapping Chromosome Segmentation using U-Net: Convolutional Networks with Test Time Augmentation,” *Procedia Comput. Sci.*, vol. 159, pp. 524–533, 2019.

[290] E. Altinsoy, C. Yilmaz, J. Wen, L. Wu, J. Yang, and Y. Zhu, “Raw G-Band Chromosome Image Segmentation Using U-Net Based Neural Network,” in *International Conference on Artificial Intelligence and Soft Computing*, 2019, pp. 117–126.

[291] H. Bai, T. Zhang, C. Lu, W. Chen, F. Xu, and Z. -B. Han, “Chromosome Extraction Based on U-Net and YOLOv3,” *IEEE Access*, vol. 8, pp. 178563–178569, 2020, doi: 10.1109/ACCESS.2020.3026483.

[292] Y. M. Kassim, O. Glinskii, V. Glinsky, V. Huxley, G. Guidoboni, and K. Palaniappan, “Deep U-Net Regression and Hand-Crafted Feature Fusion for Accurate Blood Vessel Segmentation,” in *2019 IEEE International Conference on Image Processing (ICIP)*, 2019, pp. 1445–1449.

[293] A. Ojeda-Pat, A. Martin-Gonzalez, and R. Soberanis-Mukul, “Convolutional Neural Network U-Net for Trypanosoma cruzi Segmentation,” in *International Symposium on Intelligent Computing Systems*, 2020, pp. 118–131.

[294] N. Ali *et al.*, “Predictive Modeling of Antibiotic Susceptibility in E. Coli Strains Using the U-Net Network and One-Class Classification,” *IEEE Access*, vol. 8, pp. 167711–167720, 2020, doi: 10.1109/ACCESS.2020.3022829.

[295] X. Hu and H. Yang, “DRU-net: a novel U-net for biomedical image segmentation,” *IET Image Process.*, vol. 14, no. 1, pp. 192–200, 2019.

[296] S. Li, J. Xu, and R. Chen, “U-Net Neural Network Optimization Method Based on Deconvolution Algorithm.,” Nov. 2020, pp. 592–602. doi: 10.1007/978-3-030-63830-6_50.

[297] M. E. Bagdigen and G. Bilgin, “Cell Segmentation in Triple-Negative Breast Cancer Histopathological Images Using U-Net Architecture,” in *2020 28th Signal Processing and Communications Applications Conference (SIU)*, Oct. 2020, pp. 1–4. doi: 10.1109/SIU49456.2020.9302367.

[298] J. Silva-Rodríguez, E. Payá-Bosch, G. García, A. Colomer, and V. Naranjo, “Prostate Gland Segmentation in Histology Images via Residual and Multi-resolution U-NET.,” Jan. 2020, pp. 1–8.

[299] G. Bueno, M. M. Fernandez-Carrobles, L. Gonzalez-Lopez, and O. Deniz, “Glomerulosclerosis identification in whole slide images using semantic segmentation,” *Comput. Methods Programs Biomed.*, vol. 184, p. 105273, 2020.

[300] M. Dash, N. D. Londhe, S. Ghosh, A. Semwal, and R. S. Sonawane, “PsLSNet: Automated psoriasis skin lesion segmentation using modified U-Net-based fully convolutional network,” *Biomed. Signal Process. Control*, vol. 52, pp. 226–237, 2019.

[301] S. N. Hasan, M. Gezer, R. A. Azeez, and S. Gülseçen, “Skin Lesion Segmentation by using Deep Learning Techniques,” in *2019 Medical Technologies Congress (TIPTEKNO)*, 2019, pp. 1–4.
[302] Z. Al Nazi and T. A. Abir, “Automatic Skin Lesion Segmentation and Melanoma Detection: Transfer Learning Approach with U-Net and DCNN-SVM,” in *Proceedings of International Joint Conference on Computational Intelligence*, 2020, pp. 371–381.
[303] P. Tang *et al.*, “Efficient skin lesion segmentation using separable-Unet with stochastic weight averaging,” *Comput. Methods Programs Biomed.*, vol. 178, pp. 289–301, 2019.
[304] E. Z. Chen, X. Dong, X. Li, H. Jiang, R. Rong, and J. Wu, “Lesion attributes segmentation for melanoma detection with multi-task u-net,” in *2019 IEEE 16th International Symposium on Biomedical Imaging (ISBI 2019)*, 2019, pp. 485–488.
[305] G. Asaeikheybari, J. Green, X. Qian, H. Jiang, and M.-C. Huang, “Medical image learning from a few/few training samples: Melanoma segmentation study,” *Smart Health*, vol. 14, p. 100088, 2019.
[306] L. Liu, L. Mou, X. X. Zhu, and M. Mandal, “Skin Lesion Segmentation Based on Improved U-net,” in *2019 IEEE Canadian Conference of Electrical and Computer Engineering (CCECE)*, 2019, pp. 1–4.
[307] M. A. Al-Masni, M. A. Al-antari, M.-T. Choi, S.-M. Han, and T.-S. Kim, “Skin lesion segmentation in dermoscopy images via deep full resolution convolutional networks,” *Comput. Methods Programs Biomed.*, vol. 162, pp. 221–231, 2018.
[308] B. S. Lin, K. Michael, S. Kalra, and H. R. Tizhoosh, “Skin lesion segmentation: U-nets versus clustering,” in *2017 IEEE Symposium Series on Computational Intelligence (SSCI)*, 2017, pp. 1–7.
[309] D. R. Ramani and S. S. Ranjani, “U-Net Based Segmentation and Multiple Feature Extraction of Dermascopic Images for Efficient Diagnosis of Melanoma,” in *Computer Aided Intervention and Diagnostics in Clinical and Medical Images*, Springer, 2019, pp. 81–101.
[310] B. Hafhouf, A. Zitouni, A. C. Megherbi, and S. Sbaa, “A Modified U-Net for Skin Lesion Segmentation,” in *2020 1st International Conference on Communications, Control Systems and Signal Processing (CCSSP)*, May 2020, pp. 225–228. doi: 10.1109/CCSSP49278.2020.9151511.
[311] Y. Yang, C. Feng, and R. Wang, “Automatic segmentation model combining U-Net and level set method for medical images,” *Expert Syst. Appl.*, vol. 153, p. 113419, Sep. 2020, doi: 10.1016/j.eswa.2020.113419.
[312] D. Lin, Y. Li, T. L. Nwe, S. Dong, and Z. M. Oo, “RefineU-Net: Improved U-Net with progressive global feedbacks and residual attention guided local refinement for medical image segmentation,” *Pattern Recognit. Lett.*, vol. 138, pp. 267–275, Oct. 2020, doi: 10.1016/j.patrec.2020.07.013.
[313] T. L. A. van den Heuvel, H. Petros, S. Santini, C. L. de Korte, and B. van Ginneken, “Automated Fetal Head Detection and Circumference Estimation from Free-Hand Ultrasound Sweeps Using Deep Learning in Resource-Limited Countries,” *Ultrasound Med. Biol.*, vol. 45, no. 3, pp. 773–785, Mar. 2019, doi: 10.1016/j.ultrasmedbio.2018.09.015.
[314] T. Włodarczyk *et al.*, “Estimation of Preterm Birth Markers with U-Net Segmentation Network,” in *Smart Ultrasound Imaging and Perinatal, Preterm and Paediatric Image Analysis*, Cham, 2019, pp. 95–103.

[315] B. Du *et al.*, “A novel transcranial ultrasound imaging method with diverging wave transmission and deep learning approach,” *Comput. Methods Programs Biomed.*, vol. 186, p. 105308, Apr. 2020, doi: 10.1016/j.cmpb.2019.105308.
[316] Y. Wang, C. Wei, Z. Wang, Q. Lu, and C. Wang, “A More Streamlined U-net for Nerve Segmentation in Ultrasound Images,” in *2018 Chinese Automation Congress (CAC)*, Dec. 2018, pp. 101–104. doi: 10.1109/CAC.2018.8623052.
[317] Q. Zhang, Z. Cui, X. Niu, S. Geng, and Y. Qiao, “Image Segmentation with Pyramid Dilated Convolution Based on ResNet and U-Net,” in *Neural Information Processing*, Cham, 2017, pp. 364–372.
[318] K. HATANO, S. MURAKAMI, H. LU, J. K. TAN, H. KIM, and T. AOKI, “Detection of Phalange Region Based on U-Net,” in *2018 18th International Conference on Control, Automation and Systems (ICCAS)*, Oct. 2018, pp. 1338–1342.
[319] W. Wu, J. Zhang, H. Xie, Y. Zhao, S. Zhang, and L. Gu, “Automatic detection of coronary artery stenosis by convolutional neural network with temporal constraint,” *Comput. Biol. Med.*, vol. 118, p. 103657, Mar. 2020, doi: 10.1016/j.compbiomed.2020.103657.
[320] M. Gherardini, E. Mazomenos, A. Menciassi, and D. Stoyanov, “Catheter segmentation in X-ray fluoroscopy using synthetic data and transfer learning with light U-nets,” *Comput. Methods Programs Biomed.*, vol. 192, p. 105420, Aug. 2020, doi: 10.1016/j.cmpb.2020.105420.
[321] M. Amiri, R. Brooks, and H. Rivaz, “Fine Tuning U-Net for Ultrasound Image Segmentation: Which Layers?,” in *Domain Adaptation and Representation Transfer and Medical Image Learning with Less Labels and Imperfect Data*, Cham, 2019, pp. 235–242.
[322] M. Byra *et al.*, “Breast mass segmentation in ultrasound with selective kernel U-Net convolutional neural network,” *Biomed. Signal Process. Control*, vol. 61, p. 102027, Aug. 2020, doi: 10.1016/j.bspc.2020.102027.
[323] M. Amiri, R. Brooks, B. Behboodi, and H. Rivaz, “Two-stage ultrasound image segmentation using U-Net and test time augmentation.,” *Int. J. Comput. Assist. Radiol. Surg.*, vol. 15, no. 6, pp. 981–988, Apr. 2020, doi: 10.1007/S11548-020-02158-3.
[324] N. Abraham, K. Illanko, N. Khan, and D. Androutsos, “Deep Learning for Semantic Segmentation of Brachial Plexus Nervesin Ultrasound Images Using U-Net and M-Net,” in *2019 3rd International Conference on Imaging, Signal Processing and Communication (ICISPC)*, Jul. 2019, pp. 85–89. doi: 10.1109/ICISPC.2019.8935668.
[325] S. Moradi *et al.*, “MFP-Unet: A novel deep learning based approach for left ventricle segmentation in echocardiography,” *Phys. Med.*, vol. 67, pp. 58–69, 2019.
[326] J. Yang, M. Faraji, and A. Basu, “Robust segmentation of arterial walls in intravascular ultrasound images using Dual Path U-Net,” *Ultrasonics*, vol. 96, pp. 24–33, Jul. 2019, doi: 10.1016/j.ultras.2019.03.014.
[327] M. Xie *et al.*, “Vessel lumen segmentation in carotid artery ultrasounds with the U-Net convolutional neural network,” in *2020 IEEE International Conference on Bioinformatics and Biomedicine (BIBM)*, Dec. 2020, pp. 2680–2684. doi: 10.1109/BIBM49941.2020.9313434.
[328] M. Xia, W. Yan, Y. Huang, Y. Guo, G. Zhou, and Y. Wang, “Extracting Membrane Borders in IVUS Images Using a Multi-Scale Feature Aggregated U-Net,” in *2020 42nd Annual International Conference of the IEEE Engineering in Medicine & Biology Society (EMBC)*, Jul. 2020, pp. 1650–1653. doi: 10.1109/EMBC44109.2020.9175970.

[329] M. Xie *et al.*, “Two-stage and dual-decoder convolutional U-Net ensembles for reliable vessel and plaque segmentation in carotid ultrasound images,” in *2020 19th IEEE International Conference on Machine Learning and Applications (ICMLA)*, Dec. 2020, pp. 1376–1381. doi: 10.1109/ICMLA51294.2020.00214.

[330] V. Zyuzin, A. Mukhtarov, D. Neustroev, and T. Chumarnaya, “Segmentation of 2D Echocardiography Images using Residual Blocks in U-Net Architectures,” in *2020 Ural Symposium on Biomedical Engineering, Radioelectronics and Information Technology (USBEREIT)*, May 2020, pp. 499–502. doi: 10.1109/USBEREIT48449.2020.9117678.

[331] L. S. Hesse and A. I. L. Namburete, “Improving U-Net Segmentation with Active Contour Based Label Correction.,” Jul. 2020. doi: 10.1007/978-3-030-52791-4_6.

[332] X. Li *et al.*, “Multi-Task Refined Boundary-Supervision U-Net (MRBSU-Net) for Gastrointestinal Stromal Tumor Segmentation in Endoscopic Ultrasound (EUS) Images,” *IEEE Access*, vol. 8, pp. 5805–5816, 2020, doi: 10.1109/ACCESS.2019.2963472.

[333] L. Xu *et al.*, “DW-Net: A cascaded convolutional neural network for apical four-chamber view segmentation in fetal echocardiography,” *Comput. Med. Imaging Graph.*, vol. 80, p. 101690, Mar. 2020, doi: 10.1016/j.compmedimag.2019.101690.

[334] J. Ding, Z. Huang, M. Shi, and C. Ning, “Automatic Thyroid Ultrasound Image Segmentation Based on U-shaped Network,” in *2019 12th International Congress on Image and Signal Processing, BioMedical Engineering and Informatics (CISP-BMEI)*, Oct. 2019, pp. 1–5. doi: 10.1109/CISP-BMEI48845.2019.8966062.

[335] D. M. Alex and D. A. Chandy, “Investigations on Performances of Pre-trained U-Net Models for 2D Ultrasound Kidney Image Segmentation,” Aug. 2020, pp. 185–195. doi: 10.1007/978-3-030-60036-5_13.

[336] W. Zhang, H. Cheng, and J. Gan, “MUNet: A Multi-scale U-Net Framework for Medical Image Segmentation,” in *2020 International Joint Conference on Neural Networks (IJCNN)*, Jul. 2020, pp. 1–7. doi: 10.1109/IJCNN48605.2020.9206703.

[337] S. Marques *et al.*, “Segmentation of gynaecological ultrasound images using different U-Net based approaches,” in *2019 IEEE International Ultrasonics Symposium (IUS)*, Oct. 2019, pp. 1485–1488. doi: 10.1109/ULTSYM.2019.8925948.

[338] L. Ding, K. Zhao, X. Zhang, X. Wang, and J. Zhang, “A Lightweight U-Net Architecture Multi-Scale Convolutional Network for Pediatric Hand Bone Segmentation in X-Ray Image,” *IEEE Access*, vol. 7, pp. 68436–68445, 2019, doi: 10.1109/ACCESS.2019.2918205.

[339] Y. Shu, X. Wu, and W. Li, “LVC-Net: Medical Image Segmentation with Noisy Label Based on Local Visual Cues,” in *Medical Image Computing and Computer Assisted Intervention – MICCAI 2019*, Cham, 2019, pp. 558–566.

[340] Y. Mu, D. Xue, J. Guo, H. Xu, W. Wang, and H. Li, “Automatic calcaneus fracture identification and segmentation using a multi-task U-Net,” in *2020 5th International Conference on Communication, Image and Signal Processing (CCISP)*, Nov. 2020, pp. 140–144. doi: 10.1109/CCISP51026.2020.9273509.

[341] M. Frid-Adar, A. Ben-Cohen, R. Amer, and H. Greenspan, “Improving the Segmentation of Anatomical Structures in Chest Radiographs Using U-Net with an ImageNet Pre-trained Encoder,” in *Image Analysis for Moving Organ, Breast, and Thoracic Images*, Cham, 2018, pp. 159–168.

[342] S. Reza, O. B. Amin, and M. M. A. Hashem, “TransResUNet: Improving U-Net Architecture for Robust Lungs Segmentation in Chest X-rays,” in *2020 IEEE Region 10 Symposium (TENSYMP)*, Jun. 2020, pp. 1592–1595. doi: 10.1109/TENSYMP50017.2020.9230835.

[343] D. Waiker, P. D. Baghel, K. R. Varma, and S. P. Sahu, “Effective Semantic Segmentation of Lung X-Ray Images using U-Net Architecture,” in *2020 Fourth International Conference on Computing Methodologies and Communication (ICCMC)*, Mar. 2020, pp. 603–607. doi: 10.1109/ICCMC48092.2020.ICCMC-000112.

[344] T. J. Jun, J. Kweon, Y.-H. Kim, and D. Kim, “T-Net: Nested encoder–decoder architecture for the main vessel segmentation in coronary angiography,” *Neural Netw.*, vol. 128, pp. 216–233, Aug. 2020, doi: 10.1016/j.neunet.2020.05.002.

[345] H. Toda *et al.*, “Shape Recovery of Polyp Using Blood Vessel Detection and Matching Estimation by U-Net,” in *2019 8th International Congress on Advanced Applied Informatics (IIAI-AAI)*, 2019, pp. 450–453.

[346] S. K. Hasan and C. A. Linte, “U-NetPlus: A Modified Encoder-Decoder U-Net Architecture for Semantic and Instance Segmentation of Surgical Instruments from Laparoscopic Images,” in *2019 41st Annual International Conference of the IEEE Engineering in Medicine and Biology Society (EMBC)*, 2019, pp. 7205–7211.

[347] J. Leng, Y. Liu, T. Zhang, P. Quan, and Z. Cui, “Context-aware u-net for biomedical image segmentation,” in *2018 IEEE International Conference on Bioinformatics and Biomedicine (BIBM)*, 2018, pp. 2535–2538.

[348] D. J. Matuszewski and I.-M. Sintorn, “Reducing the U-Net size for practical scenarios: Virus recognition in electron microscopy images,” *Comput. Methods Programs Biomed.*, vol. 178, pp. 31–39, 2019.

[349] J. I. Orlando *et al.*, “U2-Net: A Bayesian U-Net Model With Epistemic Uncertainty Feedback For Photoreceptor Layer Segmentation In Pathological OCT Scans,” in *2019 IEEE 16th International Symposium on Biomedical Imaging (ISBI 2019)*, Apr. 2019, pp. 1441–1445. doi: 10.1109/ISBI.2019.8759581.

[350] Y. He *et al.*, “Fully Convolutional Boundary Regression for Retina OCT Segmentation.,” Oct. 2019, vol. 11764, pp. 120–128. doi: 10.1007/978-3-030-32239-7_14.

[351] J. Kugelman, D. Alonso-Caneiro, S. A. Read, S. J. Vincent, F. K. Chen, and M. J. Collins, “Effect of Altered OCT Image Quality on Deep Learning Boundary Segmentation,” *Ieee Access*, vol. 8, pp. 43537–43553, Jan. 2020, doi: 10.1109/ACCESS.2020.2977355.

[352] I. Z. Matovinovic, S. Loncaric, J. Lo, M. Heisler, and M. Sarunic, “Transfer Learning with U-Net type model for Automatic Segmentation of Three Retinal Layers In Optical Coherence Tomography Images,” in *2019 11th International Symposium on Image and Signal Processing and Analysis (ISPA)*, Sep. 2019, pp. 49–53. doi: 10.1109/ISPA.2019.8868639.

[353] S. Liu, D. P. Shamonin, G. Zahnd, A. F. W. van der Steen, T. van Walsum, and G. van Soest, “Healthy Vessel Wall Detection Using U-Net in Optical Coherence Tomography,” in *Machine Learning and Medical Engineering for Cardiovascular Health and Intravascular Imaging and Computer Assisted Stenting*, Cham, 2019, pp. 184–192.

[354] Z. Chen, D. Li, H. Shen, H. Mo, Z. Zeng, and H. Wei, “Automated segmentation of fluid regions in optical coherence tomography B-scan images of age-related macular degeneration,” *Opt. Laser Technol.*, vol. 122, p. 105830, Feb. 2020, doi: 10.1016/j.optlastec.2019.105830.

[355] R. Tennakoon, A. K. Gostar, R. Hoseinnezhad, and A. Bab-Hadiashar, "Retinal fluid segmentation in OCT images using adversarial loss based convolutional neural networks," Apr. 2018, pp. 1436–1440. doi: 10.1109/ISBI.2018.8363842.

[356] R. Asgari, S. Waldstein, F. Schlanitz, M. Baratsits, U. Schmidt-Erfurth, and H. Bogunović, "U-Net with Spatial Pyramid Pooling for Drusen Segmentation in Optical Coherence Tomography," in *Ophthalmic Medical Image Analysis*, Cham, 2019, pp. 77–85.

[357] M. Zhang *et al.*, "A neural network approach to segment brain blood vessels in digital subtraction angiography," *Comput. Methods Programs Biomed.*, vol. 185, p. 105159, 2020.

[358] R. Kimura, A. Teramoto, T. Ohno, K. Saito, and H. Fujita, "Virtual digital subtraction angiography using multizone patch-based U-Net.," Oct. 2020. doi: 10.1007/S13246-020-00933-9.

[359] S. Liu *et al.*, "Segmenting nailfold capillaries using an improved U-net network," *Microvasc. Res.*, vol. 130, p. 104011, Jul. 2020, doi: 10.1016/j.mvr.2020.104011.

[360] Y. Han and J. C. Ye, "Framing U-Net via deep convolutional framelets: Application to sparse-view CT," *IEEE Trans. Med. Imaging*, vol. 37, no. 6, pp. 1418–1429, 2018.

[361] Y. Liu *et al.*, "Artifact Suppression for Passive Cavitation Imaging Using U-Net CNNs with Uncertainty Quantification," in *2019 IEEE 4th International Conference on Signal and Image Processing (ICSIP)*, Jul. 2019, pp. 1037–1042. doi: 10.1109/SIPROCESS.2019.8868593.

[362] R. Souza *et al.*, "Dual-domain cascade of U-nets for multi-channel magnetic resonance image reconstruction," *Magn. Reson. Imaging*, vol. 71, pp. 140–153, Sep. 2020, doi: 10.1016/j.mri.2020.06.002.

[363] H. Lan, D. Jiang, C. Yang, F. Gao, and F. Gao, "Y-Net: Hybrid deep learning image reconstruction for photoacoustic tomography in vivo," *Photoacoustics*, vol. 20, p. 100197, Dec. 2020, doi: 10.1016/j.pacs.2020.100197.

[364] Z. Cheng, K. Guo, C. Wu, J. Shen, and L. Qu, "U-Net cascaded with dilated convolution for medical image registration," in *2019 Chinese Automation Congress (CAC)*, 2019, pp. 3647–3651.

[365] M. Salem *et al.*, "A fully convolutional neural network for new T2-w lesion detection in multiple sclerosis," *NeuroImage Clin.*, vol. 25, p. 102149, 2020.

[366] D. Wei *et al.*, "Deep morphological simplification network (MS-Net) for guided registration of brain magnetic resonance images," *Pattern Recognit.*, vol. 100, p. 107171, Apr. 2020, doi: 10.1016/j.patcog.2019.107171.

[367] B. R. Thomson *et al.*, "MR-to-US Registration Using Multiclass Segmentation of Hepatic Vasculature with a Reduced 3D U-Net.," Oct. 2020, pp. 275–284. doi: 10.1007/978-3-030-59716-0_27.

[368] L. Sun *et al.*, "Topological correction of infant cortical surfaces using anatomically constrained U-net," in *International Workshop on Machine Learning in Medical Imaging*, 2018, pp. 125–133.

[369] I. Olaciregui-Ruiz, I. Torres-Xirau, J. Teuwen, U. A. van der Heide, and A. Mans, "A Deep Learning-based correction to EPID dosimetry for attenuation and scatter in the Unity MR-Linac system," *Phys. Med.*, vol. 71, pp. 124–131, 2020.

[370] G. Li, L. Bai, C. Zhu, E. Wu, and R. Ma, "A Novel Method of Synthetic CT Generation from MR Images Based on Convolutional Neural Networks," in *2018 11th International Congress on Image and Signal Processing, BioMedical Engineering and Informatics (CISP-BMEI)*, 2018, pp. 1–5.

[371] O. Lucena, R. Souza, L. Rittner, R. Frayne, and R. Lotufo, "Convolutional neural networks for skull-stripping in brain MR imaging using silver standard masks," *Artif. Intell. Med.*, vol. 98, pp. 48–58, 2019.
[372] T. Nair, D. Precup, D. L. Arnold, and T. Arbel, "Exploring uncertainty measures in deep networks for multiple sclerosis lesion detection and segmentation," *Med. Image Anal.*, vol. 59, p. 101557, 2020.
[373] X. Xia and B. Kulis, "W-net: A deep model for fully unsupervised image segmentation," *ArXiv Prepr. ArXiv171108506*, 2017.
[374] Z. Khan and J. Yang, "Bottom-up unsupervised image segmentation using FC-Dense u-net based deep representation clustering and multidimensional feature fusion based region merging," *Image Vis. Comput.*, vol. 94, p. 103871, 2020.
[375] F. Chen, Y. Jiang, X. Zeng, J. Zhang, X. Gao, and M. Xu, "PUB-SalNet: A Pre-Trained Unsupervised Self-Aware Backpropagation Network for Biomedical Salient Segmentation," *Algorithms*, vol. 13, no. 5, p. 126, 2020.
[376] M. Tan and Q. V. Le, "Efficientnet: Rethinking model scaling for convolutional neural networks," *ArXiv Prepr. ArXiv190511946*, 2019.
[377] X. Yi, E. Walia, and P. Babyn, "Generative adversarial network in medical imaging: A review," *Med. Image Anal.*, vol. 58, p. 101552, 2019.
[378] N. Papernot, P. McDaniel, I. Goodfellow, S. Jha, Z. B. Celik, and A. Swami, "Practical black-box attacks against machine learning," in *Proceedings of the 2017 ACM on Asia conference on computer and communications security*, 2017, pp. 506–519.
[379] M. I. Razzak, S. Naz, and A. Zaib, "Deep learning for medical image processing: Overview, challenges and the future," in *Classification in BioApps*, Springer, 2018, pp. 323–350.
[380] N. Siddique, S. Paheding, Md. Z. Alom, and V. K. Devabhaktuni, "Recurrent residual U-Net with EfficientNet encoder for medical image segmentation," in *Proceedings of SPIE Pattern Recognition and Tracking XXXII*, Apr. 2021, vol. 11735. doi: 10.1117/12.2591343.
[381] G. Larsson, M. Maire, and G. Shakhnarovich, "FractalNet: Ultra-Deep Neural Networks without Residuals.," 2017. [Online]. Available: https://openreview.net/forum?id=S1VaB4cex
[382] M. Tan and Q. V. Le, "EfficientNet: Rethinking Model Scaling for Convolutional Neural Networks," May 2019, pp. 6105–6114.
[383] Z. Bai, H. Jiang, S. Li, and Y.-D. Yao, "Liver Tumor Segmentation Based on Multi-Scale Candidate Generation and Fractal Residual Network," *Ieee Access*, vol. 7, pp. 82122–82133, Jun. 2019, doi: 10.1109/ACCESS.2019.2923218.
[384] A. Kumar *et al.*, "CSNet: A new DeepNet framework for ischemic stroke lesion segmentation.," *Comput. Methods Programs Biomed.*, vol. 193, May 2020, doi: 10.1016/J.CMPB.2020.105524.
[385] K. P. Murphy, *Machine learning: a probabilistic perspective*. MIT press, 2012.
[386] L. R. Dice, "Measures of the amount of ecologic association between species," *Ecology*, vol. 26, no. 3, pp. 297–302, 1945.
[387] P. Jaccard, "The distribution of the flora in the alpine zone. 1," *New Phytol.*, vol. 11, no. 2, pp. 37–50, 1912.
[388] S. S. M. Salehi, D. Erdogmus, and A. Gholipour, "Tversky loss function for image segmentation using 3D fully convolutional deep networks," 2017, pp. 379–387.
[389] H. Kervadec, J. Bouchtiba, C. Desrosiers, E. Granger, J. Dolz, and I. B. Ayed, "Boundary loss for highly unbalanced segmentation," 2019, pp. 285–296.

[390] M. M. Fraz *et al.*, “An Ensemble Classification-Based Approach Applied to Retinal Blood Vessel Segmentation,” *IEEE Trans. Biomed. Eng.*, vol. 59, no. 9, pp. 2538–2548, Sep. 2012, doi: 10.1109/TBME.2012.2205687.

[391] N. Codella *et al.*, “Skin lesion analysis toward melanoma detection 2018: A challenge hosted by the international skin imaging collaboration (isic),” *ArXiv Prepr. ArXiv190203368*, 2019.

[392] P. Tschandl, C. Rosendahl, and H. Kittler, “The HAM10000 dataset, a large collection of multi-source dermatoscopic images of common pigmented skin lesions,” *Sci. Data*, vol. 5, p. 180161, 2018.

[393] D. M. Powers, “Evaluation: from precision, recall and F-measure to ROC, informedness, markedness and correlation,” *ArXiv Prepr. ArXiv201016061*, 2020.

[394] T. Fawcett, “An introduction to ROC analysis,” *Pattern Recognit. Lett.*, vol. 27, no. 8, pp. 861–874, 2006.

[395] S. Ioffe and C. Szegedy, “Batch normalization: Accelerating deep network training by reducing internal covariate shift,” *ArXiv Prepr. ArXiv150203167*, 2015.

[396] A. L. Maas, A. Y. Hannun, and A. Y. Ng, “Rectifier nonlinearities improve neural network acoustic models,” 2013, vol. 30, no. 1, p. 3.

[397] N. Srivastava, G. Hinton, A. Krizhevsky, I. Sutskever, and R. Salakhutdinov, “Dropout: a simple way to prevent neural networks from overfitting,” *J. Mach. Learn. Res.*, vol. 15, no. 1, pp. 1929–1958, 2014.

[398] Z. Zhang, Q. Liu, and Y. Wang, “Road extraction by deep residual u-net,” *IEEE Geosci. Remote Sens. Lett.*, vol. 15, no. 5, pp. 749–753, 2018.

[399] S. Y. Shin, S. Lee, I. D. Yun, and K. M. Lee, “Deep vessel segmentation by learning graphical connectivity,” *Med. Image Anal.*, vol. 58, p. 101556, 2019.

[400] J. Zhuang, “Laddernet: Multi-path networks based on u-net for medical image segmentation,” *ArXiv Prepr. ArXiv181007810*, 2018.

[401] L. Li, M. Verma, Y. Nakashima, H. Nagahara, and R. Kawasaki, “Iternet: Retinal image segmentation utilizing structural redundancy in vessel networks,” 2020, pp. 3656–3665.

PUBLICATIONS

N. Siddique, S. Paheding, C. Elkin, and V. K. Devabhaktuni, "U-Net and its variants for medical image segmentation: A review of theory and applications," *IEEE Access*, vol. 9, pp. 82031–82057, Jun. 2021. doi: 10.1109/ACCESS.2021.3086020.

N. Siddique, S. Paheding, M. Z. Alom, and V. K. Devabhaktuni, "Recurrent residual U-Net with EfficientNet encoder for medical image segmentation," in *Proc. SPIE 11735, Pattern Recognition and Tracking XXXII, 117350L*, vol. 11735, Apr. 2021. doi: 10.1117/12.2591343.